Svetlana Shafrova

First-year sea ice features: Investigation of ice field strength heterogeneity and modelling of ice rubble behaviour

Thesis for the degree of philosophiae doctor

Trondheim, August 2007

Norwegian University of
Science and Technology
Faculty of Engineering Science and Technology
Department of Civil and Transport Engineering

NTNU
Innovation and Creativity

UNIS
The University Centre in Svalbard
Department of Arctic Technology

NTNU
Norwegian University of Science and Technology

Thesis for the degree of philosophiae doctor

Faculty of Engineering Science and Technology
Department of Civil and Transport Engineering

ISBN 978-82-471-3859-5 (printed ver.)
ISBN 978-82-471-3862-5 (electronic ver.)
ISSN 1503-8181

Theses at NTNU, 2007-176

Printed by Tapir Uttrykk

Svetlana Shafrova

First-year sea ice features:
Investigation of ice field strength heterogeneity and modelling of ice rubble behaviour

Longyearbyen, October 2007

Doctoral thesis for the philosophiae doctor degree (PhD)

Norwegian University of Science and Technology
Faculty of Engineering Science and Technology
Department of Civil and Transport Engineering

NTNU

The University Centre in Svalbard
Department of Arctic Technology

UNIS

To my mother,
who gave me the possibility

ABSTRACT

For the nearest years the design load level for offshore structures in Arctic regions is likely to be controlled by first-year sea ice ridges and rubble fields if the icebergs are not present in the area. Drifting ridges may hit fixed or moored surface structure such as platforms or ships, or they may gouge the seabed endangering pipelines and wellheads. Both the temporal and spatial properties of the consolidated layer and the unconsolidated part (the ice rubble) of the ice ridge are important input into ridge-load models. A better understanding of the ice rubble behaviour will enable us to determine the ice-ridge load more accurately. This thesis deals with two separate but connected subjects, namely: *the ice strength field heterogeneity of both first-year sea ice ridge and level ice and the mechanical behaviour of the ice rubble.*

Field mechanical testing of first-year sea ice by uniaxial compression has been done in order to improve the knowledge of the ice fields strength heterogeneity. The in-plane ice strength non-homogeneity of different ice fields on the landfast level ice in the Spitsbergen fjords were investigated. A typical ice strength variability was found to be about 20-40% for the vertical ice samples and 10-20% for the horizontal ones. The weak zones were found within the entire ice fields. It was established that the strength of the ice samples taken from a certain depth from the ice cover surface at the different locations of the same ice field varied by a factor of 3 to 4. Furthermore, two first-year sea ice ridges have been examined with respect to the 2D spatial strength distribution: one in the North-western Barents Sea and one in the Arctic Ocean nearby Spitsbergen. The ice ridges are characterized by high strength heterogeneity of 40-55%, where the ice strength varied more than 3 times along both vertical and horizontal directions.

Special Finite Difference program “Inhomogeneity” was used to study the influence of the ice strength heterogeneity on the ice loads. It was shown that the ice heterogeneity might be one of the reasons for the scale effect.

In order to investigate the nature of freeze bonds between the ice blocks, series of field and laboratory small scale tests were conducted with submerged ice blocks. The small scale field tests were carried out in Adventfjorden on Spitsbergen. An opening was made in the landfast level ice. The level ice was sawed into cubic blocks which then were submerged down into the water. Some of the ice blocks were cut in two parts and then frozen together in order to simulate the freeze bonds between the ice blocks. The other blocks were submerged without forming the adfreeze bond. In addition to that, laboratory tests with both artificial ice (fresh and sea water) and natural sea ice were conducted in the cold laboratories at the University Centre in Svalbard (UNIS). The temporal development of the freeze bonding strength and the

local strength of the ice blocks in the ice rubble, their changes with block size, confinement and ice properties were studied. The average freeze bonding strength from the field tests was found as 32 ± 18 kPa after 48 hours of submerging. The corresponding freeze bonding strength from the laboratory tests was 67 ± 52 kPa for the natural sea ice and 274 ± 142 kPa for the artificial freshwater ice within 60 hours of testing. Moreover, the ratio of freeze bonding strength to the strength of the submerged ice was found in the range of 0.008 to 0.082 with an average around 0.03 after 48 hours of submerging in the field. The corresponding strength ratio varied from 0.14 to 0.38 for the artificial fresh water ice and from 0.015 to 0.40 for the sea ice within 60 hours of testing in the laboratory.

A pseudo-discrete continuum model has been developed to study the behaviour of the ice rubble and in particularly its initial failure mechanism that is associated with the breakage of the freeze bonding contacts (rubble skeleton). The model is a combination of discrete particle assembly generation and Finite Element analysis of this assembly. The model provides a possibility to simulate the contacts between the ice blocks. A parametric analysis simulating 2D direct shear tests shows that the pseudo-discrete continuum model is very sensitive to both strength and morphology of the freeze bonds between the ice blocks. An attempt to extend the model to study large deformations within the ice rubble (that is associated with rotation, rearrangement of the ice blocks and their breakage) was considered.

ACKNOWLEDGEMENTS

I would like to acknowledge those who made this thesis possible, those who supported me during the work as well as those who made this time exciting.

My supervisor Professor Sveinung Løset from Norwegian University of Science and Technology (NTNU) and University Centre in Svalbard (UNIS) introduced me to the Arctic engineering in 1999 during my fist visit on Svalbard. His enthusiasm and valuable support made this study possible.

My co-supervisor Associate Professor Knut V. Høyland from UNIS and NTNU educated me a lot both with respect to the theoretical background and field experience. His support and great encouragements together with interesting and helpful discussions are sincerely acknowledged.

My co-supervisor Professor Karl N. Shkninek from the Saint-Petersburg State Polytechnical University (SPbSPU) first made me familiar with offshore engineering thought my university years and after made a lot of efforts to follow my work; his good ideas and willingness to help is much appreciated.

My co-supervisor Professor Ove Tobias Gudmestad from Statoil ASA, University of Stavanger and NTNU firstly supported me a lot during my MSc project and after was always interested about the current stage and progress of my work, that reminded me to be back to real problems.

I learned a lot from Dr. Pavel Liferov from Barlindhaug Consult in Tromsø (now Statoil ASA); his ideas about ice rubble behaviour were the main force at the beginning of the work. The encouragement and help from Professor Lars Grande from NTNU is also greatly appreciated.

The cooperation and valuable support from Dr. Per Olav Moslet from UNIS (now Dr. techn. Olav Olsen a.s.), Mr. Rinat Kamalov from NTNU, Ms. Ekaterina Kim from SPbSPU and Mr. Sèbastien Barrault from UNIS are highly acknowledged.

The students from the Arctic Technology Department at UNIS in the years 2004 to 2006 provided essential support for the field and laboratory testing.

The invaluable library services from Ms. Berit Jakobsen from UNIS is highly valued and I will never forget the delicious dinners and nice music at 238-13B. I would also like to thank Ms. Monika Trümper for the pleasant entertainment during lunch and coffee breaks at my final term at UNIS.

Last but not least, I would like to thank my mother, Natalia, that I am able to submit this thesis.

CONTENT

1 INTRODUCTION

1.1 General

Hydrocarbon deposits have been discovered in ice-infested waters in the European Arctic (Barents, Pechora and Kara Seas), North American Arctic (Beaufort Sea), North Caspian Sea and Offshore Sakhalin. For the development of production facilities in such areas emphasis will be on the adequate design of structures and pipelines that can resist actions from the ice features.

The ice loads on offshore and coastal structures depend on many factors describing both the ice field and offshore structure. The ice strength is one of the key parameters for the calculation of the ice loads. The strength depends on the physical properties of the ice, such as salinity, temperature, density and as a result the ice porosity. All these parameters are continuously changing with the space and the time which leads to a large variation in the ice strength values. As a result the temporal and spatial variations of the ice properties are of high importance for both probabilistic and deterministic analysis of ice loads.

A better knowledge about ice properties within the sea ice ridges together with knowledge about their deformation behaviour will lead to more precise estimation of the ice load. Thus, the capital costs for the offshore structures will decrease resulting in more economic field development for the Arctic offshore.

1.2 Objectives, scope and organization of the thesis

The main intent of this work has been to increase the knowledge about mechanical properties of the sea ice features in general and to study the ice rubble behaviour via numerical modelling. Special attention has been a focus on ice strength spatial distribution within both level ice and ice ridges. The influence of the ice strength heterogeneity on the ice loads was investigated using a special numerical program. Another aim of the thesis was to investigate the morphology and strength of the freeze bonds between ice blocks in the sea ice ridge. The in-situ ridge investigations together with small-scale field and laboratory testing has been carried out. Based on these results, a pseudo-discrete continuum model was established to study the ice rubble deformation behaviour.

The main objectives of the thesis are:

1. Field and laboratory experiments:
   - To estimate the ice strength heterogeneity both in-plane and through the ice thickness, within first-year sea ice features.
   - To investigate the morphology of the freeze bonds between the ice blocks within ice ridges.
   - To study the temporal development of the freeze-bonding strength by small scale testing.
2. Numerical work:
   - To investigate the influence of the ice strength heterogeneity on the ice loads using the special 2D Finite Difference numerical program - "Inhomogeneity".
   - To develop and verify a numerical model that can be used to simulate the mechanical behaviour of ice rubble.
   - To study the behaviour and to derive the mechanical properties of the ice rubble from numerical simulations of direct shear tests.

The present work is a follow up of previous research on ice rubble behaviour by Dr. Pavel Liferov. He introduced (Liferov, 2005) the numerical model that was verified and extended within the present study.

The thesis consists of seven papers submitted to or accepted in scientific journals and international conference proceedings. This thesis is organized as follows:

Chapter 2 gives a brief introduction to ice physics and mechanics. The formation and structure of the first-year sea ice ridges are also discussed.

Chapter 3 analyses field measurements of the uniaxial compression strength of first-year sea ice. The chapter consists of three papers. One of them deals with the ice strength spatial distribution within the ice ridges and drift ice that were examined in the Barents Sea (2005) and Arctic Ocean (2006). Besides it reports morphology data of the freeze bonds between ice blocks in the ridge sails. Two other papers describe and analyze the in-plane strength variability for the different ice fields in landfast level ice in Spitsbergen fjords during the years 2004 and 2005.

Chapter 4 discussed the influence of the ice strength heterogeneity on the ice loads based on numerical simulations that were conducted using the 2D Finite Difference program "Inhomogeneity". The program was introduced and the wide range of numerical experiments were performed. The chapter comprises one paper.

Chapter 5 describes and discusses small scale field and laboratory testing of ice rubble during the years 2005 and 2006. The strength of the freeze bonds between the ice blocks together with the local strength of the corresponding ice blocks in the ice rubble were examined. The influence of different aspects such as time, block size, confinement, ice salinity and ice temperature on the corresponding strength values were under investigation. The chapter consists of one paper.

Chapter 6 describes the ice rubble material model with focus on application of Mohr-Coulomb material model. The review of classical theory of elasto-plasticity and brief introduction into the finite element numerical modelling are given in this chapter.

Chapter 7 deals with an analysis of the deformation and strength of ice rubble. Finite element numerical modelling was performed to simulate the rubble behaviour. The chapter consists of two papers.

Chapter 8 presents the main conclusions of the present study and gives the recommendation for further work.

1.3 Readership

The present work was carried out to improve the knowledge about ice field strength heterogeneity that is one of factors that can be responsible for non-simultaneous ice failure of an ice feature which may link to the ice strength scale effect. There is still a lack of information since the strength variability has not been considered in detail yet. Special attention was given to study the ice rubble morphology and deformation behaviour. The target readership is engineers and scientists working with, and person interested in:

- Hydrocarbon field development in ice-infested waters.
- Ice research with focus on first-year sea ice features.
- Design of structures subjected to loads from level ice and ice rubble.
- Field activities in Arctic waters.

1.4 Reference

Liferov, P. (2005). First-year ice ridge scour and some aspects of ice rubble behaviour. Doctoral Theses at NTNU 2005:84, Department of Civil and Transport Engineering, Norwegian University of Science and Technology, Trondheim, 155 p.

2 SEA ICE ENVIRONMENT

2.1 Introduction

Sea ice features are often a key consideration in the engineering as well as in geophysical perspective. They may determine the design load for marine and coastal structures such as platforms, ships, pipelines and bridges. From a geophysical point of view they are important for both ice volume estimations and for analysis of the strength of pack ice. The current knowledge about sea ice features and their loads on structures is not exhaustive, both physico-mechanical properties and morphology characteristics need more investigations. It is vital to increase the background information for both analytical and numerical ice load prediction models.

2.2 Sea ice features

2.2.1 General

Sea ice in the ocean can be found in a number of different forms depending on the physical process that the ice has been exposed to after the formation. Sea ice that is unaffected by deformation is known as level ice. Other sea ice features correspond to various forms of deformed ice, such as rafted ice, ridges, rubble, stamukha and hummocks.

The sea ice condition can be divided into drifting and landfast ice. The landfast ice is normally the level sea ice which is attached to the shore. In landfast ice the thermal expansion and tide may cause stresses and loads on nearby structures. But the design load level is usually determined by the drift ice features i.e. ice ridges and surrounding level ice fields if icebergs are not dominating in the area. Furthermore, the ice is usually categorized based on the age as first-year, second-year or multi-year type. The present thesis deals with first-year features only. Since the main work of the study deals with ice ridges, the formation and structure of these features will be briefly discussed in the next section.

2.2.2 First-year ice ridges

Ice ridges form when the level ice cover is compressed or sheared by environmental driving forces and are often found in the transition area (shear zone) between the landfast and the drift ice. They are in general long, non-symmetrical and curvilinear three-dimensional features. The ice broken during the ridge formation creates ice rubble both above (sail) and below (keel) the water level, which is in hydrostatic

equilibrium. The central part of the ridge along the water line is refrozen forming the consolidated layer of the ridge.

A typical sketch of the cross-section of a first-year ridge together with the basic geometrical parameters that describe the ridge shape is schematically shown in Fig. 2.1. Fig. 2.2 shows photo of first-year ice ridges from the North-Western Barents Sea area.

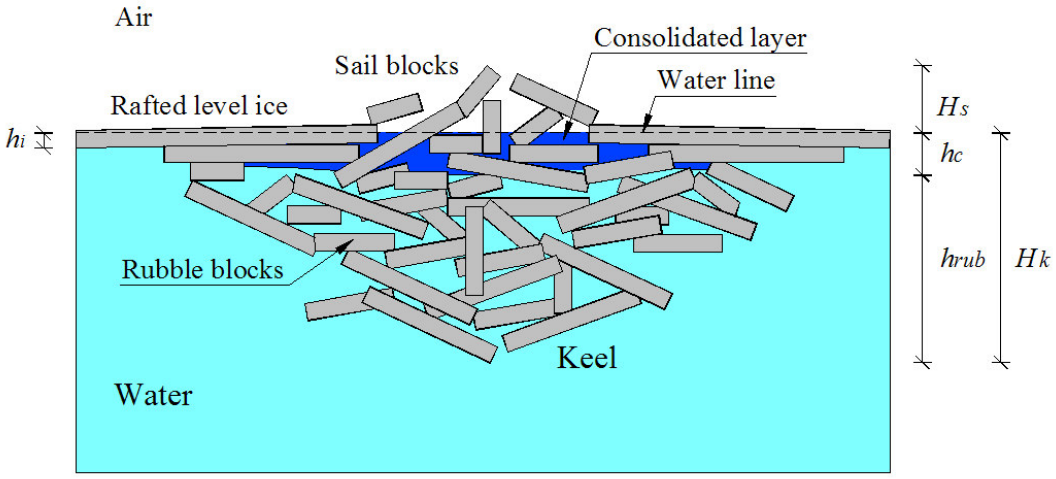

Fig. 2.1. Principal cross section sketch of an ice ridge.

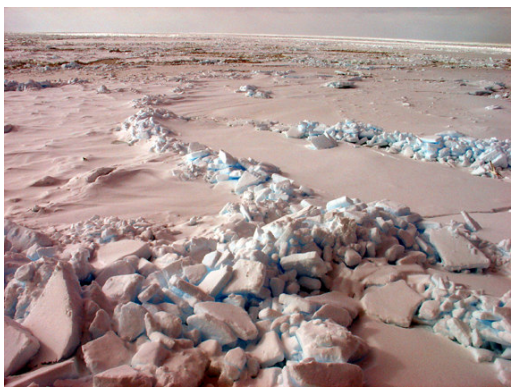

Fig. 2.2. Photo of first-year ridges in the Barents Sea, May 2005.

Published studies of the morphology and shapes of the first-year ice ridges is given by Tucker and Govoni (1981), Veitch et al. (1991), Leppäranta and Hakala (1992), Leppäranta et al. (1995), Timco and Burden (1997), Bonnemaire et al. (2003), Zubakin et al. (2005) and Høyland (2007).

The macro porosity (η) and total porosity (η_t) of an ice ridge can be defined after Høyland, (2002) as follows:

$$\eta = \frac{V_{sea\ water}}{V_{sea\ water} + V_{pure\ ice} + V_{brine\ pockets}} \tag{2.1}$$

$$\eta_t = \frac{V_{sea\ water} + V_{brine\ pockets}}{V_{sea\ water} + V_{pure\ ice} + V_{brine\ pockets}} \tag{2.2}$$

The parameters in these equations are defined in Fig. 2.3.

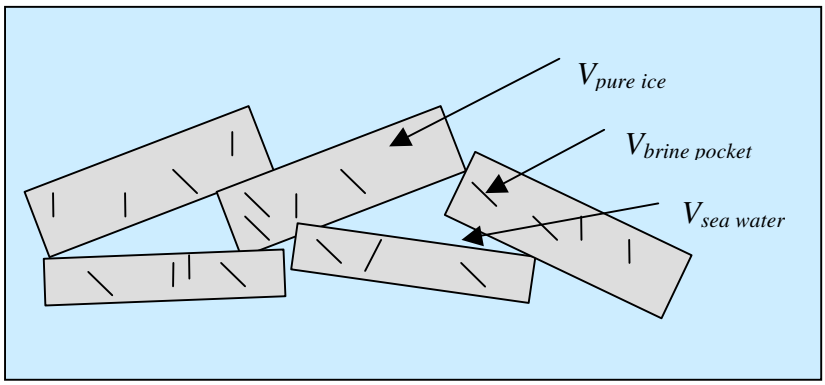

Fig. 2.3. Definition of porosity in a ridge (after Løset et al., 2006).

Typical key parameters of a first-year ice ridge are:

- Sail height: H_s= 1-6 m (often 2-4 m)
- Keel depth: H_k= 4-25 m (often 8-15 m)
- Keel to sail ratio: H_k/H_s= 4-5
- The ratio between the consolidated layer and level ice thickness: h_c/h_i=1.2–2.1 (often 1.5-1.8)
- Salinity: 4-8 ppt
- Macro-porosity: 25-40% (often 30-35%).

The internal morphology of ridges from various locations is reported by Sayed and Frederking (1989) from the Beafort Sea, Veitch et al. (1991) from the Gulf of Bothnia, Bonnemaire et al. (2003) and Høyland (2007) both from the Barents Sea. Høyland (2007) found that the average thickness of the ice blocks in the sail was 0.38 m and the ice blocks with thickness up to 2 m were found. Altogether 432 blocks were inspected. The average length/thickness, the width/thickness and the length/width ratios from the same study were 3.5, 2.4 and 1.6, respectively. Fig. 2.4 shows ice blocks from the sail and ice rubble blocks from the keel of the same ice ridge.

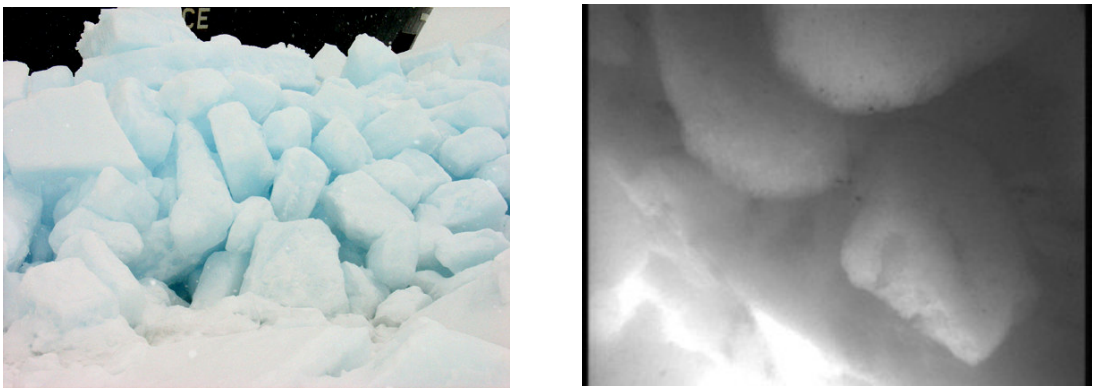

a) Ridge sail b) Ridge keel (underwater video)

Fig. 2.4. The typical view of the ice blocks within the same ice ridge, Barents Sea, May 2005.

The internal morphology of the ice ridge is important for the description of the ice rubble deformation behaviour. Most of the studies like Prodanovic (1979), Urroz and Ettema (1987) and Timco et al. (2000) aiming that the rubble strength is generally treated in accordance with soil mechanics theory for granular materials and in particular the linear Mohr-Coulomb failure criteria is used, where the strength deviation is based on angle of internal friction and cohesion:

$$\tau = \sigma \tan\varphi + c \tag{2.3}$$

where τ and σ are the shear and normal stresses on the failure surface respectively, φ is the angle of internal friction and c is the cohesion.

The reported values of the rubble strength show a great scatter. Heinonen and Määttänen, (2000) obtained from in-situ tests that the rubble cohesion is 2.3 kPa and the angle of internal friction is 14°. Most of the experiments were performed in the laboratory and the corresponding strength results were in the range: 0 - 25 kPa for the rubble cohesion and 8 - 70° for the angle of internal friction.

2.3 Ice physics and mechanics

2.3.1 Physical and mechanical properties of sea ice

Several parameters affect the ice loads on marine and coastal structures, in particular, the type of ice feature, the ice properties, the scenario of ice-structure interaction and the structure's geometry. The influence of ice properties on the ice load are schematically shown in Fig. 2.5.

The temperature of sea ice is highly variable and mainly controlled by air temperature, wind speed and snow cover thickness. During the winter the temperature profile through the sea ice is assumed to be approximately linear, ranging between the mean air temperature at the upper layers and the freezing point of sea water at lower layers. During the spring the temperature profile will become non-linear corresponding to a parabolic or "C-shape" as the result of the air temperature increase and as the thermal changes propagate through the ice cover. Fig. 2.6 shows typical temperature profiles through the first-year landfast ice in Van Mijenfjorden, Svalbard.

As Fig. 2.5 shows that the ice strength is dependent on several physical properties and the temperature is one of them. The temperature affects the brine volume of the ice and will therefore have an important indirect effect on the strength of the saline ice (Kämäräinen, 1993). The pure ice content increases with decreasing temperature and as a result the ice becomes stronger (higher strength) and harder (higher modulus of elasticity). In addition the ice becomes more brittle with decreasing temperature.

Salinity of the sea ice is another important parameter that together with temperature govern the brine volume and thereby the porosity. When the ice crystals form, the salt accumulates into the cells that are called the brine pockets. Any temperature gradient in the sea ice will result in brine cells migration along the gradient in the direction of higher temperature which leads to continuous brine drainage within the ice. The increase of brine volume corresponds to strength decrease, since the presence of impurities (brine, air) reduces the pure ice content. The salinity profile of the level ice typically has a "C-shape" profile as shown in Fig. 2.7.

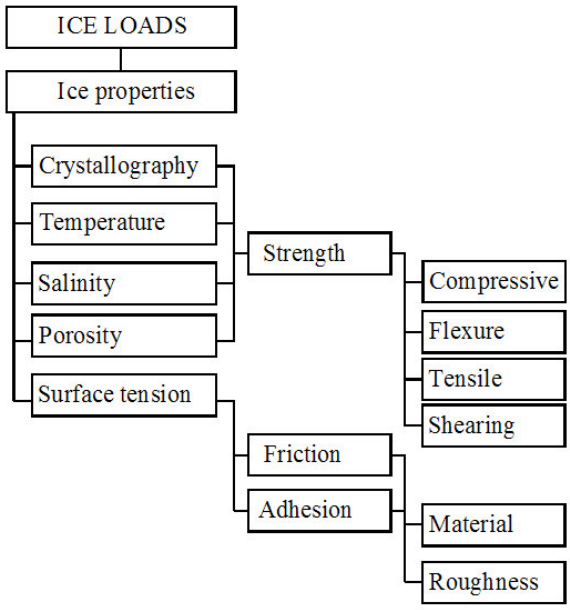

Fig. 2.5. Ice properties affecting ice loads on structures.
(after Løset et al., 2006).

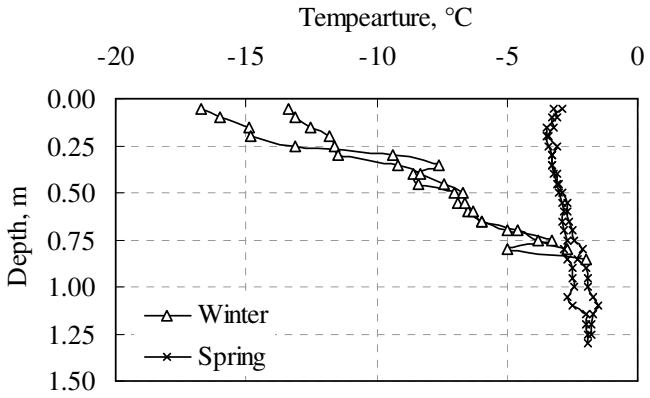

Fig. 2.6. Typical temperature profiles through the first-year sea ice
in winter (middel of March) and in spring (end of April),
Van Mijenfjorden, Svalbard, 2004.

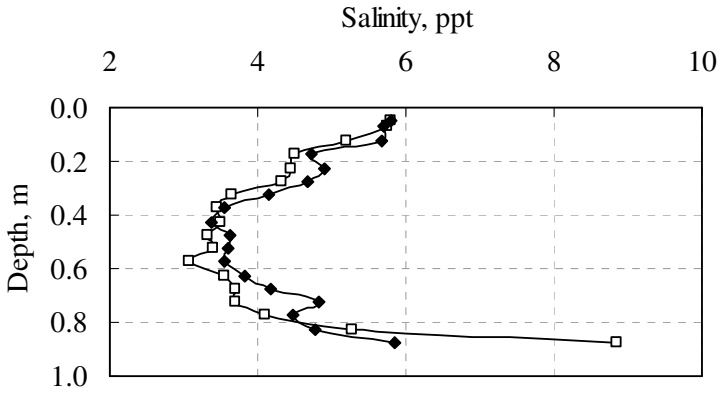

Fig. 2.7. Typical salinity profiles through the first-year sea ice in Van Mijenfjorden, Svalbard, April, 2004.

As already mentioned the temperature together with the salinity and the density determine the air and brine volume contents and as a result the porosity within the ice. The porosity of ice is a key parameter for the thermo-mechanical behaviour of ice, and it is of interest to derive the porosity from relatively simple measurements of ice temperature (T_i), ice salinity (S_i) and ice density (ρ_i). The present derivations follows Cox and Weeks (1983) for ice colder than -2ºC and Leppäranta and Manninen (1988) for warm ice. Sea ice consists of pure ice, water, salt and air. The salt is either dissolved in the water (brine) or exists as solid salts. The vital assumption behind these models is that the pure ice, the brine and the solid salts exist in thermal equilibrium and the relationship between the components is given by the temperature and the salinity. The air is assumed to exist independently of the other substances.

For the ice colder than -2ºC, the brine and air volume can be written as:

$$\nu_b = \frac{\rho_i \cdot S_i}{F_1(T_i)}, \tag{2.4}$$

$$\nu_a = 1 - \frac{\rho_i}{\rho_{pi}} + \rho_i \cdot S_i \frac{F_2(T_i)}{F_1(T_i)}, \tag{2.5}$$

where the functions F1(T) and F2(T) are unique functions of the temperature that given by Cox and Weeks (1983). The density of pure ice (ρ_{pi}) is defined from Pounder (1965) as:

$$\rho_{pi} = 0.917 - 1.403 \cdot 10^{-4} T_i, \tag{2.6}$$

where T_i is given in ºC.

In the warm ice there is no solid salts, and the formulas for the brine and air volume become:

$$V_b = \frac{\rho_i \cdot S_i}{S_b \cdot \rho_b}, \tag{2.7}$$

$$V_a = 1 - \frac{\rho_i}{\rho_{pi}} + V_b \cdot \left(\frac{\rho_b}{\rho_{pi}} - 1 \right) \tag{2.8}$$

Where the salinity (S_b) and density (ρ_b) of the brine is given by Leppäranta and Manninen (1988) at different temperature based on UNESCO equations for S_b (T_i) and ρ_b (S_b, T_i).

In general the ice becomes weaker and softer with increasing porosity. But there is no proper link between the ice porosity and the corresponding strength. The ice strength shows substantial variation in both the vertical and horizontal planes due to changes of the ice properties. The reasons behind these variations are explicitly defined but the corresponding effect on the ice strength is not fully understood.

The mechanical behaviour of ice is also affected by the grain size distribution (type of material) and loading rate. The grain size is the crucial factor to distinguish between nucleation control (brittle material) and propagation control (ductile material) fracture. When the ice behaves brittle the fracture will be unstable and nucleation controlled while for the ductile failure it will propagate in a stable manner (Løset et al., 2006). For low strain rate the ice can be considered as a ductile material that is subjected to yielding. For high strain rates the ice demonstrates brittle behaviour.

2.3.2 Mechanical behaviour of sea ice

Sea ice is a polycrystalline material. The common forms of natural polycrystalline ice are granular and columnar ice. The granular ice is a conglomerate of randomly oriented crystals. If the crystal orientations are truly random, then the mechanical properties of ice are isotropic. Sea ice is mostly composed of secondary ice with a columnar crystal structure when the crystals are elongated in the vertical direction with their *c*-axes randomly distributed in the horizontal plane. Sea ice is transversely isotropic (orthotropic) material and its mechanical properties are the same in all directions in the horizontal plane because the *c*-axes are randomly oriented in the horizontal plane (S2 ice). While with a preferred orientation of the *c*-axes in the horizontal plane (S3 ice), then sea ice is fully anisotropic. Thus, the mechanical behaviour of sea ice in the horizontal plane differs from that in the vertical direction.

Fig. 2.8 shows a typical creep diagram for sea ice. The time-depended deformation curve is usually divided into different stages: instantaneous deformation, primary creep deformation (transient), secondary creep deformation (steady state) and a tertiary stage resulting in failure. The total strain is often decomposed based on Sinha's model (Sinha, 1983). The model represents time-dependent deformation mechanisms containing both viscoelastic (primary creep) and viscoplastic (secondary creep) strain terms in addition to the elastic deformation.

$$\varepsilon^{tot} = \varepsilon^{e} + \varepsilon^{d} + \varepsilon^{v}, \tag{2.9}$$

where ε^{e} is the immediate elastic strain, ε^{d} is the viscoelastic (or delayed elastic) strain and ε^{v} is the viscoplastic (creep or permanent) strain.

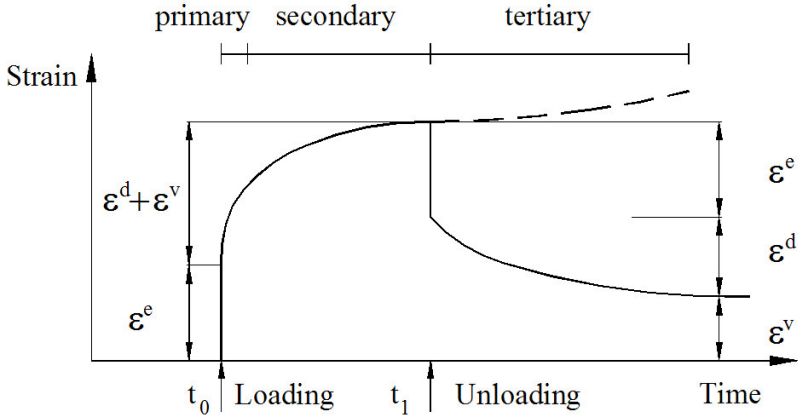

Fig. 2.8. Strain history diagram for creep test.
(A constant stress is applied at time t_0 and removed at time t_1).

The elastic strain is interpreted as elastic response of the crystal lattice due to applied stress and described by Hooke's law as:

$$\varepsilon^{e} = \frac{\sigma}{E}, \tag{2.10}$$

where σ is the applied stress, E is the modulus of elasticity (the material parameter).

Both viscoelastic (recoverable) and viscoplastic (permanent) strains are time-dependent parameters. The recoverable strain (ε^{d}) represents the effect of the grain boundary sliding on the total deformation of the material and the permanent

strain (ε^v) describes the effect of the movement of dislocations in crystals on the deformation body (Løset et al., 1998). According to Sinha (1983) the viscoelastic strain is expressed in terms of stress σ and time t, while the viscoplastic strain is given in rate form by Norton's law as:

$$\varepsilon^d = c_1 \frac{d_1}{d}\left(\frac{\sigma}{E}\right)^s \left(1 - exp\left(-\left(a_T t\right)^b\right)\right), \tag{2.11}$$

$$\dot{\varepsilon}^v = \dot{\varepsilon}_0 \left(\frac{\sigma}{\sigma_0}\right)^n, \tag{2.12}$$

where c_1, b are the constants, d is the average grain diameter, d_1 is the unit of grain diameter, s is the stress component for the delayed elastic strain, E is the modulus of elasticity, a_T is the inverse of relaxation time, $\dot{\varepsilon}_0$ is the visco-plastic strain rate for the unit stress σ_0. The stress exponent n is normally equal to 3.

The deformation, failure mechanisms and strength of ice are significantly affected by the strain rate. Typically, the strain rate is classified into the following ranges: ductile, transitional or brittle. Depending on the type (grain size) of ice and the state of the ice (stress, strain, strain rate and temperature), the ice behaviour transforms from almost purely ductile through a transition phase and into brittle behaviour. The ice fails in brittle manner if the strain rate is high enough or the ice temperature is low enough. The assumption that the nucleation controlled failure implies the brittle behaviour and propagation controlled failure defines the ductile behaviour is usually made. The formation of the first cracks manly depends on the vicoelastic strain. Based on the laboratory observations it was found that the critical value of ε^d (that is inversely proportional to grain size) can be used to define the loading conditions resulting in crack formation. The brittle-to-ductile transition behaviour is demonstrated by Sanderson (1988) for the S2 columnar ice and given in Fig. 2.9. Thus, depending on the loading conditions, the ice behaviour can be expressed by continuum mechanics approach describing elastic and ductile deformations or by fracture mechanics characterising brittle processes in crack formation.

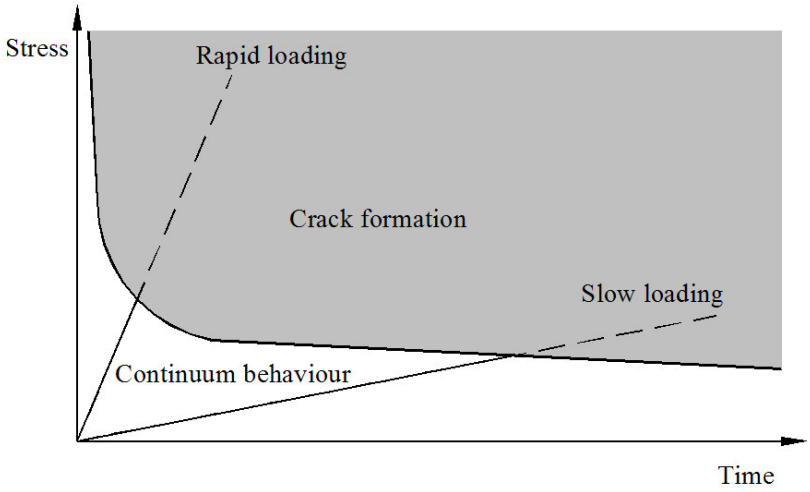

Fig. 2.9. Formation of first cracks during tests at constant strain-rate (after Sanderson, 1988). The shaded section represents crack formation.

2.4 References

Bonnemaire, B., Hoyland, K.V., Liferov, P., and Moslet, P. (2003). An ice ridge in the Barents Sea, Part I: Morphology and physical parameters. *In Proc. of the 17th Int. Conf. on Port and Ocean Engineering under Arctic Conditions (POAC),* NTNU, Trondheim, Norway, Vol. 2, pp. 559-568.

Cox, G.F. and Weeks, W.F. (1983). Equations for determining the gas and brine volumes in sea ice samples. *Journal of Glaciology*, Vol. 29, (102): 306-316.

Heinonen, J. and Määttänen, M. (2000). LOLEIF ridge loading experiments – analysis of rubble strength in the ridge keel punch test. *In Proc. of the 14th Int. Symp. on Ice (IAHR)*, Gdansk, Polland, pp. 63-71.

Høyland, K.V. (2002). Consolidation of first-year sea ice ridges. *Journal of Geophysical research*, 107 (C6): 15,1-15,15.

Høyland, K.V. (2007). Morphology and small-scale strength of ridges in the North-western Barents Sea. *Cold Regions Science and Technology*, (48): 169-187.

Leppäranta, M. and Hakala, R. (1995). The structure and strength of first-year ridges in the Baltic Sea. *Cold Regions Science and Technology*, (20): 295–311.

Leppäranta, M., Lensu, M., Koslof, P., and Veitch, B. (1995). The life story of a first-year sea ice ridge. *Cold Regions Science and Technology*, (23): 279-290.

Leppäranta, M. and Manninen, T. (1988). The brine and gas content of sea ice with attention to low salinities and high temperatures. Technical Report 1988 (2), Finnish Institute of marine research. 14 p.

Løset, S., Shkhinek, K.N., Gudmestad, O.T. and Høyland, K.V. (2006). Actions from Ice on Arctic Offshore and Coastal Structures. Trondheim, St. Petersburg, Stavanger and Longyearbyen, 271 p.

Løset, S., Shkhinek, K.N. and Høyland, K.V. (1998). Ice Physics and Mechanics. Trondheim, 101 p.

Kämäräinen, J. (1993). Studies in ice mechanics. Helsinki University of Technology. 182 p.

Pounder, E.R. (1965). The physics of ice. Oxford, Pergamon press, 151 p.

Prodanovic, A. (1979). Model tests of ice rubble strength. *In Proc. of the 5th Int. Conf. on Port and Ocean Engineering under Arctic conditions (POAC)*, Trondheim, Norway, Vol. 1, pp. 89-105.

Sanderson, T.J.O. (1988). Ice Mechanics. Risk to offshore structures. Graham and Trotman, 253 p.

Sayed, M. and Frederking, R.M.W. (1989). Measurements of ridge sails in the Beaufort Sea. *Canadian Journal of Civil Engineering*, Vol. 16, (1): 16-21.

Sinha, N.K. (1983). Creep model of ice for monotonically increasing stress. *Cold Regions Science and Technology*, (8): 25-33.

Timco, G.W. and Burden, R. (1997). An analysis of the shapes of sea ice ridges. *Cold Regions Science and Technology*, (25): 65-77.

Timco, G.W., Croasdale, K. and Wright, B. (2000). An overview of first-year sea ice ridges. PERD/CHC report 5-112, 159 p.

Tucker, W. and Govoni, J. (1981). Morphological investigations of first-year sea ice pressure ridge sails. *Cold Regions Science and Technology*, (5): 1-12.

Urroz, G.E. and Ettema, R. (1987). Simple shear box experiments with floating ice rubble. *Cold Regions Science and Technology*, (14): 185-199.

Veitch, B., Lensu, M., Riska, K., Koslof, P., Keiley, P., and Kujala, P. (1991). Field observations of ridges in the northern Baltic Sea. *In Proc. of the 11th Int. Conf. on Port and Ocean Engineering under Arctic Conditions (POAC),* St. Johns, Canada, pp. 381-438.

Zubakin, G.K., Gudoshnikov, Yu. P., Naumov, A.K., Stepanov, I.V, Kubyshkin, N.V. (2005). Peculiarities of the structure and properties of the Ice Ridges in the eastern Barents Sea based on the 2003 expedition data. *International Journal of Offshore and Polar Engineering*, Vol. 15, (1): 28-33.

3 FIELD MEASUREMENTS OF ICE STRENGTH SPATIAL HETEROGENEITY

3.1 Introduction

This chapter deals with field measurements of the uniaxial compression strength within the first-yea sea ice features. First-year sea ice ridges and surrounding level ice (drift ice) in the Barents Sea (2005) and Arctic Ocean (2006) were examined with respect to ice strength spatial distribution. Furthermore, the in-plane strength heterogeneity within the different ice fields in landfast level ice in Spitsbergen fjords during the field testing programs of 2004-2005 was analyzed and discussed. The major purpose behind these field studies are the following:

1. To improve the knowledge of field measurements of sea ice strength. Recently the surface layer of sea ice fields has been examined in-situ using an express method known as the drop ball technique. Most available studies on the sea ice strength are based on the uniaxial compression test data. But only a few of them deals with field testing. Usually, the ice samples were collected on the site, transported to the laboratory and then compressed. The borehole-jack test is an alternative way of testing ice strength in the field, but the boundary conditions are less clear than in a uniaxial compression experiment.
2. To study the spatial distribution of ice strength within different first-year sea ice features. It can be important for design ice load evaluations. The presence of weak/strong zones (both in vertical and horizontal directions) in level ice and first-year ice ridges is the main explanation for non-simultaneous failure, which may further be linked to the apparent size effect in nominal pressure. As a result by taking into account the ice strength variability, the estimated ice load can be reduced.
3. To establish the proper link between physical and mechanical properties of sea ice.

This chapter consists of three papers, each composing a section. Section 3.2 presents investigations for the first-year sea ice ridges. In addition the morphology data of the freeze bonds between the ice blocks for the ridge sails was described and analyzed. Sections 3.3 and 3.4 deal with the landfast level ice data. All sections are almost identical to the referred papers with some misprints corrected.

Publication references:

(3.2) Shafrova, S. and Høyland, K.V. (2007). Morphology and 2D spatial strength distribution in two Arctic first-year sea ice ridges. Cold Regions Science and Technology, doi:10.1016/j.coldregions. 2007.05.011.

(3.3) Shafrova, S. and Moslet, P.O. (2006). In-situ uniaxial compression tests of level ice. Part I: Ice strength variability versus length scale. In Proceedings of the 25th International Conference on Offshore Mechanics and Arctic Engineering (OMAE), Hamburg, Germany, OMAE-92450, 9p.

(3.4) Shafrova, S. and Moslet, P.O. (2006). In-situ uniaxial compression tests of level ice. Part II: Ice strength spatial distribution. In Proceedings of the 25th International Conference on Offshore Mechanics and Arctic Engineering (OMAE), Hamburg, Germany, OMAE-92451, 10p.

Journal of Cold Regions Science and Technology, doi:10.1016/j.coldregions.2007.05.011

3.2 Morphology and 2D spatial strength distribution in two Arctic first-year sea ice ridges

Svetlana Shafrova[1] and Knut V. Høyland

The University Centre in Svalbard (UNIS), Longyearbyen, Norway

Norwegian University of Science and Technology (NTNU), Trondheim, Norway

Abstract

Geometry and morphology of two first-year sea ice ridges, one in the North-western Barents Sea in 2005 and one in the Arctic Ocean in 2006, were examined. Altogether 130 freeze bonding contacts between the ice blocks in the ridge sail were examined; and the average freeze bond length and width were 0.28 m and 0.14 m, respectively; the average length/width ratio was 2.2 (2005) and 1.8 (2006). The average freeze bond length to average block length ratio was 0.33 (2005) and 0.35 (2006). Furthermore the uniaxial compression tests were conducted in the field on the first-year sea ice. The temperature, salinity and density were measured for each ice sample and the brine and air volume was calculated. Both vertical and horizontal ice samples were tested. The ratio between vertical and horizontal strength was 2.0 for the level ice and 1.1 both for the consolidated layer and for the unconsolidated part of the ice ridge. Weak zones were discovered in the ice ridges, and the ice strength varied by a factor of more than 3 along both vertical and horizontal directions. The strength variation for the vertical samples within different parts of an ice ridge was at the same level: 50-55% for the 2005 feature and around 40% for the 2006 ridge. The corresponding strength variation for the level ice (2006) was estimated as 42.2% for the vertical samples and 25.2% for the horizontal ones.

Key words: First-year ice ridges; The Barents Sea; The Arctic Ocean; Morphology; Uniaxial compression strength; Spatial distribution of properties.

1. Introduction

Sea ice ridges are formed by compression or shear in the ice cover. When a ridge forms, most of the ice blocks go below the waterline and form the keel, whereas a smaller amount of ice pieces form the sail above the waterline. The sail is composed

[1] Corresponding author.
E-mail address: svetlana.shafrova@unis.no

of dry ice blocks with snow- and/or air filled pores. The keel consists of a consolidated layer of refrozen ice that grows through the cold season, and unconsolidated or partly consolidated ice rubble beneath. During the initial phase of the consolidation the originally low ice temperature is spent in creating freeze bonds between the blocks. Thus, the ridge is a combination of ice blocks (that are bonded together and aligned in different directions) with slush, water and air between.

In the Arctic region, first-year sea ice ridges and rubble fields often give the design load level for the offshore structures (when icebergs aren't present, or if they are managed). Ridges may drift and hit fixed or moored surface structures such as platforms or ships, or they may scour the seabed endangering pipelines and wellheads. Both the temporal and spatial variation of properties of the ice rubble (unconsolidated part) and the consolidated layer are important input into the ridge-load models.

Different ridge actions have been described in the literature. Bjerkås (2006) found both crushing and bending when examining the Nordströmsgrund lighthouse (vertical waterline with diameter of 7.5 m) in the Gulf of Bothnia. On contrast Wright and Timco (2001) found no first-year ridge crushing against the wide (about 100 m, almost vertical waterline) Molikpaq platform. However, they did find that failure of the level ice behind the ridges often took place. Inclined structures on the other hand tend to provoke bending failure and subsequent rubble build up, and this was observed by Brown and Määttänen (2002) both at the Kemi I lighthouse (diameter 9.9 m) and the Confederation bridge piers (diameter 14.1 m). However, it is interesting to note that a similar rubble build-up (wedge) was also observed by Bjerkås (2006) in front of the vertical Nordströmsgrund lighthouse. Thus, three typical modes of interaction between a first-year ice field and a structure can occur: (1) failure of a consolidated ridge or rubble field against the structure; (2) failure of level ice on the structure; (3) failure of level ice surrounding a ridge or a ridge-field.

The ice rubble (the unconsolidated part) will deform and fail during an ice ridge-structure/sea bed interaction. Let us identify at least three different physical mechanisms that can take place during rubble deformation: (1) Failure of the freeze bonds between the ice blocks; (2) Rotation and rearrangement of the blocks; (3) Failure of the ice blocks. In other words, the strength and morphology of the freeze bonds, the size, shape, orientation and strength of the rubble blocks are all important for estimating the overall ice ridge strength. Several investigation have been done on the strength and the morphology of the freeze bonds and Dolgopolov et al. (1975), Ettema and Schaefer (1986), Kärnä and Nykänen (2004), Shafrova et al. (2004), Liferov (2005), Vershinin et al. (2005) and Shafrova (2007) all argue for their importance in relation to rubble strength and/or ice ridge action. There is more available information on the morphology (size, shape and orientation) of the

ice blocks constituting the ridge and a correlation between the morphology of the freeze bonds in between the blocks and the morphology of the blocks themselves will obviously be useful. The importance of the block shape and size has been investigated in particular by Hopkins and Hibler (1991) and Tuhkuri and Polojärvi (2005) in their discrete numerical simulations. Vershinin et al. (2005) also argue for the importance of the general morphology of the ice ridge.

Ice ridges fail non-simultaneously across the height and width of the structure. One possible explanation is the inhomogeneity and the presence of the weak zones throughout the ridges. Thus, the investigation of the spatial ice strength distribution through the ice ridge is needed.

The University Centre in Svalbard (UNIS) does annual ice ridge investigations in the Marginal Ice Zone (MIZ) in the vicinity of Svalbard, and the main objectives of the 2005 and 2006 expeditions included:

- study of the ice ridge morphology with focus on freeze bonds between the ice blocks;
- estimation of 2D spatial distribution of the ice strength through the ice ridge.

The results of the current investigations could be used for the verification and improvement of the existing numerical/analytical models for predicting ice ridge loads from ice ridge interaction with structure or/and seabed.

2. Site and Experimental set-up

Two first-year ice ridges were examined, one in the MIZ southwest of Svalbard in the Barents Sea (2005) and another north of Svalbard in the Arctic Ocean (2006). In 2005, the investigations were done on 9-13 of May, and the ridge was found between Hopen and Edgeøya (Fig. 1). In 2006, a suitable ice floe was located around 81º N, 9º E, and the field studies were carried out on 19-24 of May.

The geometry of the ice ridges was estimated from drilling cross-section in the ridges. The surface topography was mapped with a theodolite (Fig. 2). The size and inclination angle to the horizontal plane of the ice blocks and freeze bonds between them were measured in the ridge sail. The inclination angle was determined using compass and defined from 0 to 180º.

Fig. 1. The positions of the ice ridges, 6 refers to 2006 and 5 to 2005.

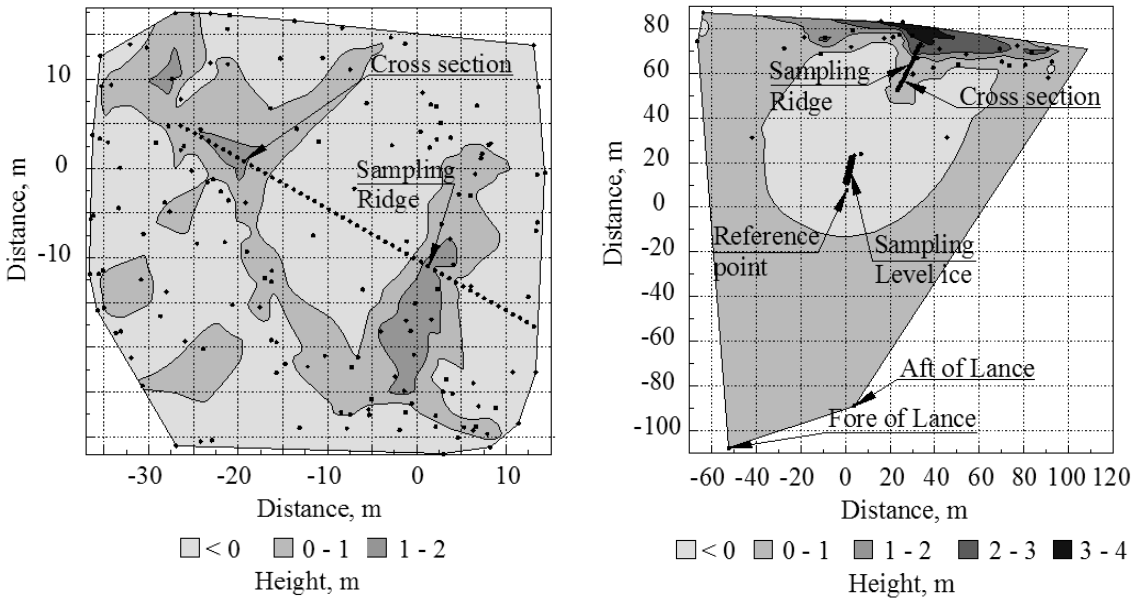

a) 2005 b) 2006

Fig. 2. The topography maps of the ice ridges, dots are the measured points.

Uniaxial compression tests were conducted in the field to measure ice strength. Ice samples 70 mm in diameter and 175 mm long were tested. The strength is defined as the maximum force divided by the initial sample cross-section, and throughout the paper is called σ. The piston speed corresponded to a nominal strain rate of $10^{-3}s^{-1}$. The compression rig (Kompis) and testing procedure is described by Shafrova and Moslet (2006a) and by Moslet (2007). The ice samples were weighed before the test and then compressed. The density was estimated from the measured weight assuming that the volumes of the samples were identical. Immediately after compression, the ice temperature was measured. Then the samples were melted and salinity was evaluated. The porosity was calculated as described by Cox and Weeks (1983) for the ice colder than -2ºC and by Leppäranta and Manninen (1988) for the warm ice.

Ice samples, both from the level ice and from the ice ridges, were tested. The samples from the ridge were characterized as consolidated layer or rubble-blocks in relation to the thickness of the consolidated layer as found by drilling, taking into account the local variations. In 2005, the ice cores were taken in straight line across the ridge (Fig. 2a). Vertical and horizontal ice samples relative to the ice ridge surface were examined. In 2006, vertical ice cores from a straight line across the ridge (Fig. 2b) and horizontal samples taken from a single hole were examined. In addition to that, the vertical and horizontal ice samples from the level ice were tested. Those were sampled every meter in a straight line towards to the ridge. When taking the horizontal samples, we first used a large core (200 mm) and then a small core (70 mm).

3. Results

3.1 Geometry and consolidation

A more detailed analysis of the 2005 ridge is given by Høyland (2007). The main results will be briefly repeated here in comparison with the 2006 feature. The topography maps of the ice floes for 2005 and 2006 expeditions are given in Fig. 2, and Table 1 gives the key data on geometry and consolidation. Respectively 50 and 29 holes were drilled in the cross-sectional mapping of the ridges in 2005 and 2006, and the corresponding cross-sections are given in Fig. 3. We used the mechanical drilling to estimate the average thickness of the level ice and the consolidated layer. The effective thickness of the consolidated layer $(h_{cl})_{eff}$ was defined as the ratio of the cross-sectional area of the consolidated layer to its bottom perimeter (see also Table 1).

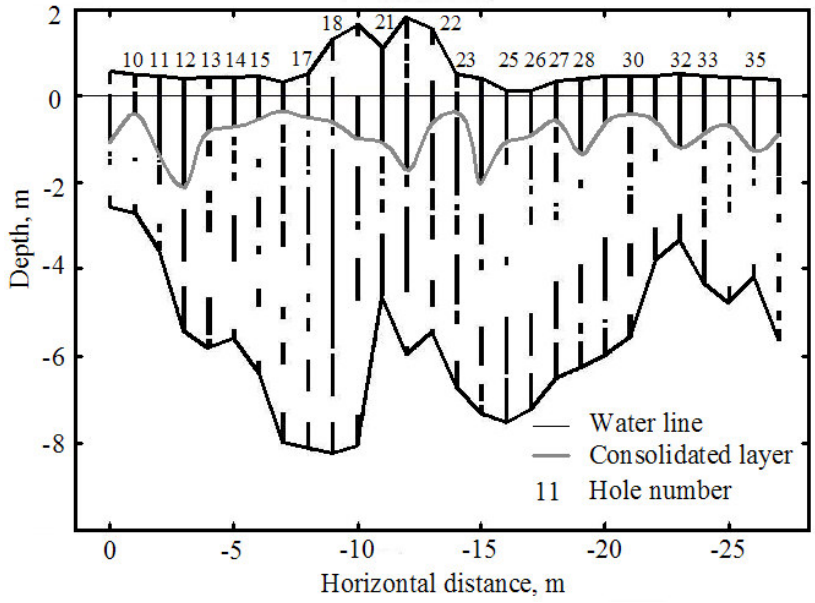

a) 2005
(has also been published by Høyland, 2007)

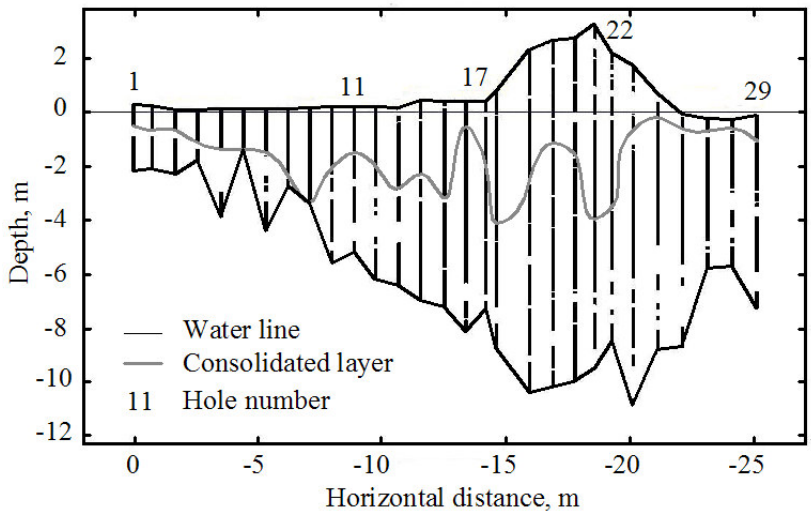

b) 2006

Fig. 3. The drilled cross-section, the black lines are ice (hard or soft) and the white in-between are the pores (voids or slush).

Table 1. The key geometrical parameters, the maximum sail height (H_s^{max}), the maximum keel depth (H_k^{max}), the level ice thickness (h_i), the thickness of the consolidated layer: the average ($(h_{cl})_{av}$), minimum ($h_{cl}^{\min}$), maximum ($h_{cl}^{\max}$), and effective ($(h_{cl})_{eff}$) values.

	H_s^{max} (m)	H_k^{max} (m)	h_i (m)	$(h_{cl})_{av}$ (m)	$h_{cl}^{\min}$ (m)	$h_{cl}^{\max}$ (m)	$(h_{cl})_{eff}$ (m)	Holes (-)
2005	2.1	8.2	0.48	1.05 ± 0.52	0.37	2.22	0.91	50
2006	3.3	10.8	0.80	1.76 ± 1.12	0.23	4.11	1.11	29

3.2 Ridge morphology

The ice blocks and the freeze bonds were examined in the sails of the ridges. We measured length, width and inclination angle of the freeze bonds. The inclination angle was defined as the angle between the horizontal plane and the long axis of the freeze bonds, as shown in Fig. 4a where a typical view of the freeze bonds is shown. Altogether 130 freeze bonding contacts were investigated in 2005-2006 and Table 2 gives the key results. In 2005, the ridge keel was examined using the underwater video camera. The ice rubble blocks from the ridge keel, both from underwater video and blocks that floated up on the side of the ridge are shown in Fig. 4b.

The size and the inclination angle were measured on respectively 210 and 50 randomly chosen blocks in 2005 and in 2006. The 2005 data are summarized and analyzed by Høyland (2007), and the key values for 2006 are given in Table 3. In 2006, the average block thickness was 0.35 m whereas the maximum value was 1.2 m. The 22 blocks (44% from the total amount of inspected blocks) had thickness between 0.25 m and 0.35 m and 42 blocks (84%) had thickness between 0.1 m and 0.45 m. Fig. 5 shows frequency histograms of the relative length for the ice blocks and for the freeze bonds (all 2005 and 2006 data).

The frequency histograms of the inclination angle for both the ice blocks and the freeze bonds are given in Fig. 6. The inclination angle for the freeze bonds was mostly located within sectors of 0-60° and 120-180°. The freeze bonds were less inclined than the ice blocks. For the statistical treatment of the results, the measured data was recalculated into the values below 90° and the adjusted data are also given in Tables 2-3.

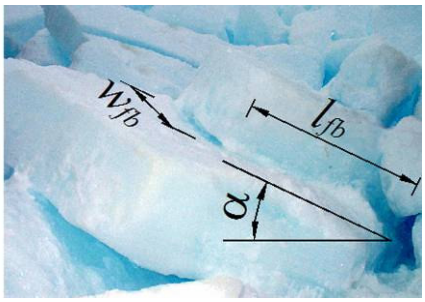

a) Sail

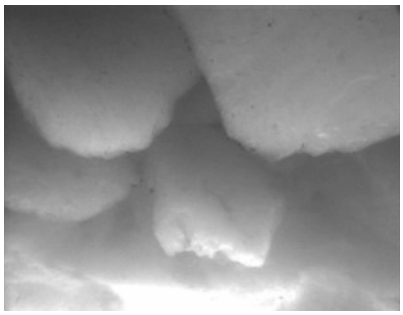

Underwater video

Blocks that popped up during anchoring to the floe

b) Keel

Fig. 4. The typical views of the ice blocks and freeze bonds (sail) in the ridge, (2005).

3.3 Uniaxial compression tests

Table 4 summarizes the relative strength ($\sigma_{rel} = \sigma / \sigma_{av}$), the coefficient of variation (k_v) and the number of tests with the different types of ice. Høyland (2007) presents the 2005 data, where the ice strength was analyzed in relation to the physical properties (basically porosity and temperature), sample orientations and failure mechanisms. In this paper we focus on the spatial distribution of the ice strength, and its relationship to the spatial distribution of the porosity. In addition we compare ridge- and level ice strength spatial variation.

Table 2. The key morphological values for the freeze bonds between the blocks, l_{fb}, w_{fb} and A_{fb} are the length, the width and the area of the freeze bonds and α_{fb} is the angle between the horizontal plane and the long axis of the freeze bonding area (ranging from [1]0 to 180º and [2]0 to 90º), l_b is the length of the ice blocks.

	w_{fb} (m)	l_{fb} (m)	A_{fb} (m^2)	α_{fb} (º)	l_{fb}/w_{fb} (-)	l_b (m)	l_{fb}^{av}/l_b^{av} (-)
2006							
av	0.13	0.24	0.041	79[1]/56[2]	1.8	0.96	0.35
st. dev	0.08	0.17	0.047	38/15	0.8	0.66	-
n	11	11	11	11	11	50	-
2005							
av	0.14	0.27	0.045	75/31	2.2	0.83	0.33
st. dev	0.08	0.16	0.050	61/22	1.5	0.42	-
n	119	119	119	119	119	210	-
Total							
av	0.14	0.27	0.045	75/33	2.2	0.86	0.32
st. dev	0.08	0.16	0.050	60/23	1.5	0.48	-
n	130	130	130	130	130	260	-

Table 3. The key morphological values, h_b is the block thickness, l_b and w_b are the block length and width and α_b is the angle between the horizontal plane and the long axis of the block ([1]0 to 180º and [2]0 to 90º).

	h_b (m)	w_b (m)	l_b (m)	α_b (º)	l_b/h_b (-)	w_b/h_b (-)	l_b/w_b (-)
2006							
av	0.35	0.68	0.96	69[1]/47[2]	3.1	2.1	1.6
st. dev	0.23	0.58	0.66	46/23	1.6	1.2	0.53
n	50	50	50	49	50	50	50

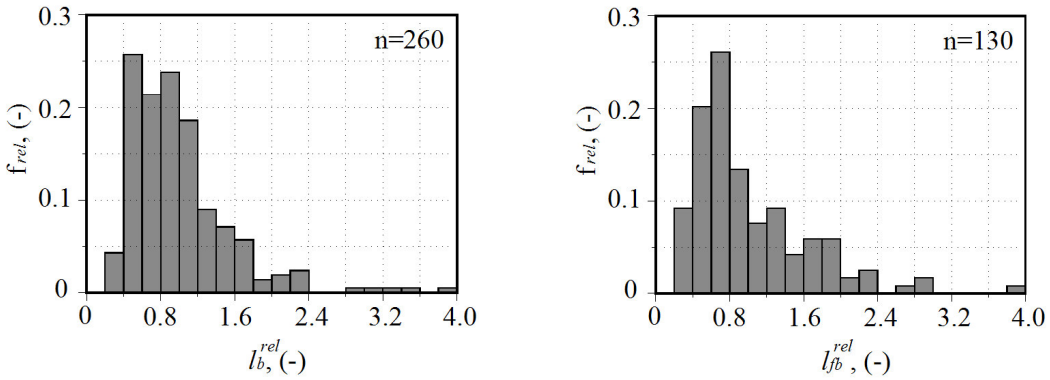

a) Ice blocks b) Freeze bonds

Fig. 5. Frequency histograms for relative length of the ice blocks and freeze bonds in the ridge sail, (2005-2006).

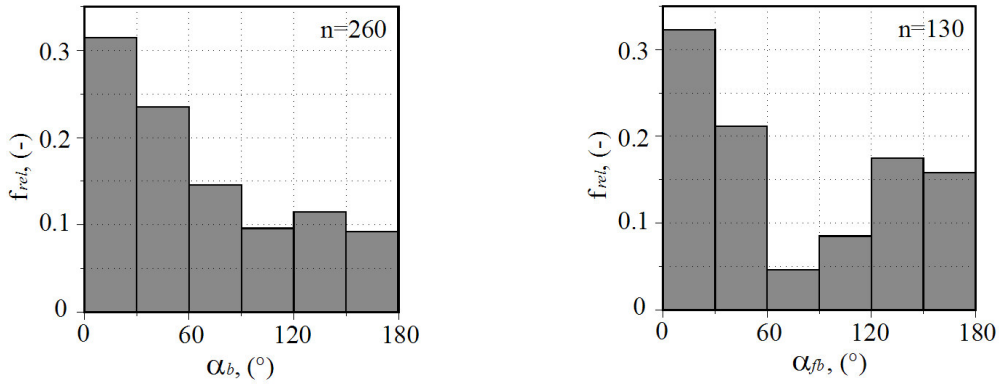

a) Ice blocks b) Freeze bonds

Fig. 6. Frequency histograms for the angles between the horizontal plane and the long axis of the ice blocks and freeze bonds, (2005-2006).

Table 4. Overview of the in-situ tested samples with relative strength values ($\sigma_{rel}=\sigma/\sigma_{av}$) and coefficients of variation (k_v) for the different types of ice.

Year	Ice type	Direction	σ_{rel} (-)	k_v (%)	n (-)
2005	Sail	Vert	0.17 – 2.3	52.7	30
		Hor	0.19 – 2.2	44.1	21
	Cons. layer	Vert	0.10 – 2.7	54.7	35
		Hor	0.26 – 2.5	50.1	28
	Rubble-blocks	Vert	0.08 – 2.2	49.9	68
		Hor	0.64 – 1.4	23.8	14
2006	Level ice	Vert	0.48 – 2.3	42.2	41
		Hor	0.40 – 1.8	25.2	41
	Cons. layer	Vert	0.28 – 1.8	37.9	42
		Hor	0.56 – 1.4	29.7	12
	Rubble-blocks	Vert	0.28 – 1.7	40.1	38
		Hor	0.58 – 1.4	36.4	6

3.3.1 Spatial strength distribution

3.3.1.1 Level ice

In 2006 the ice samples were taken along a straight line towards to the ridge (Fig. 2b). The distance between the sampling points was 1 m, and the total length of the investigated profiles was 10 m for the vertical ice sampling and 9 m for the horizontal one. The maps of the vertical and horizontal ice strength distribution in the level ice are given in Fig. 7. The ice strength varied considerably within short distances, and the strongest ice was in the bottom layers. The vertical and horizontal spatial distributions of porosity for 2006 level ice are given in Fig. 8, whereas Fig. 9 shows typical temperature, salinity and density profiles for the level ice (data from the compressed ice samples).

Furthermore the strength data was recalculated in terms of relative values (σ_{rel}) and the corresponding frequency histograms are given in Fig. 10. The strength histogram for vertical samples is more flat and stretched along x-axis compared to the horizontal one, so it shows a larger strength variation.

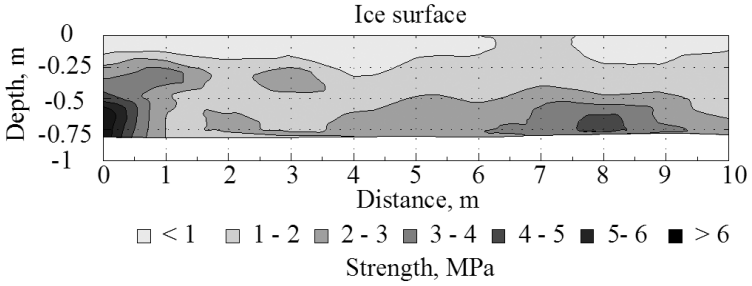

a) Vertical ice samples

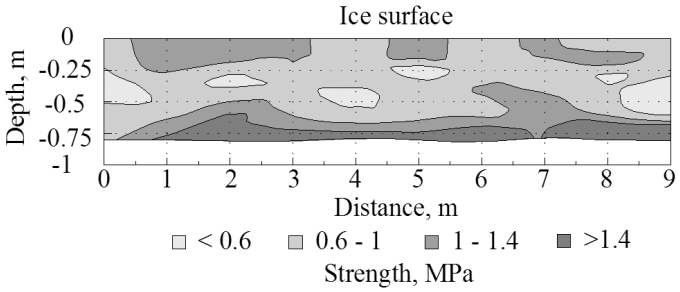

b) Horizontal ice samples

Fig. 7. The ice strength distribution for the level ice, (2006).

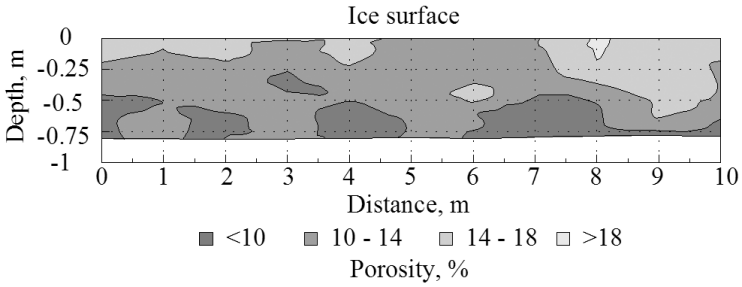

a) Vertical ice samples

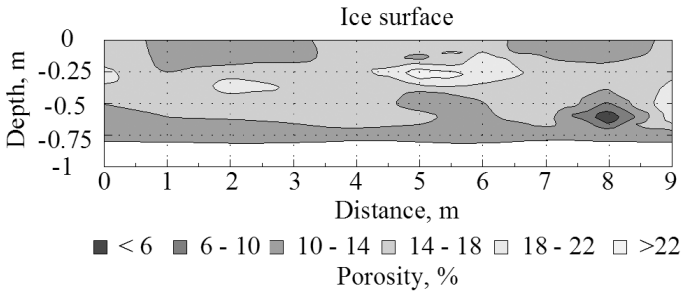

b) Horizontal ice samples

Fig. 8. The porosity distribution for the level ice, (2006).

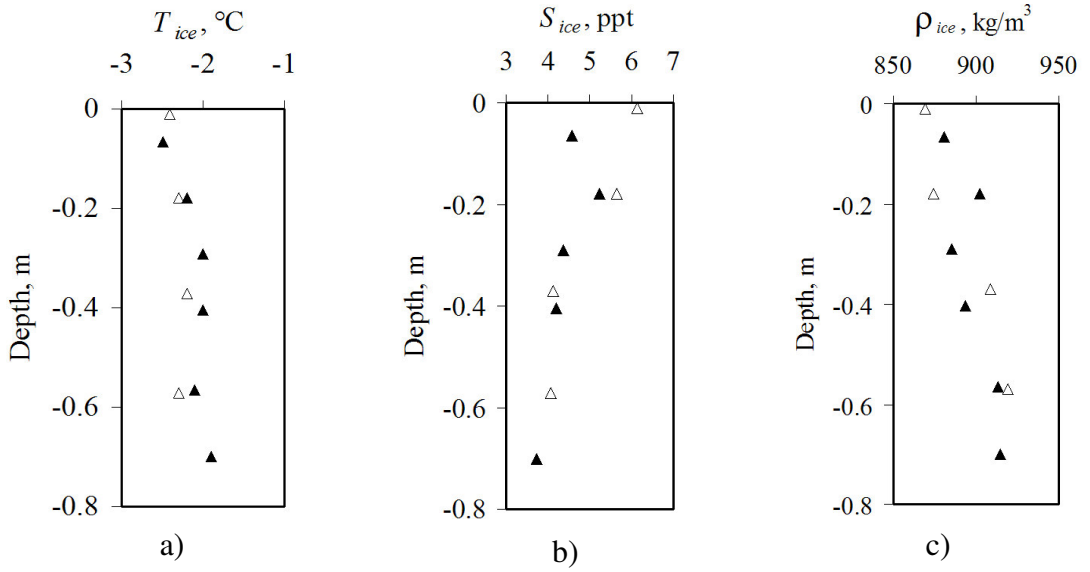

Fig. 9. Typical temperature, salinity and density profiles for level ice, (2006). (data from compressed vertical (white triangles) and horizontal (black triangles) ice samples).

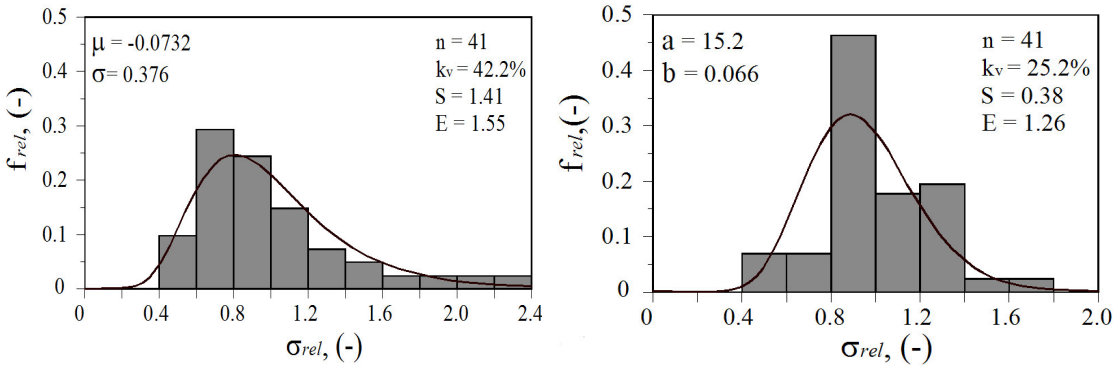

a) Vertical samples
Lognormal distribution

b) Horizontal samples
Gamma distribution

Fig. 10. Frequency histograms for relative ice strength for level ice, (2006).

n is the number of compressed ice samples, k_v is the coefficient of variation, S is the skewness, E is the excess; μ, σ and a, b are the parameters of the corresponding lognormal and gamma distributions.

3.3.1.2 Ice ridge

In 2005, vertical ice cores were sampled along a straight line across the ridge mostly every meter over a distance of 17 m. The horizontal samples were taken from two parts of the ice ridge: in front of the sail and behind it. Horizontal samples from 9 sampling points were tested. The maps of the spatial strength distribution in the 2005 ridge (through the cross-section given in Fig. 3a) are shown in Fig. 11.

In 2006, vertical ice samples were taken every two meters in along a straight line across the ridge (Fig. 3b). The length of the profile was 8 m. Horizontal samples from a single hole were tested. The results are shown as a map of the strength distribution along the line (Fig. 12a) and as a profile for both vertical and horizontal samples taken from hole 11 (Fig. 12b). The frequency histograms for the relative ice strength in different parts of the ridges are given in Fig. 13.

The ice strength variation in the vertical direction is shown in Fig. 14. The strength decreased through the consolidated layer but it is difficult to see any trend for the ice rubble-blocks. The rubble-blocks were significantly weaker than both the level ice and the consolidated layer even for comparable physical properties (temperature and salinity). Generally, their strength was below 0.5 MPa. But local spots with higher strength were also found. The absolute minimum and maximum values of the ice rubble-block strength were 0.03 MPa and 1.67 MPa respectively. The rubble-blocks strength variability for the vertical samples was less for 2005 and higher for 2006 than the corresponding strength variability inside the consolidated layer. For the horizontal samples the strength variability is the lowest ones, but only a few samples were tested.

The porosity of the ice samples from the ice ridge (not the same as the macro porosity of the ridge) versus the depth is given in Fig. 15. The 2005 data show increasing porosity with the depth through the sail and the consolidated layer. No trend can be found for 2006 data.

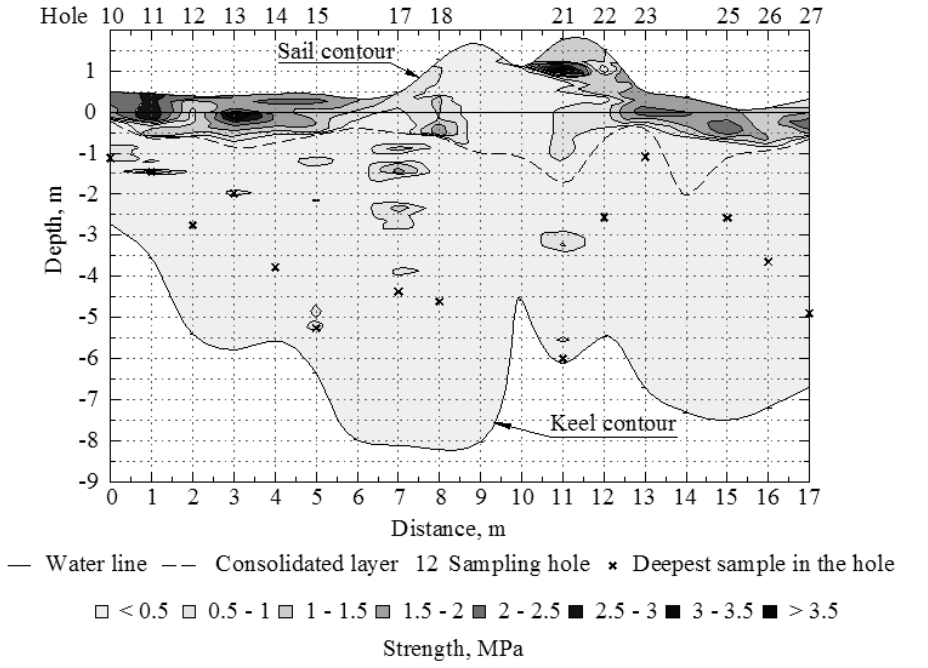

a) Vertical ice samples

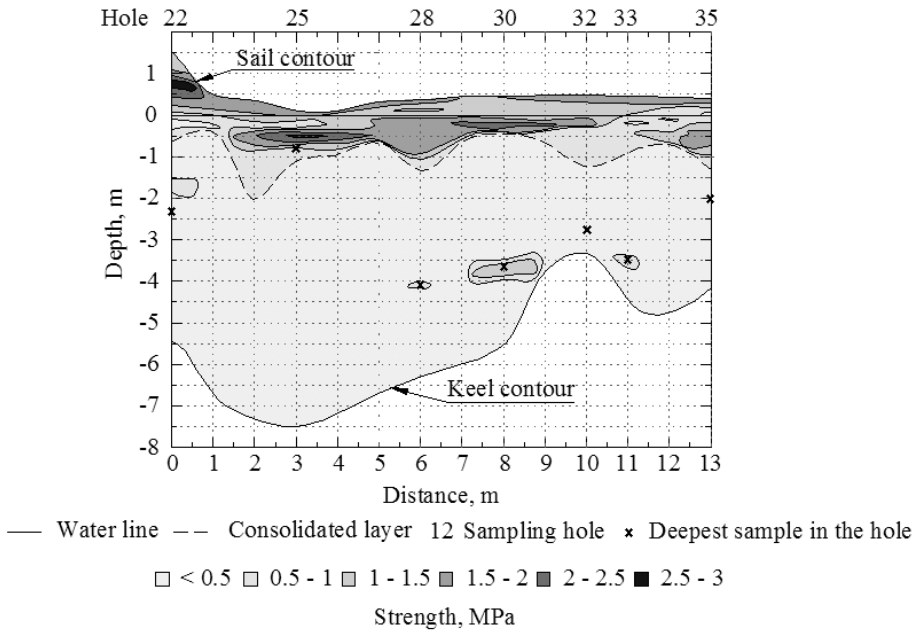

b) Horizontal ice samples

Fig. 11. The ice strength distribution for the ice ridge, Barents Sea, (2005).

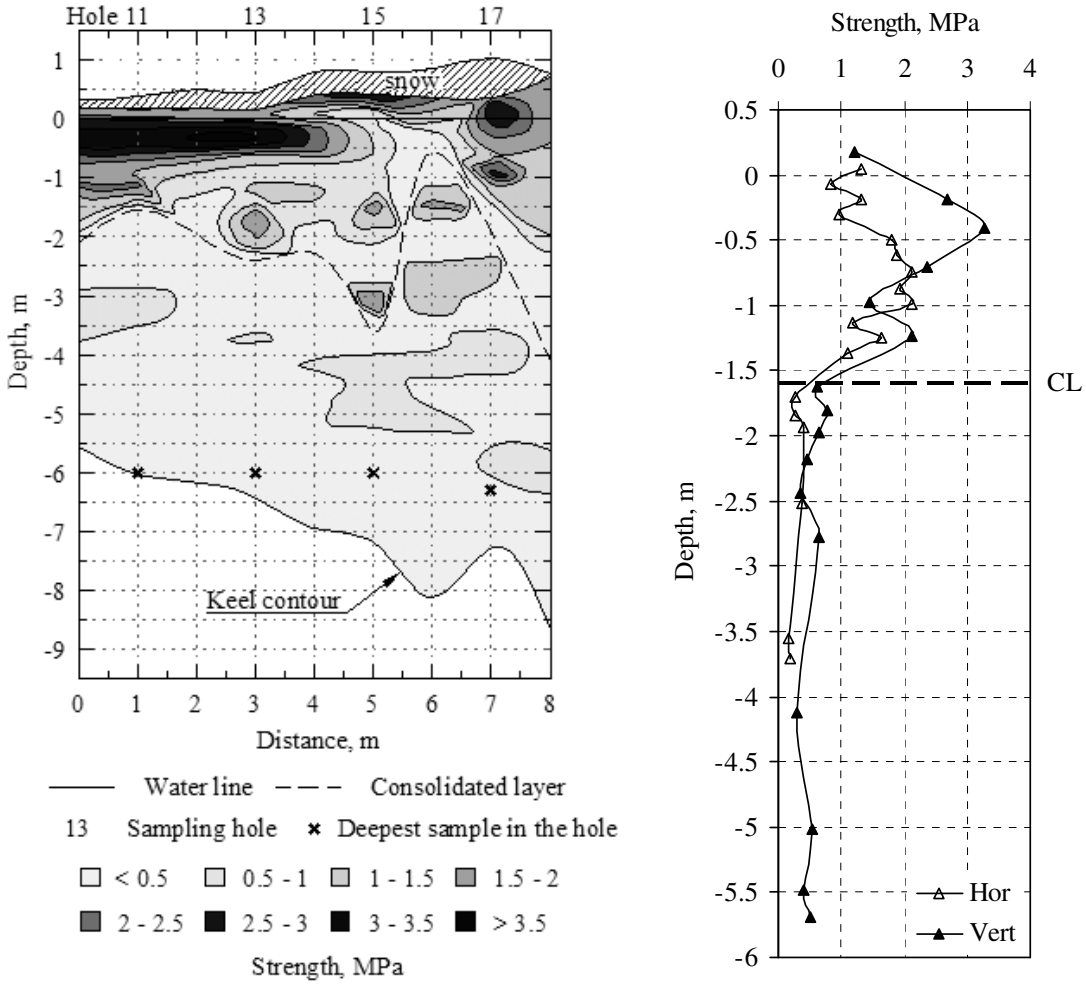

a) Vertical samples

b) Hole 11

Fig. 12. The ice strength distribution for the ice ridge, Arctic Ocean, (2006).

3.3.2 Strength versus physical properties

The maps of spatial strength and porosity distributions demonstrate generally a similar pattern with strong, low-porous ice close to the bottom of the ice sheet (Figs. 7 and 8). Table 5 gives a summary of the main physical and mechanical properties (temperature T_{av}, salinity S_{av}, total porosity $(\eta_{tot})_{av}$ and ice strength σ_{av}) of the different types of ice for vertical and horizontal samples.

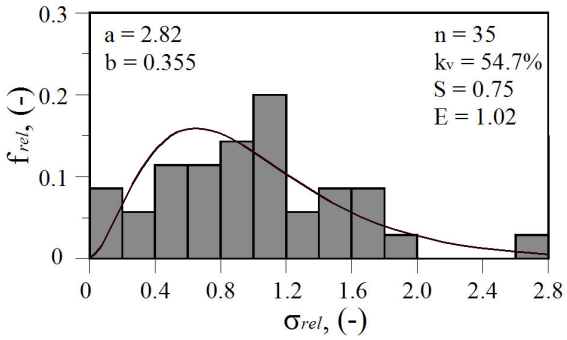

a) Consolidated layer, Gamma distribution

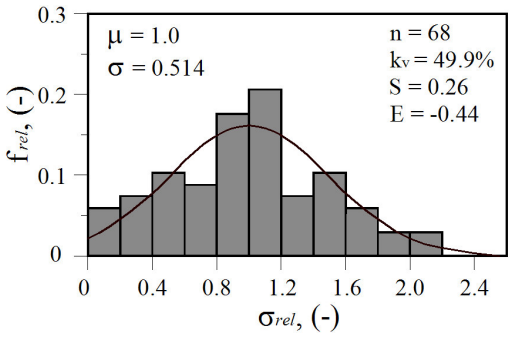

b) Ice rubble-blocks, Normal distribution

2005

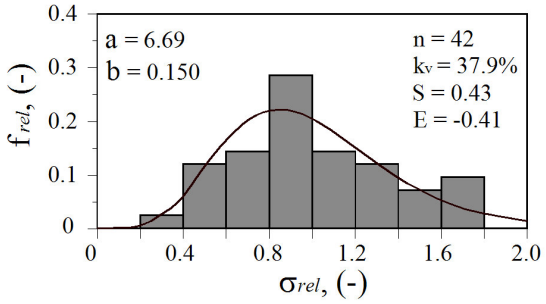

c) Consolidated layer, Gamma distribution

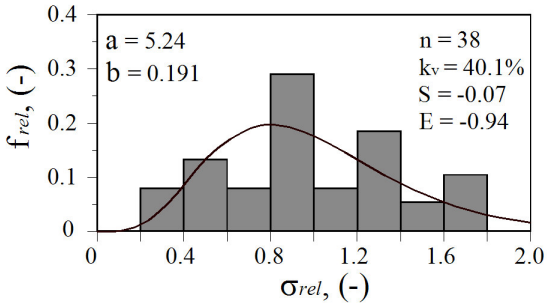

d) Ice rubble-blocks, Gamma distribution

2006

Fig. 13. Frequency histogram for relative ice strength in the ice ridge, (vertical samples only).
n is the number of compressed ice samples, k_v is the coefficient of variation, S is the skewness, E is the excess; a, b and μ, σ are the parameters of the corresponding gamma and noramal istributions.

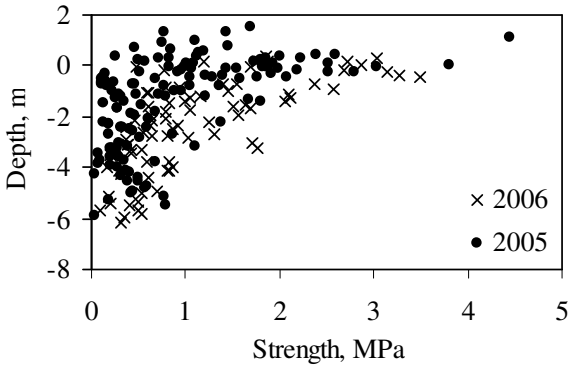

Fig. 14. The depth versus ice strength, ridge data.
(the 2005 data has also been published by Høyland, 2007).

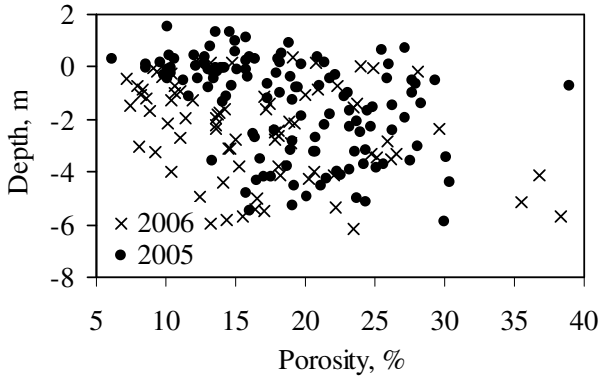

Fig. 15. The depth versus porosity, ridge data.

Table 5. Summary of the ice properties for the different types of ice, the ice strength (σ_{av} ± the standard deviation), the ice temperature (T_{av}), the salinity of ice (S_{av}) and the total porosity of ice ($\langle \eta_{tot} \rangle_{av}$).

Ice type	σ_{av} (MPa)	T_{av} (ºC)	S_{av} (ppt)	$\langle \eta_{tot} \rangle_{av}$ (%)
Vertical samples, 2005				
Sail	1.53 ± 0.95	-2.20 ± 0.59	3.98 ± 1.46	15.7 ± 5.2
Cons. layer	1.22 ± 0.80	-1.89 ± 0.33	4.56 ± 0.93	15.9 ± 5.5
Rubble-blocks	0.48 ± 0.38	-1.51 ± 0.23	4.88 ± 0.99	22.0 ± 4.9
Horizontal samples, 2005				
Sail	1.46 ± 0.66	-1.78 ± 0.29	3.25 ± 1.23	16.5 ± 4.0
Cons. layer	1.22 ± 0.60	-1.78 ± 0.27	4.16 ± 0.63	18.1 ± 4.9
Rubble-blocks	0.55 ± 0.26	-1.44 ± 0.20	3.90 ± 0.78	20.5 ± 3.3
Vertical samples, 2006				
Level ice	1.86 ± 1.24	-2.29 ± 0.20	4.88 ± 0.80	12.3 ± 2.5
Cons. layer	1.63 ± 0.82	-2.28 ± 0.35	5.25 ± 2.79	14.9 ± 6.7
Rubble-blocks	0.54 ± 0.26	-1.77 ± 0.26	5.28 ± 2.19	20.2 ± 7.1
Horizontal samples, 2006				
Level ice	0.94 ± 0.35	-1.92 ± 0.32	4.08 ± 0.83	14.6 ± 3.5
Cons. layer	1.52 ± 0.45	-1.88 ± 0.31	3.05 ± 0.73	12.7 ± 4.9
Rubble-blocks	0.27 ± 0.10	-1.66 ± 0.16	3.09 ± 0.71	19.0 ± 4.4

One can see that the horizontal samples were warmer than the corresponding vertical samples. In addition to that, the salinity of the horizontal samples was less than the salinity of the vertical samples for all types of ice.

Table 6 gives more details on the strength as a function of porosity for the 2006 samples. Both the strength and its variation decreased with increasing porosity. The table also shows that the strength of vertical level ice samples was higher than the corresponding strength of the consolidated layer only for the porosities less than 10%. For the two other comparable groups vertical samples from the consolidated layer were actually stronger.

Table 6. The average and the standard deviation of the strength versus groups of porosity (2006).[1]

Porosity (%)	Level ice		Ice ridge			
			Consolidated layer		Rubble-blocks	
	σ_{av} (MPa)	n (-)	σ_{av} (MPa)	n (-)	σ_{av} (MPa)	n (-)
Vertical samples						
5-10	3.38 ± 1.55	9	1.78 ± 0.93	12	-	-
10-15	1.54 ± 0.72	26	1.78 ± 0.84	15	0.65 ± 0.27	11
15-20	0.96 ± 0.37	6	1.40 ± 0.64	7	0.50 ± 0.18	13
20-25	-	-	1.42 ± 0.79	7	0.42 ± 0.23	6
25-30	-	-	0.78	1	0.65 ± 0.31	6
30-	-	-	-	-	0.14 ± 0.06	2
Horizontal samples						
5-10	-	-	1.38 ± 0.59	2	-	-
10-15	1.11 ± 0.35	23	1.57 ± 0.47	9	0.18	1
15-20	0.74 ± 0.20	14	1.33	1	0.30 ± 0.08	3
20-25	0.53 ± 0.23	3	-	-	0.27 ± 0.13	2

[1]The 2005 data has been published by Høyland (2007).

Figs. 16 and 17 show both vertical and horizontal ice strength as a function of the total porosity separately for the level ice and ice ridge. The vertical to horizontal strength ratio is shown in Table 7 and 8. The main trend is that the vertical level ice samples were the strongest followed by the consolidated layer samples (vertical and

horizontal respectively) with the horizontal level ice samples being the weakest ($\sigma_i^v > \sigma_{cl}^v > \sigma_{cl}^h > \sigma_i^h$). Ice from the rubble blocks was weaker than any other ice samples. In other words, we found a trend of higher vertical than horizontal strength (in particular for the sail and the level ice). In addition to that, a trend of decreasing strength ratio with the ridge depth may exist. By contrast, the 2006 level ice strength data (Table 8) shows that both ice strength and strength ratio increase with depth.

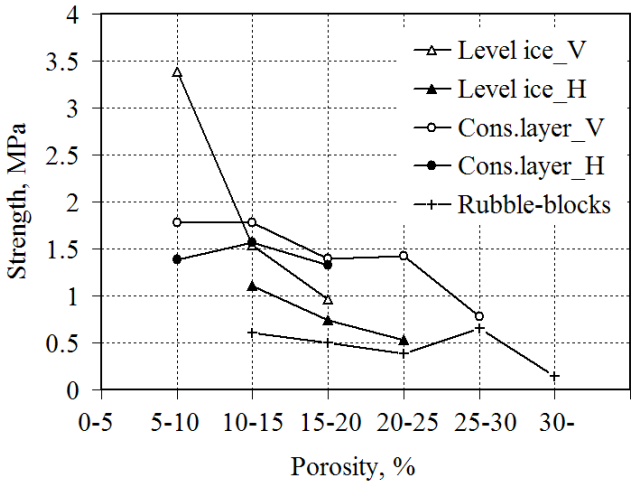

Fig. 16. The ice strength versus groups of porosity, (2006).

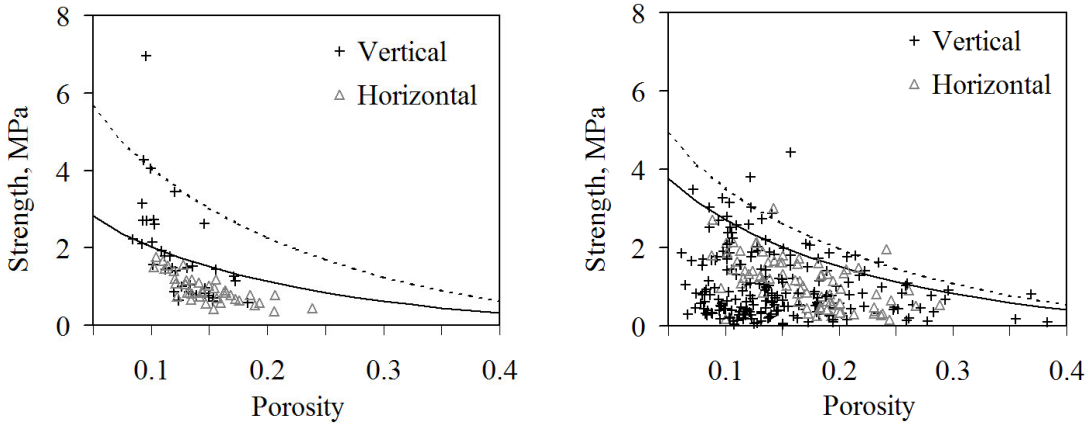

a) Level ice (2006) b) Ridge (2005-2006)

Fig. 17. The ice strength versus porosity.
The lines are fit to maximum values for vertical (point line) and horizontal (solid line) strength.

Table 7. The ratio between the vertical and horizontal strength for the groups of porosity (2005-2006).

Poro-sity (%)	Level ice			Ice ridge								
				Sail			Cons. layer			Rubble-blocks		
	σ^v/σ^h	n_v	n_h	σ^v/σ^h	n_v	n_h	σ^v/σ^h	n_v	n_h	σ^v/σ^h	n_v	n_h
10-15	$\frac{\underline{1.52}^a}{1.79}$	$\frac{\underline{26}}{18}$	$\frac{\underline{23}}{18}$	1.28	10	7	1.07	32	18	-	-	-
15-20	$\frac{\underline{1.38}}{1.86}$	$\frac{\underline{6}}{3}$	$\frac{\underline{14}}{12}$	1.35	11	10	1.20	16	12	1.23	30	9
20-25	-	-	-	-	-	-	-	-	-	0.96	32	9
25-30	-	-	-	-	-	-	0.30	4	4	-	-	-

[a] all level ice
columnar ice only

Table 8. The average strength (σ^v, σ^h), the ratio between the vertical and horizontal strength (σ^v/σ^h) and coefficient of variation (k_v) for the groups of samples in relation to the sampling depth (Level ice, 2006).

Depth (m)	Vertical samples			Horizontal samples			Ratio	
	σ^v (MPa)	k_v (%)	n (-)	σ^h (MPa)	k_v (%)	n (-)	σ^v/σ^h (-)	k_v (%)
0-0.2	0.83 ± 0.25	29.8	11	0.92 ± 0.18	19.3	7	0.93 ± 0.32	34.3
0.2-0.4	1.71 ± 0.78	45.7	10	0.78 ± 0.24	31.3	11	2.45 ± 1.35	55.8
0.4-0.6	2.06 ± 0.91	44.2	11	0.72 ± 0.19	26.7	8	3.05 ± 1.58	51.8
0.6-0.8	3.03 ± 1.66	54.8	9	1.17 ± 0.42	36.2	15	3.10 ± 2.49	80.4

Table 9 shows the average values of the air and brine volumes versus corresponding ice strength for groups of porosity. As can be seen the brine volume was the major contributor to the total porosity for porosities less than 20% and 15% for the vertical and horizontal samples respectively. For the higher porosities the air volume became essential and comparable with the brine volume.

Table 9. The air (η_{air}) and brine volume (η_{brine}) contents for the groups of porosity (2005-2006).

Porosity (%)	Level ice			Ice ridge					
				Consolidated layer			Rubble-blocks		
	η_{air} (%)	η_{brine} (%)	n (-)	η_{air} (%)	η_{brine} (%)	n (-)	η_{air} (%)	η_{brine} (%)	n (-)
Vertical samples									
5-10	1.20	8.09	9	1.19	7.42	14	-	-	-
10-15	1.83	10.5	26	3.53	8.65	22	3.44	9.57	15
15-20	5.04	11.5	6	4.18	13.7	16	4.25	13.3	30
20-25	-	-	-	5.41	17.1	9	6.92	15.8	32
25-30	-	-	-	12.6	15.3	5	7.54	19.4	15
30-	-	-	-	-	-	-	14.7	19.2	6
Horizontal samples									
5-10	-	-	-	0.90	8.30	2	-	-	-
10-15	3.44	9.39	23	2.67	9.54	18	-	-	-
15-20	6.01	10.8	14	6.86	10.8	12	7.67	10.3	9
20-25	10.4	11.3	3	9.74	11.5	3	10.3	12.3	9
25-30	-	-	-	17.7	9.27	4	-	-	-

4. Analysis

4.1 Geometry and consolidation

UNIS has so far investigated 5 ridges in the Barents Sea in the years 2002-2005 (Høyland, 2007) and one in the Arctic Ocean (2006). The average keel depth to sail height ratio (H_k^{max}/H_s^{max}) for those ridges was 3.7 and varied from 1.5 to 5.1 with the coefficient of variation of 31%. The ratio was lower than the average value of 4.4 found by Timco and Burden (1997) based on data from 97 first-year ice ridges. They also reported that there is a large scatter in the keel-to-sail ratio. The ratio varied from 1.25 up to 10 and the corresponding coefficient of variation was 41%. However, 65% of examined ridges (63 features) had a ratio from 2.8 to 5.2. Our data fits well to this range.

The thickness of the consolidated layer in 2006 (1.76 m) estimated by the drilling corresponds well to results of 1.7-1.9 m found by Høyland (2002) for the landfast ridges in West Spitsbergen fjords. In 2005, the consolidated layer was only 1.05 m thick. However, the ratio between the surrounding level ice and consolidated layer thickness was 2.2 in both years. This is a bit higher compared to the other published results (see Høyland (2002) for a review). Høyland (2002) reported that for the landfast Spitsbergen ridges, the h_{cl}/h_i ratio increased during the season and approached its maximum by the end of the season. Our measurements were carried out in May, thus a higher ratio is expected.

Table 1 shows a considerable variation of the consolidated layer thickness. Høyland (2007) found that maximum-to-average thickness ratio for h_{cl} was around 2, and the minimum-to-average thickness ratio was 0.38. The variation becomes even lager when 2006 data are included, and the ratios changes to 2.1 and 0.36 respectively. These data shows larger variation than Timco and Burden (1997) reported. As discussed by Høyland (2007), a larger variation may be expected on ridges in drifting ice. While some of the ridges described by Timco and Burden (1997) were situated in the landfast ice. Thus, it is reasonable to find higher variation in our data.

The consolidated layer is a major contributor to the total ice ridge load on a structure. Even though most estimation use level ice-like models and apply only the average thickness and strength, we think that both thickness – and strength variation are important (the ice strength variation will be discussed in Section 4.3). The thickness variation can be characterized in several different ways: as the standard deviation, coefficient of variation, or similar statistical measures. Perhaps the simplest way is to use the effective thickness ($\left(h_{cl}\right)_{eff}$), one then sticks to one parameter, which is sensitive to thickness variations and can be used in the simplest formulas.

4.2 Ridge morphology

As showed in the introduction, several authors consider information about the morphology of the freeze bonds to be important for the mechanical behaviour of ice rubble. Our results (Tables 2 and 3) show that the length to widths ratio (l_{fb}/w_{fb}) for the freeze bonds was slightly higher than the corresponding ratio (l_b/w_b) for the ice blocks but is in the same range. The frequency histograms of the relative length for both the ice blocks and freeze bonds show large scatter in the data (Fig. 5), and they look similar. The relative length varied from 0.2 to 4.0 in both cases. In addition, the higher frequency corresponds to the same ranges (0.6-1.4). Therefore, we suggest using a correlation between the corresponding lengths and introduce the average freeze bond length to the average block length ratio (l_{fb}^{av}/l_b^{av}). This ratio was

0.33 (2005) and 0.35 (2006) for the two ridges. Introduction of such a parameter facilitates the building of discrete and pseudo-discrete models of ice rubble behaviour. In a recent paper by Shafrova (2007) the shear strength of ice rubble is investigated using a pseudo-discrete continuum model where the freeze bonds are included.

The length of the freeze bonds (contact area) is one of main input parameters that affect the strength properties (mainly the cohesion). Shafrova et al. (2004) and Liferov (2005) analyzed the direct shear test simulations, and suggest that shear strength of rubble is linearly proportional to the contact area. They observed that increasing of size of the contact area from 7.6 m^2/m to 14.7 m^2/m leads to increasing of rubble strength from 5.9 kPa/m to 10.8 kPa/m.

The main contribution to ice ridge load comes from the keel (in particular when it comes to scouring). We have conducted detailed investigations of the morphology in the ridge sails only. This is, of course because the sail is easier to examine, and because there is reason to believe that the keel morphology is quite similar. The underwater videos (Fig. 4b) show that the ridge keel may consist of rubble blocks connected to each other by freeze bonds, like in the sail. The keel blocks are smoother and more eroded than the blocks in the sail, but visually they look similar.

The blocks size and the inclination angles given in Table 3 compare well with the other ridge data from the Barents Sea 2002-2005 presented by Høyland (2007), and with other available literature data reviewed in the same paper.

4.3 Uniaxial compression tests

4.3.1 Spatial strength distribution

4.3.1.1 Level ice

Several investigations (1991-2005) have been conducted in order to evaluate the in-plane strength heterogeneity for the both landfast and drift level ice. The results of the published field studies (together with the current data) are summarized in Table 10. The Table shows that the typical in plane ice strength heterogeneity in terms of coefficient of variation is 20-40% that corresponds to strength variation by a factor of 2 to 5.

Our results (Fig. 7) can be compared with the field studies for the Sakhalin offshore area by Polomoshnov et al. (1992) and Astafiev et al. (2001) where vertical ice samples were taken along a straight line and tested in uniaxial compression in the laboratory. The distance between sampling points was 20 m, and the total length of the profiles was 100 m. The investigations were carried out within several seasons from 1982 to 1995, and a typical map of ice strength distribution for the drift level ice in the Sakhalin area is given in Fig. 18. As can be seen, the strength of the drift ice

Table 10. Key information on ice strength in-plane heterogeneity.

Author(s)	Type of ice, Location	k_v (%)	Strength variation	D[1]	n[2]	Comments
Surkov and Truskov (1993)	Landfast ice, Chaivo Bay	45	< 3 times	V	125	Line 100 m, step 10 m, 2-4 differ. depth
Takeuchi et al. (1995)	Landfast ice, Lake Saroma	26	> 3.5 times 0.6-2.2 MPa	H	256	Line 38 m, step 0.15 m Single depth
Truskov et al. (1996)	Drift ice, Sakhalin area	-	< 3 times 1.3-3.7 MPa	V	125	Cross 100x100 m, step 20 m, 5 differ. depths
Farafonov (2006)	Landfast ice, Amur Bay	8-45	1.5-8 times 0.73-9 MPa	3)	536	8 Areas 100x100 m^2, Step 0.39 - 25 m, Surface layer
		-	5-7 times 0.4-4.4 MPa	V	28	Cross 160x160 m, step 20 m, 2 differ. depths
Shafrova and Moslet (2006b)	Landfast ice, Spitsbergen fjords	41	> 2 times 3.6-8.1 MPa	V	25	Area 3.1 x 3.1 m^2, step 0.78 m, depth 0.05 m
		27	> 5 times 2.3-12 MPa	V	36	Area 10x10 m^2, step 2 m, depth 0.3 m
		20-36	3-4 times 3.2-13 MPa	V	98	2 Areas 150x150 m^2, step 25 m, depth 0.3 m
Current paper	Drift ice, Arctic Ocean	30-55	2.5-4 times 0.58-7 MPa	V	41	Lines 10 m, step 1 m 3-4 differ. depths.
		20-38	1.7-5 times 0.35-1.8MPa	H	41	

[1] The direction of ice samples is either vertical (V) or horizontal (H).
[2] Number of compressed ice samples.
[3] Express method, drop ball test.

varied by a factor of 1.5-3 along both horizontal and vertical directions, and this agrees well with our results. Furthermore, Astafiev et al. (2001) and Polomoshnov et al. (1992) reported that the zones of maximum ice strength occupy 10-20% of the examined area. If we define maximum strength as 2 times average strength value - $\sigma_{rel} > 2$, we find that the areas with the maximum strength were 14% ($\sigma_{rel} > 2$) and 12% ($\sigma_{rel} > 1.5$) for the vertical and horizontal ice strength maps respectively (Fig. 7). The size of our study area is one tenth of the area in the Sakhalin investigations. Thus, the hypothesis of decreasing ice strength variability with the reduction of length scale is considered to be questionable. Further investigations should be done preferably with confined tests (e.g. borehole jack).

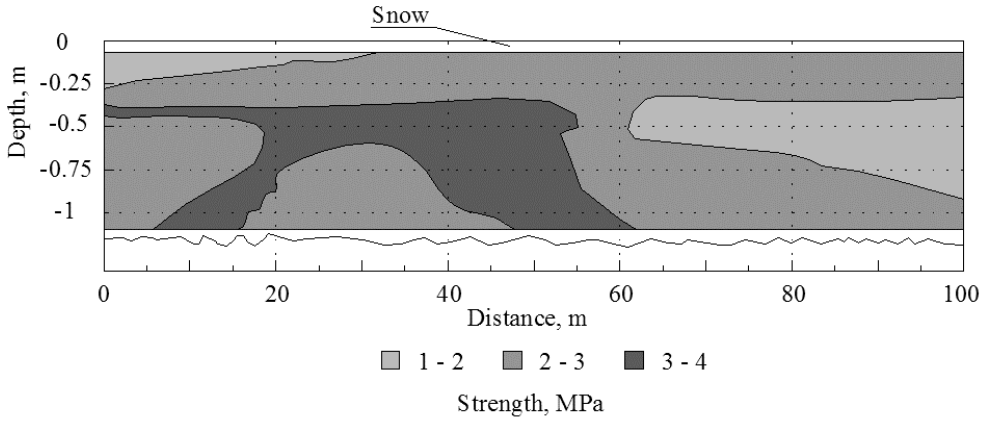

Fig. 18. The ice strength distribution for the drift ice. Vertical ice samples, after Astafiev et al. (2001).

As shown in Fig. 7a, the ice strength varied by a factor of 4 for samples from a constant depth in the level ice. This agrees well with strength maps by Shafrova and Moslet (2006b) who investigated the in-plane strength non-homogeneity of the different ice fields from the Spitsbergen fjords (Table 10). They reported that the strength of ice samples taken from the same depth at the different points in the landfast level ice field can vary by a factor of 3 to 4.

4.3.1.2 Ice ridges

The maps of the absolute strength distributions of the different parts of the ice ridge show that strength data for ridged ice from the same ice depth varies significantly. Local zones with high strength were adjacent to the regions of low strength. Moreover their arrangement pattern seems to be random (stochastic). The size of

these zones also changes randomly. The presence of those zones demonstrates the high variability of properties in geophysical materials such as sea ice, and the strength of ridge samples varied by a factor of more than 3 in both vertical and horizontal directions. We found a higher strength variation for the vertical samples for all types of the first-year sea ice features (Table 4 and Table 8) compared to the horizontal ones.

One of the main objectives of the 2006 expedition was to compare strength and other physical properties of level ice with corresponding data from different parts of an ice ridge. We found that the strength variability in the level ice was partly higher (vertical samples) and partly lower (horizontal samples) compared to the consolidated layer. The level ice strength varied from 0.35 MPa to 6.96 MPa, whereas the consolidated layer strength varied within a narrower range of 0.48 MPa to 3.49 MPa. The bigger range of the level ice strength is due to bigger differences in relation to ice texture between vertical and horizontal ice samples. But the horizontal level ice samples themselves had smaller variation than both horizontal and vertical consolidated layer samples. Thus, no clear trend of the level ice strength homogeneity compared to the strength homogeneity within the ice ridge can be found in our data (in Section 4.3.2 we discuss these differences and similarities in relation to physical properties). The situation with the ice-rubble blocks is not clear, but only a few horizontal samples were tested.

The field data do not support the statement that strength inhomogeneity in ice ridges is any higher than in the level ice. However, when considering about ice action on structures, high variation in the consolidated layer thickness and the total thickness of the ridges make those ice features more inhomogeneous than the level ice.

The ice rubble blocks were weaker than both the consolidated layer and level ice. As shown in the strength maps of the ice ridges, solid ice samples from the rubble blocks were collected at the depth down to 6 m. Even though the average strength of the ice from the rubble blocks was less than 0.5 MPa, some ice samples (even from the depth about 5 m) have strength exceeding 1 MPa. The relative strength distributions for the ice rubble blocks and consolidated layer exhibited some similarity (Fig. 13). The strength variation within the different parts of an ice ridge was at the same level: 50-55% for the 2005 feature and around 40% for the 2006 ridge, and the frequency histograms for the consolidated layer and ice-rubble blocks were similar for both years.

Four theoretical distributions (normal, t location-scale, gamma and lognormal) were tested to determine the distribution law for the relative ice strength. The results of goodness-of-fit analysis for the best fit distributions for the different ice features show that the ice strength data can be described (in 5 out of 6 cases) by asymmetrical lognormal or gamma distributions (Fig. 10 and Fig. 13). The level ice strength

distribution (vertical samples) has a longer tail and a peak shifted towards lower values compared to the consolidated layer. This means that for the level ice, the mode value is less than the mean value of the data set. This is due to presence of 9 strong samples from the bottom layer. By contrast, the consolidated layer data is evenly distributed and the mean value correspond well to the mode of the distribution.

The obtained data on ice strength spatial distribution are important for ice load estimations. The presence of weak/strong zones in first-year ice features is the principal explanation for non-simultaneous failure, which may further be linked to the apparent size effect in nominal pressure (Sanderson, 1988). Farafonov (2006) claims that for offshore structures larger than 35 m, the total ice load can be reduced by 12% due to ice strength heterogeneity in the Amur Bay area. By contrast, Shkhinek et al. (2007) argue that by taking into account the ice strength heterogeneity the total ice load can be increased. They report that the presence of strong zones in the entire ice field increased the ice load significantly. The weak zones diminish the ice load, but this diminishing has a local character and should be ignored because zones with the higher strength always occur before or after weak ones. Further investigations on this subject are currently underway. A more detailed field data of the ice strength spatial distribution will help to develop a proper characterization of the ice strength heterogeneity.

4.3.2 Strength versus physical properties

Ice strength decrease with increasing porosity was demonstrated by many authors, e.g. Timco and Frederking (1990). Moslet (2007) presents new data and includes an up-to-date review of the previous studies. He suggests that this phenomenon is due to both reduction of the pure ice content and a result of crack nucleation and propagation. Based on his own data he suggests Eq. 1 for the maximum ice strength as a function of the total porosity of first-year level ice in uniaxial tests, with parameter A as 24 MPa and 8 MPa for respectively vertical and horizontal samples. The same equation fits our data with A equals 10.5 MPa and 5.25 MPa for vertical and horizontal level ice samples and 9.1 MPa and 7 MPa for vertical and horizontal consolidated layer samples. We used a constant proportionality of 2 between vertical and horizontal level ice strength, and a proportionality factor of 1.3 for the ridged ice.

$$\sigma = A \cdot \left(1 - \sqrt{\frac{\eta_{tot}}{0.7}}\right)^2, \tag{1}$$

The vertical samples were generally stronger than the horizontal ones for all types of the first-year sea ice (Table 7). The ratio between vertical and horizontal strength of

ice was significantly higher for the level ice (2.0) than the corresponding values for the consolidated layer (1.1) and the ice rubble (1.09). This is not surprising and is due to the difference in ice texture as shown and argued for by Poplin and Wang (1994) and Høyland (2007). The level ice basically has columnar structure, whereas the ridge has a more random ice texture. The isotropic behaviour of the surface layer in level ice is clearly seen in Table 8, where the vertical to horizontal strength ratio was 0.93 for the surface layer and 2.45-3.1 for the columnar ice. Polomoshnov and Truskov (1993) and Astafiev et al. (2001) observed a similar trend for both landfast and drift ice offshore Sakhalin. They found a strength ratio (σ^v / σ^h) around 1.0 for the surface layer in level ice. For the columnar ice they report a typical ratio of 1.7 – 2.8 for the drift ice and 1.5 – 2.4 for the landfast ice, which is lower than we found. Sakhalin studies were conducted during the cold season (January – March), whereas the present study was carried out close to the end of the season (May). Moslet (2007) suggests that the vertical to horizontal strength ratio depends on the ice temperature: the colder the ice is the lower the ratio is. The ratios reported for the Sakhalin studies are lower than what we measured, and since ice in the Sakhalin studies was likely colder, the ratio is expected to be smaller.

Table 5 shows that the horizontal samples were less saline and more porous than the vertical ones. This is probably because brine channels basically run vertically and a horizontal sample would drain faster than a vertical one. This also helps with explaining the generally higher porosity. A lack of low porosity horizontal samples was also found by Høyland (2007) who reported that only 7 horizontal samples from 75 that were tested from the consolidated layer of the ridge had porosity less than 5%. By contrast, 38 (from 170) vertical samples were in this porosity range. The lack of low porosity samples may also be explained by the predominant brine channel spacing. If this spacing is in-between the size of the small and large core (70 mm and 200 mm), some of the vertical samples may have been sampled in-between brine channels but the horizontal ones would certainly include at least one channel. Finally this may be the effect of the double coring technique, it may enhance brine drainage. The fact that the horizontal samples were always warmer than the vertical ones is more difficult to understand. It may also be an indirect effect of brine drainage. If the remaining brine had a lower average salinity, it would also have a higher freezing point and if it is to be kept at the critical point the temperature have to increase. Another explanation deals also with double coring technique, the horizontal ice samples can be artificially warmed up before testing.

The ice strength is a key parameter for the ice loads analysis, but so far, there is no proper link between physical and mechanical properties of ice. However, it is significantly easier and cheaper to measure and estimate physical - (such as temperature, salinity and porosity) instead of mechanical properties of ice. Thus, the relationships between these parameters will be obviously useful. Figs. 7 and 8 suggest

a clear spatial correlation between ice strength and porosity data. The occurrence of (relatively) strong and low-porous ice in the lower layers of the level ice is due to the temperature profile and the effect of radiation in melting ice. As mentioned above the same dependence was also developed based on the ridge data and the relationship between for the maximum ice strength as a function of the total porosity is given as Eq. (1). In general our study confirms the connection between ice strength and ice properties (basically ice texture and porosity).

5. Conclusions

Two ridges were examined during the annual UNIS scientific expeditions: one in the North-western part of the Barents Sea and one in the Arctic Ocean in the years 2005 and 2006, respectively. Measurements of ice ridge geometry and morphology were presented. In addition to that, first-year sea ice both from ice ridges and level ice were sampled and uniaxial compression test were conducted in field. The main conclusions are:

- Altogether 130 freeze bonding contacts were inspected. The average length was 0.27 m, and width was 0.14 m. The average length to width ratio was 2.2 (2005) and 1.8 (2006).
- The average freeze bond length to the average block length ratio was introduced; it is 0.33 (2005) and 0.35 (2006).
- The solid samples of ice from the ice rubble blocks in the ridge keel were significantly weaker than the consolidated layer with an average strength below 0.5 MPa. Several rubble blocks samples with strength higher than 1.0 MPa were found.
- Weak (and strong) zones in the ice were discovered in the ice ridges, and the ice strength varied by a factor of more than 3 along both vertical and horizontal directions.
- The strength and porosity maps of the level ice correlate well to each other. The maximum strength of the drift ice for the both level ice and ice ridge can be estimated from the total porosity and the corresponding equations have been developed.
- The strength variation was higher (vertical samples) and lower (horizontal) for level ice than for the ice ridge data.
- The vertical samples were stronger than the horizontal ones and showed a bigger strength variation for all types of the first-year sea ice. The ratio between vertical and horizontal strength of ice was found to be 2.0 for the level ice and around 1.1 both for the consolidated layer and for the ice rubble blocks.

Acknowledgement

This field data was collected together with students of the Arctic Technology department in the UNIS course AT-208 in the years 2005 and 2006. We would like to thank all of them for their excellent work both in the field and on the processing of data. The encouragement and help from Per Olav Moslet (2005) and Sébastien Barrault (2006) is greatly appreciated. We also would like to thank the crew on RV "Lance" for always being helpful and friendly. The authors would like to thank Dr. Dmitri G. Matskevitch for comments and review of this paper.

References

Astafiev, S.V., Kalinin, E.N., Polomoshnov, A.M., Surkov, G.A. (2001). Ice investigations on the Northern Sakhalin Shelf. Download from www.science.sakhalin.ru/Geography/2001/A1/ (in Russian).

Bjerkås, M. (2006). Ice actions on offshore structures. Doctoral thesis. Norwegian University of Science and Technology, NTNU, Trondheim, Norway, 179p.

Brown T.G. and Määttänen, M. (2002). Comparison on Kemi-I and Confederation bridge cone ice load measurement results. *In Proc. of the 16th Int. Symp. on Ice (IAHR),* Dunedin, New-Zealand, pp. 503- 513.

Cox, G.F. and Weeks, W.F. (1983). Equations for determining the gas and brine volumes in sea ice samples. *Journal of Glaciology*, Vol. 29, (102): 306-316.

Dolgopolov, Yu., Afanasiev, V., Koren'kof, V. and Panfilov, D. (1975). Effect of hummocked ice on the piers of marine hydraulic structures. *In Proc. of the 3rd Int. Symp. on Ice (IAHR)*, Hanover, USA, pp. 463-477.

Ettema, R. and Schaefer, J.A. (1986). Experiments on freeze-bonding between ice blocks in floating ice rubble. *Journal of Glaciology*, Vol. 32, (112): 397-403.

Farafonov, A.E. (2006). Heterogeneity of the ice cover and its estimation for the ice loads evaluation on the sea water engineering constructions. Abstract of the Candidate of Science thesis. Far-East State Technical University, Vladivostok, Russia. 24p. (in Russian).

Hopkins, M.A. and Hibler, W.D. (1991). On the shear strength of geophysical scale ice rubble. *Cold Regions Science and Technology*, (19): 201-212.

Høyland, K.V. (2002). Consolidation of first-year sea ice ridges. *Journal of Geophysical research*, 107 (C6): 15,1-15,15.

Høyland, K.V. (2007). Morphology and small-scale strength of ridges in the North-western Barents Sea. *Cold Regions Science and Technology*, (48): 169-187.

Kärnä, T. and Nykänen, E. (2004). An approach for ridge load determination in probabilistic design. *In Proc. of the 17th Int. Symp. on Ice (IAHR),* Saint-Petersburg, Russia, pp. 68- 76.

Leppäranta, M. and Manninen, T. (1988). The brine and gas content of sea ice with attention to low salinities and high temperatures. Technical Report 1988(2), Finnish Institute of marine research. 14 p.

Liferov, P. (2005). Review of ice rubble behaviour and strength, Part II: Modelling. *Cold Regions Science and Technology*, (41): 153–163.

Moslet, P.O. (2007). Field testing of uniaxial compression of columnar sea ice. *Cold Regions Science and Technology,* (48): 1–14.

Polomoshnov, A.M., Truskov, P.A. and Tambovsky, V.S. (1992). Determination of design values for sea ice physico-mechanical properties. *In Proc. of the 2nd Int. Offshore and Polar Engineering Conference, (ISOPE),* San Francisco, USA, Vol. 2, pp. 641–650.

Polomoshnov, A.M. and Truskov, P.A. (1993). Sea ice strength variability due to various ice column axis orientation. *In Proc. of the 3rd Int. Offshore and Polar Engineering Conference, (ISOPE)*, Singapore, Vol. 2, pp. 643–647.

Poplin, J. and Wang, A. (1994). Mechanical properties of rafted annual sea ice. *Cold Regions Science and Technology*, (23, 1): 41-67.

Sanderson, T.J.O. (1988). Ice mechanics risks to offshore structures. Graham and Trotman. London, 253p.

Shafrova, S. (2007). Initial failure of the ice rubble in plane strain direct shear tests. *In Proc. of the 19th International Conference on Port and Ocean Engineering under Arctic conditions, (POAC),* Dalian, China, Vol. 1, pp. 256-266.

Shafrova, S., Liferov, P., Shkhinek, K. (2004). Modelling ice rubble with pseudo-discrete continuum model. *In Proc. of the 17th Int. Symp. on Ice (IAHR),* Saint-Petersburg, Russia, Vol. 2, pp. 265-274.

Shafrova, S. and Moslet, P.O. (2006a). In-situ uniaxial compression tests of level ice. Part I: Ice strength variability versus length scale. *In Proc. of the 25th Int. Conf. on Offshore Mechanics and Arctic Engineering (OMAE),* Hamburg, Germany, OMAE-92450, 9p.

Shafrova, S. and Moslet, P.O. (2006b). In-situ uniaxial compression tests of level ice. Part II: Ice strength spatial distribution. In *Proc. of the 25th Int. Conf. on Offshore*

Mechanics and Arctic Engineering (OMAE), Hamburg, Germany, OMAE-92451, 10p.

Shkhinek, K., Blanchet, D., Jilenkov, A., Shafrova, S. (2007). Ice loads dependence on the field heterogeneity. *In Proc. of the 19th International Conference on Port and Ocean Engineering under Arctic conditions, (POAC),* Dalian, China, Vol. 1, pp. 245-255.

Surkov, G.A. and Truskov, P.A. (1993). Analysis of spatial heterogeneity of ultimate ice compressive strength. *In Proc. of the 3rd Int. Offshore and Polar Engineering Conference, (ISOPE)*, Singapore, Vol. 2, pp. 596–599.

Takeuchi, T., Akagawa, S. and Iwai, T. (1995). On the distribution of strength of in-situ sea ice sheet. *In Proc. of the Civil Engineering in the Ocean Conference,* Vol. 11, pp. 241-245 (in Japanese).

Timco, G.W. and Burden, R. (1997). An analysis of the shapes of sea ice ridges. *Cold Regions Science and Technology*, (25): 65-77.

Timco, G.W. and Frederking, R.M.W. (1990). Compressive strength of sea ice sheets. *Cold Regions Science and Technology*, (17): 227-240.

Truskov, P.A., Surkov, G.A., Astafiev, V.N. (1996). 3-D variability of sea ice uniaxial compressive strength. *In Proc. of the 13th Int. Symp. on Ice (IAHR),* Beijing, China, pp. 94-101.

Tuhkuri, J. and Polojärvi, A. (2005). Effect of particle shape and in 2D ridge keel deformation simulations. *In Proc. of the 18th Int. Conf. on Port and Ocean Eng. under Arctic Conditions (POAC),* Potsdam, USA, Vol. 2, pp. 939–948.

Vershinin, A.S., Truskov, P.A., Kuzmichev, K.V. (2005). Ice actions on the structures of the Sakhalin Shelf. Institute Giprostroimost, Moscow, 208p (in Russian).

Wright, B.D. and Timco, G.W. (2001). First-year ridge interaction with the Molikpaq in the Beaufort Sea. *Cold Regions Science and Technology*, (32): 27-44.

In Proceedings of the 25th International Conference on Offshore Mechanics and Arctic Engineering (OMAE), 2006, Paper No. - OMAE-92450

3.3 In-situ uniaxial compression tests of the level ice. Part I: Ice strength variability versus length scale

Svetlana Shafrova and Per Olav Moslet

The University Centre in Svalbard (UNIS), Longyearbyen, Norway

Abstract

Field programs of the ice strength determination through the uniaxial compression tests were carried out on the landfast level ice both in the Van Mijenfjorden and in the Adventfjorden on Svalbard, Norway in 2004 and 2005. The ice strength was examined in relation to the different length scales. The step (horizontal distance) between the ice samples was continuously reduced in order to find out how the ice strength variability develops. The spatial variation of the physical properties of the ice such as temperature, salinity, density have been measured. The typical ice strength variability for the areas larger than 40 m^2 is found as 20 – 30% for the vertical ice cores of the certain depth from the ice cover surface. For the horizontal ones it is slightly less about 10 – 20%.

Introduction

For the Arctic region the ice forces in most cases determine the design load level for the offshore structures. The ice forces on structures depends on many factors, some of them relate to the ice itself and some to the structure. The geometry, type of the ice features and its physical and mechanical properties are the most important factors that affect the ice load. Several methods were developed for the ice load calculation. The most common approach is based on the Korzhavin's method (SNiP (1996) and API (1995)), where the load is determined by multiplication of the uniaxial compression strength of the ice on several coefficients describing both the structure and the ice field. Therefore it is important to made a proper analysis of the ice strength evaluation.

Many researchers (Butkovich (1959), Peyton (1966), Wang (1981), Frederking and Timco (1980), (1983), Timco and Frederking (1990)) have measured (both in laboratory and in-situ) the uniaxial compressive strength of small ice samples. It has been found that the ice strength is a function of both the testing conditions (loading rate, confinement condition, sample size, stiffness of testing machine) and the physical properties of the ice (temperature, salinity, density, porosity, ice type, grain

size). As a result considerable variation of ice strength from different experiments has been reported.

Field studies of an ice cover (Surkov et al., 1993, Truskov et al., 1996) show that the ice strength characterized by spatial heterogeneity both for an individual point of the ice field and for the entire ice field. Besides the ice strength changes significantly through the season. The continuous change of the ice properties in space and time often lead to a big variability in the ice strength and as a result in the ice force analysis. So, the study of the ice strength heterogeneity seems to be vital, since a precise evaluation of the ice strength has a great importance for the design ice load analysis.

It is known that the ice strength depends significantly on its temperature (T_{ice}) and salinity (S_{ice}). For the in-situ testing, it is important to minimize the time between sampling and testing, so that T_{ice} and S_{ice} don't change. The ice cores should be compressed within minutes after sampling and the whole test program should be done during short time period. For this purpose the portable compression equipment was used during our experiments.

Part I of this paper deals with the ice strength heterogeneity in relation to different length scales. It was proposed that the ice strength variability should decrease with reducing of the length scale. Our test programs were done in order to verify this.

Part II of this paper presents the data of the ice strength variability for the different test areas: for a small area (Point-area), for a line and for an area in the ice cover.

Experimental set-up

General

Two in-situ test programs were carried out: Test 1 in the Van Mijenfjorden and Test 2 in the Adventfjorden (Fig. 1). The horizontal spacing between the samples, hereafter called the step (*ST*), was continuously reduced during testing. The dimensions of the considered area in both directions were always twice of this distance. These linear dimensions of the study area are hereafter called the length scales (*LS*). So, the current field studies were done in order to examine the ice strength variation in relation to the horizontal spacing between the samples and as a result to the different length scales ($LS = 2ST$). The description of the test programs is summarized in Table 1.

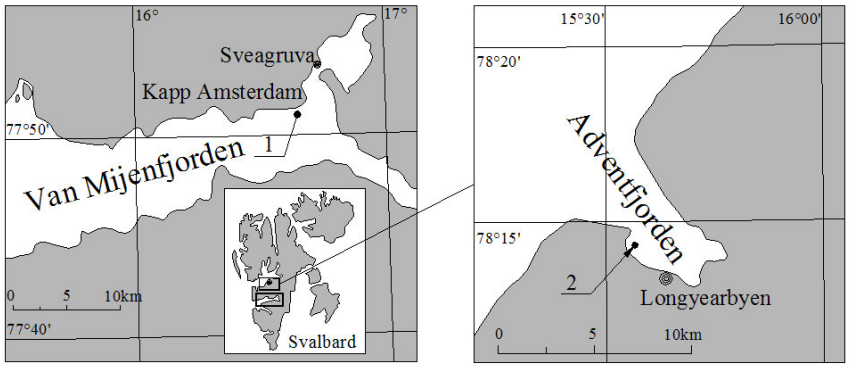

Fig. 1. The map of the test sites locations.

The sites are marked by the dots and the number of the site corresponds to the test number.

Table 1. Summary of the tests.

no.	Data	Location	Description	Depth[a]	Dir.[b]	n[c]
	Spring, 2004, Van Mijenfjorden					
1.	21 March	Kapp Amsterdam	Area of 10 x 10 m^2, step from 1 to 0.25 m, 5 square areas	0.30	V	25
	Spring, 2005, Adventfjorden					
2.	7 - 8 April	Longyearbyen	Area of 50 x 50 m^2, step from 25 to 0.4 m, 7 square areas	0.05 0.12	V H	65 29

Note: [a] The depth is from the ice cover surface to the top of the sample, (m).
[b] The direction is either vertical (V) or horizontal (H).
[c] Number of compressed ice samples.

We used the portable compression equipment (Fig. 2) for the ice strength evaluation. It consists of band saw and portable uniaxial compression machine – 'KOMPIS'. The main parts of the 'KOMPIS' machine are the following: mechanical jack (A) that transfers the rotational movement from the electrical engine (B), the load cell (C), which measures the load applied to the ice core and the displacement sensor (D), which measures the displacement of the ice core during compression. Cylindrical ice samples of Ø70 mm and 175 mm in height were tested under a constant speed. The

velocity of the lower steel plate, which was in contact with the bottom of the ice sample, was such that 175 mm long samples were subjected to a nominal strain rate of $1 \cdot 10^{-3}$ 1/s. The real strain rate was about $7 \cdot 10^{-4}$ 1/s. A more detailed description of the compression equipment is given by Moslet (2007).

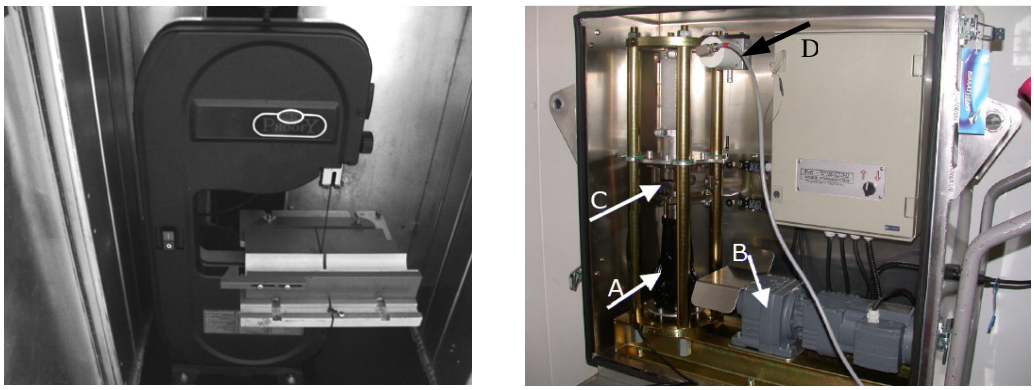

a) Band saw

b) Compression machine – "KOMPIS"
A – mechanical jack, B – electrical engine,
C – load cell, D – displacement sensor

Fig. 2. The portable compression equipment.

Vertical ice samples were prepared and compressed using the following technique. Firstly, the vertical ice core was drilled out of the level ice sheet by an ice core drill with the inner diameter of 70 mm. Then this core was cut using band saw into the 175 mm sample with the parallel ends. The sample was weighed prior test in order to determine the ice density and then compressed. Immediately after compression the ice temperature was measured. Then the core was put into the plastic bag for further melting and salinity measurements. The salinity was deducted from the conductivity measurements of the melted samples.

Each test program was finished within one or two days. In order to avoid changes of salinity and temperature, the ice cores were compressed directly on the site within 10 minutes after the ice core was sampled from the parent ice. Furthermore, since the most of the brine channels are vertical, the ice core was left horizontally as much as possible prior testing. This had to minimize the salinity drainage from the ice.

We distinguished between two failure modes: brittle and ductile. As mention by Moslet (2007), the brittle behaviour was defined as when the sample had a sudden load drop and lost all its strength immediately, while the ductile was characterized as a load peak followed by a softening phase when the ice gradually lost its strength.

The test was stopped when the sample entered the softening phase or a sudden load drop was occurred. Both failure modes are characterized by crack nucleation. But for the brittle behaviour the effect of crack nucleation followed by the rapid crack propagation.

Test 1

The area with plane dimensions of 10 m was divided into squares with 1 m sides, which gave us 121 samples. The first square with 1 m side was further divided into squares with sides of 0.5 m and finally into squares of 0.25 m sides as shown in Fig. 3. Only one ice depth (0.3 m from the ice cover surface) was tested. Thus 129 vertical samples were compressed during this test. The ice temperature was registered for the all samples.

This data set was used to evaluate the ice strength variability over the 10x10 m^2 area (See Part II of this paper). The 5 square areas with the length scales of 8 m, 4 m, 2 m, 1 m, 0.5 m can be distinguished as shown in Fig. 3. The step was continuously reduced from 4 m to 0.25 m for these areas. So that all areas, except the last one, consisted of 9 samples. The smallest area with length scale of 0.5 m contained only 5 samples as shown in Fig. 3b.

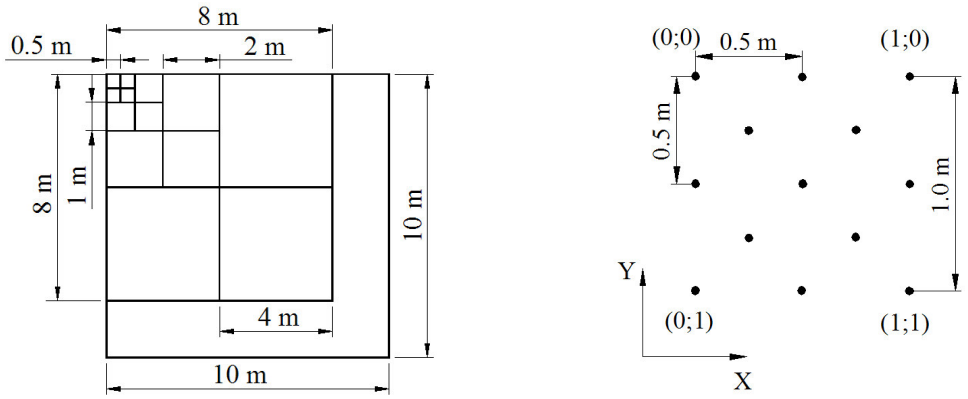

a) Plan view of area
(Samples were taken at the points of intersections)

b) Upper left corner of the test area
(Samples positions are marked by the dots)

Fig. 3. Sampling area, Test 1.

Test 2

Initially, it was planned to investigate a basin of 100x100 m^2, at such size the heterogeneity over the area is commensurable with area of distribution of the stress-strain state zone arising from ice-structure interaction (Seliverstov et al., 2001). Kärnä and Jochmann (2003) conducted ice force measurements at the lighthouse Norströmsgrund in the northern part of the Baltic Sea. They reported that for one-hinge bending failure the ratio of the circumferential crack width (B) to the waterline diameter of the structure (D) varied typically from 0.2 to 1.2. The waterline plane dimensions of the offshore structures varying from 2 - 3 m up to 100 m. So, the test area no less than 100 m in each direction with a minimum step between sampling no over 0.4 m should be considered.

During our test the area was reduced to 50x50 m^2 and divided into the squares with a minimum step between the samples of about 0.39 m as shown in Fig. 4. The step between the samples was continuously reduced from 25 m to 0.39 m. Thus 7 square areas of different length scales (50 m, 25 m, 12.5 m, 6.25 m, 3.13 m, 1.56 m and 0.78 m) were investigated. Vertical ice cores from 0.05 m depth below the ice cover surface were taken at each corner of these squares and compressed. The 9 samples within the area constitutes a data bock. Two different data blocks started at y=0 and y=3.13 were considered for the areas with the length scales of 1.56 m and 0.78 m (Fig. 4b). The part of the testing area that had a size of 3.13 m with a uniform step of 0.78 m (as given in Fig. 4b) will be analyzed in relation to the ice strength distribution in Part II of this paper.

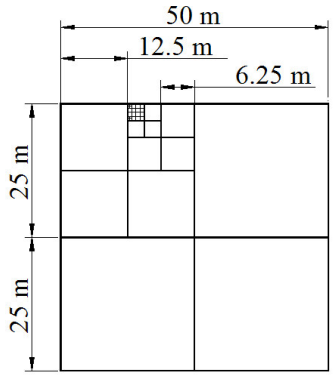

a) Plan view of area

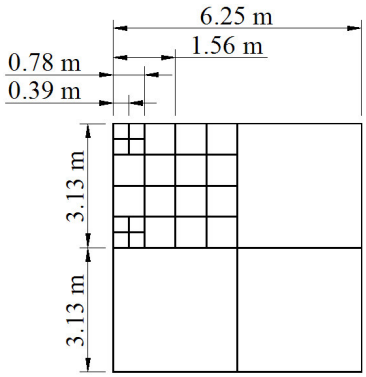

b) Part of testing area, left upper corner corresponds to the corner (12.5, 0) of the plan view

Fig. 4. Sampling area, Test 2.

Samples were taken at the points of intersections, areas with the length scales of 1.56 m and 0.78 m had two data blocks that started at (0, 0) and (0, 3.13).

In addition the horizontal ice cores were also sampled and tested at each point of the squares with the length scales from 50 m to 6.25 m. The squares for the horizontal sampling were the same as for the vertical ones. In order to get a horizontal ice core, a large core drill (Ø220 mm) was used to take a vertical ice core. From this vertical core the horizontal ice core (Ø70 mm) was drilled using a small core drill. The centre of the horizontal core was approximately 0.12 m from the top of the ice cover surface. One ice core was taken per each sampling point.

Results

Test 1

The coefficients of variation k_v (ratio of the standard deviation to the mean value) both for the ice strength and ice temperature as well as the mean strength value versus the length scales are given in Fig. 5 for Test 1. The temperature of the ice cores measured immediately after compression was in the range of -3.1°C to -5.2°C, and 87% of the samples had a temperature between -4.0°C and -5.2°C. The mean value of the ice temperature varied within 0.5 °C for the different test areas. The air temperature was around -2°C during testing.

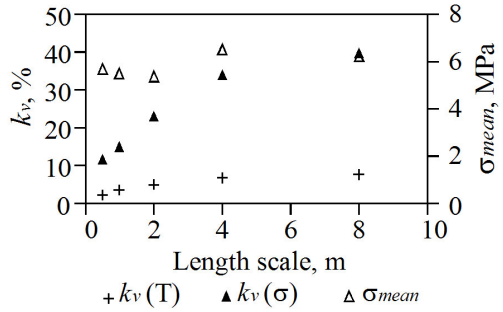

Fig. 5. Correlation plot k_v and σ_{mean} versus length scale, Test 1.

where $k_v(\sigma)$ and $k_v(T)$ are the coefficients of variation of the ice strength and ice temperature respectively, σ_{mean} is the mean value of the ice strength.

Test 2

For the Test 2 the results of statistical analysis for the vertical ice samples are shown in Fig. 6, both ice strength and corresponding temperature variability versus length scales are presented. As mentioned before, there are two data blocks for the areas with the length scales of 1.56 m and 0.78 m, which started at y=0 and y=3.13 respectively. Fig. 7 shows the results of the ice strength and corresponding temperature variability for the horizontal ice samples. The mean value of the ice temperature was found to be constant varying within 0.7°C.

The ice strength and temperature versus time scale for the both vertical and horizontal samples are given in Fig. 8. The time scale is given by sample number, which increases with the time. The vertical samples have been plotted in the two failure modes (brittle and ductile), while the horizontal ones only acted in the ductile failure mode. The ice temperature was registered in range of -2.7°C to -7.6°C, the air temperature was about -15°C at the day of the testing. The ice strength versus ice temperature for the vertical ice samples is plotted in Fig. 9. The snow depth was measured spatially during testing and was varied between 0.02 m and 0.26 m over the test area. The ice strength and ice temperature versus snow depth (h) for the vertical ice samples are given in Fig. 10. The variability and mean value for the snow depth versus length scale are shown in Fig. 11.

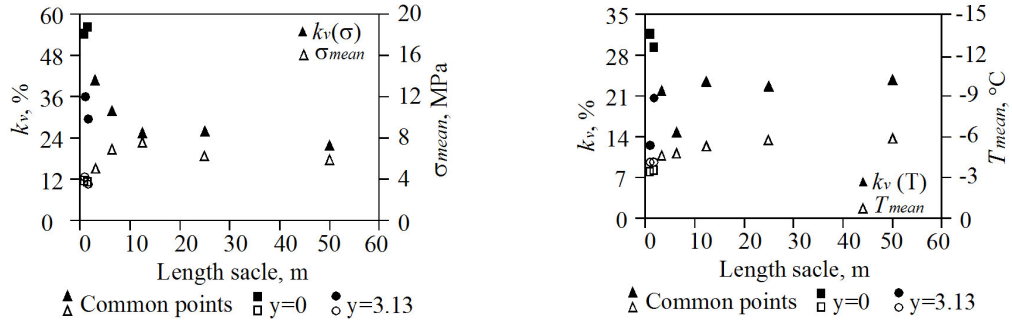

Vertical samples

Fig. 6. Correlation plots k_v , σ_{mean} and T_{mean} versus length scale, Test 2.

where $k_v(\sigma)$ and $k_v(T)$ are the coefficients of variation for the ice strength and ice temperature respectively, σ_{mean} and T_{mean} are the mean values of the ice strength and ice temperature.

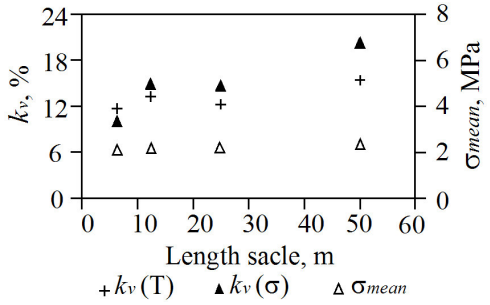

Horizontal samples

Fig. 7. Correlation plot k_v and σ_{mean} versus length scale, Test 2.

where $k_v(\sigma)$ and $k_v(T)$ are the coefficients of variation for the ice strength and ice temperature respectively, σ_{mean} is the mean value of the ice strength.

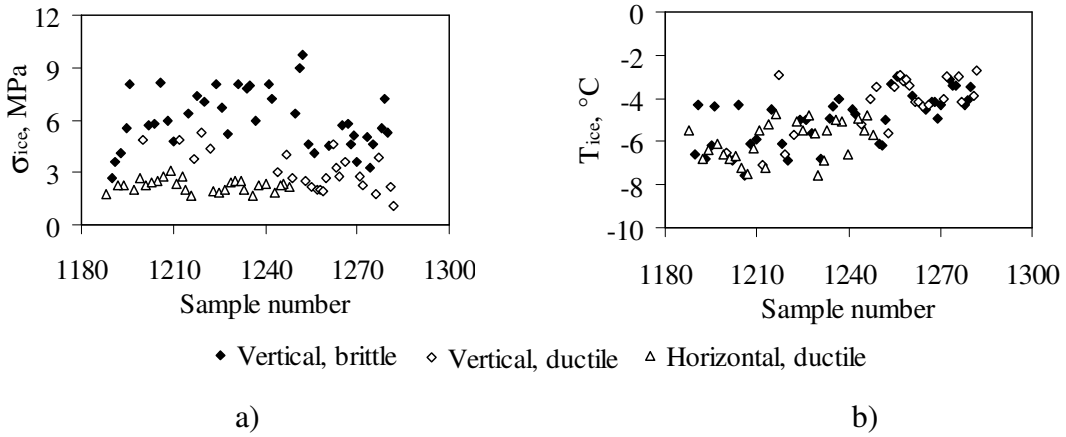

a) b)

Fig. 8. Ice properties versus time scale, Test 2.

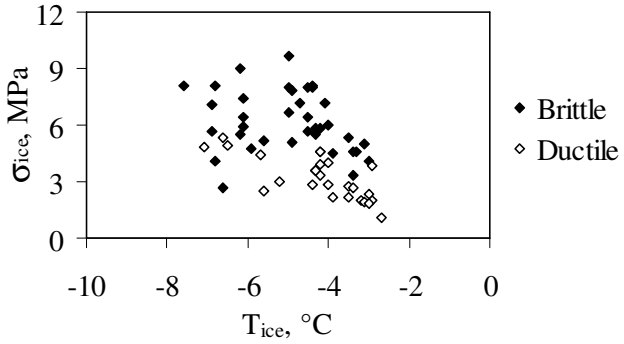

Vertical samples

Fig. 9. Ice strength versus ice temperature, Test 2.

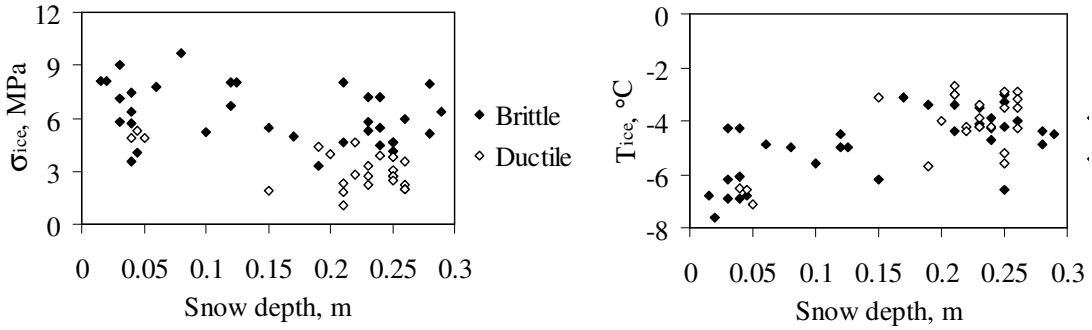

a) b)

Fig. 10. Ice properties of the vertical samples versus snow depth, Test 2.

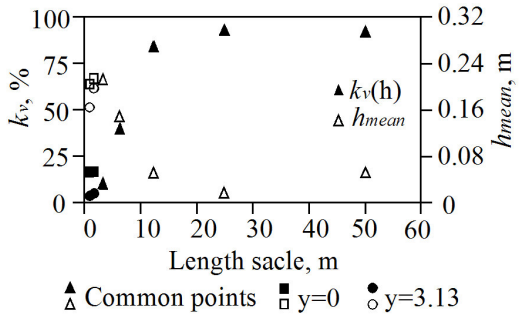

Fig. 11. Correlation plot k_v and h_{mean} versus length scale, Test 2.

where $k_v(h)$ and h_{mean} are the coefficient of variation and mean value of the snow depth.

Discussion

The vertical ice samples from 0.3 m depth were compressed during Test 1, while the air temperature was about -2°C and the measured ice temperature was found in a sufficiently narrow range. The snow was evenly distributed over the whole tested area. But even for these conditions the ice strength had a great scatter. The coefficient of variation for the ice strength decreased from 39.4% to 11.8% for the corresponding length scales of 8 m to 0.5 m as given in Fig. 5. At the same time the variation of the ice temperature decreased from 7.5% to 1.75% for the same length scales. Thus the ice strength and ice temperature variations were reduced by 70% and 77% respectively. As Fig. 5 shows the mean value of the ice strength within an area was in a narrow range varied from 5.29 MPa to 6.40 MPa. As mention previously the mean value of the ice temperature was also close to constant. Therefore the ice strength heterogeneity is correlated well with the ice temperature distribution over the considered test areas.

For Test 2 the ice strength heterogeneity didn't change with reduction of length scale from 50 m to 6.25 m for the both vertical and horizontal ice samples as shown in Figs. 6 and 7. The coefficient of variation was estimated in range of 21 - 26% for the vertical ice cores and about 15 - 20% for the horizontal ones. The corresponding mean values of the ice strength were close to constant.

Bekker et al. (1996) were conducted in-situ tests of the ice strength variability over an areas with different length scales in Amour Bay near Vladivostok (Far East). The vertical ice samples of the landfast level ice were tested using drop ball technique. As a result only surface layer were under investigation. They also reported that the ice

strength variability doesn't changes too much for the length scales from 100 m to 6.25 m.

For the vertical ice cores the further reduction in length scale to 0.4 m gave no clear tend in development of the ice strength heterogeneity. The data block corresponds to y=0 in Fig. 6a shows the higher variability for the smaller areas. Whereas, the data from y=3.13 shows a scatter. Both data blocks contradicted with the results obtained from Test 1, that show a lower variability for the small areas.

As given in Fig. 7 the ice strength and ice temperature distributions for the horizontal samples over different test areas are correlated well to each other. For the vertical ice samples the correlation is not so evident (Fig. 6b). But it is clear that the high variability of the ice strength (56.9% and 55.7%) corresponds to the higher ice temperature variation (29.5% and 31.9%). As expected the ice temperature is a key parameter for the ice strength.

Furthermore, it seems that the ice samples were affected by the air temperature, which was significantly lower than the tested ice. As shown in Fig. 8b the ice temperatures obtained from the test were higher for the last 25 to 30 samples and correspond with a lower ice strength. It looks like some of the ice samples were slightly cooled down before compression especially at the beginning of the test when both vertical and horizontal samples were under examination. It could be a reasonable explanation for the high variability and lower average strength over the small areas that were tested at the end.

Fig. 9 shows that the ice strength decreased with increasing ice temperature. But at the same time it demonstrates that there is no clear connection between ice temperature and corresponding failure mode of the ice samples. For the given temperature the average strength was higher for the brittle samples. This will be discussed further in Part II of this paper.

It can be seen from Fig. 10b that the snow depth significantly affected the ice temperature. A deep snow cover resulted in warmer ice samples. But the correlation between the ice strength and snow depth (Fig. 10a) is not so evident. This is probably a result of the different failure mechanisms that were observed for the ice samples with the same temperature (see Fig. 9).

As shown in Fig. 10a the snow depth was distributed unevenly over the considered test area. We suggest that it can explain fluctuations in the ice strength distribution, especially for the small areas. But Fig. 11 shows contradictory results. The mean value of the snow depth increased significantly from 0.12 m for the big areas to 0.24 m for the small ones. As a result the variability decreased from 92% to 4%. For the areas with length scales higher than 6.25 m the snow depth varied from 0.02 m to 0.29 m. This may have resulted in a high strength variability. In case of smaller areas the snow cover was evenly distributed with average snow depth around 0.2 m. So, the

significant increase of ice strength variability for the small areas can't be explained by the influence of the snow cover.

The data from the Test 1 (Fig. 5) shows that strength variability decreased with a reduction in the length scale from 8 m to 0.5 m. We believe that the variability can be affected by the number of samples taken per test area. An example for the 8x8 m^2 area is given in Fig. 12. The coefficient of variation of the ice strength $k_v(\sigma)$ decreased from 39.4% to 29.9% with an increasing number of samples from 9 to 25. A further increase in the sample number up to 81 lead to a variability of about 25.9%. So, the large variability in results for the both Test 1 and Test 2, sometimes can be explain due to small number of ice samples taken per area. Thus for the more precise evaluation of the ice strength heterogeneity the number of samples for each test area should be over 25, when the effect of each value to the corresponding k_v is less of importance.

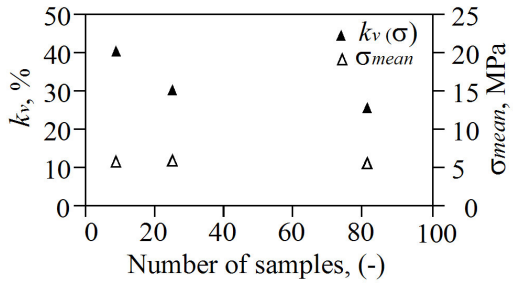

Fig. 12. Correlation plot k_v and σ_{mean} versus number of test samples, Area 8x8 m^2, Test 1.

Conclusions

Experimental studies of the ice strength variability in relation to different length scales were done on landfast level ice on Svalbard. The main conclusions are:

- For areas larger than 40 m^2 the typical ice strength heterogeneity was found in range of 20 - 30% for the vertical ice cores and about 10 - 20% for the horizontal ones.
- The development of ice strength variability for the smaller test areas is not clear. The results contradict each other. The data from the Test 1 showed significant decreasing of the ice strength heterogeneity with a reduction of length scales from 8 m to 0.5 m. The results from Test 2 showed the opposite trend.
- A high ice strength variability corresponds to the higher temperature variation.

- The hypothesis of the decreasing of ice strength variability with the corresponding reduction of the length scale was considered to be doubtful. Further investigations should be done.
- It should be proposed based on statistical laws that for more precise evaluation of the ice strength variability the number of samples should be over 25 per each test area.

Acknowledgement

We would like to thank the students of Arctic Technology department at UNIS springs of 2004 and 2005. We are grateful to all participants and contributors, especially to Basile Bonnemaire, Janne Valkonen and Rinat Kamalov. The encouragement and help from Knut V. Høyland and Sveinung Løset is greatly appreciated.

References

API RP 2N (1995). Recommended Practice for Planning, Designing and Constructing Structures and Pipeline for Arctic Conditions. American Petroleum Institute, Washington, DC 20005, 123p.

Bekker, A.T., Seliverstov, V.I., Gomolski, S.G. (1996). Experimental study of the three-dimensional ice strength distribution. *In Proc. of the 13th Int. Symp. on Ice (IAHR),* Beijing, China, pp. 110-116.

Butkovich, T.R. (1959). On the mechanical properties of sea ice, Thule, Greenland, 1957. U.S. Army Cold Regions Research and Engineering Laboratory, Research Report 54, 11p.

Frederking, R.M.W. and Timco, G.W. (1980). NRC ice property measurements during the Canmar Kigoriak trials in the Beaufort Sea winter 1979-80. NRC-DBR Paper 947, 63p.

Frederking, R.M.W. and Timco, G.W. (1983). Uniaxail compressive strength and deformation of the Beaufort sea ice. *In Proc. of the 7th Int. Conf. on Port and Ocean Engineering under Arctic conditions (POAC)*, Helsinki, Finland, Vol. 1, pp. 89–98.

Kärnä, T. and Jochmann, P. (2003). Field observations on ice failure modes. *In Proc. of the 17th Int. Conf. on Port and Ocean Engineering under Arctic conditions (POAC)*, Trondheim, Norway, Vol. 2, pp. 839–848.

Moslet, P.O. (2007). Field testing of uniaxial compression of columnar sea ice. *Cold Regions Science and Technology,* (48): 1–14.

Peyton, H.R. (1966). Sea ice strength. Final report of Naval Research Arctic project for period 1958 – 1965, 285p.

Seliverstov, V.I., Gomolski, S.G., Farafonov, A.E. (2001). Experimental studies of ice cover inhomogeneity. *In Proc. of the 11th Int. Offshore and Polar Engineering Conference (ISOPE)*, Stavanger, Norway, Vol. 1, pp. 744-748.

SNiP 2.06.04 –82*(1995). The loads and forces of ice on hydrotechnical facilities. Issue 1995, VNIIG, Saint-Petersburg (in Russian).

Surkov, G.A. and Truskov, P.A. (1993). Analysis of spatial heterogeneity of ultimate ice compressive strength. *In Proc. of the 3rd Int. Offshore and Polar Engineering Conference (ISOPE)*, Singapore, Vol. 2, pp. 596-599.

Timco, G.W and Frederking, R.M.W. (1990). Compressive strength of sea ice sheets. *Cold Regions Science and Technology*, (17): 227–240.

Truskov, P.A., Surkov, G.A. and Astafiev, V.N. (1996). 3-D variability of the sea ice uniaxial compressive strength. *In Proc. of the 13th Int. Symp. on Ice (IAHR)*, Beijing, China, pp. 94-101.

Wang, Y.S.(1981). Uniaxial compression testing of the Arctic sea ice. *In Proc. of the 2nd Int. Conf. on Port and Ocean Engineering under Arctic conditions (POAC)*, Quebec, Canada, pp. 346–355.

In Proceedings of the 25th International Conference on Offshore Mechanics and Arctic Engineering (OMAE), 2006, Paper No. - OMAE-92451

3.4 In-situ uniaxial compression tests of the level ice. Part II: Ice strength spatial distribution

Svetlana Shafrova and Per Olav Moslet

The University Centre in Svalbard (UNIS),

Longyearbyen, Norway

Abstract

Part I of this paper describes in-situ field tests of ice strength estimation in relation to the different length scales. Part II deals with the spatial heterogeneity of the ice strength in landfast level ice for the different tests areas. The paper presents a statistical analysis of the ice strength distribution for a Point-area, for a line and for an area in the ice cover. The ice strength distribution for a Point-area varied seasonally. It was estimated in terms of the coefficient of variation about 24.9% at the end of the season. For the coldest months the ice strength variability was around 40%. For the test area the strength spatial variability for the ice samples from the certain ice depth below the ice cover surface was about 19.4% for warm ice and 35.8% for cold ice. The ice strength heterogeneity for a line was determined of 14.4% in case of warm ice.

Experimental set-up

General

The current field studies was carried out in order to investigate the spatial distribution of ice strength in landfast level ice. The test locations are shown in Fig. 1, and the description of the test programs is summarized in Table 1. These field studies can be divided into two groups A and B. Group A consisted of the test programs 3 and 4 in which, the aim was to analyze the ice strength heterogeneity through the whole ice thickness for a local ice area, hereafter is called a Point-area. A more detail analysis of the ice properties is given by Moslet (2007). Test 1 and Test 2, which were presented in Part I of this paper, together with the Test 5 and Test 6 constitute Group B. The goal of Part II is to estimate the horizontal spatial variability of the physical and mechanical ice properties and particularly of the ice strength for the different test areas. The portable compression equipment described in Part I and by Moslet (2007) was also used during these tests.

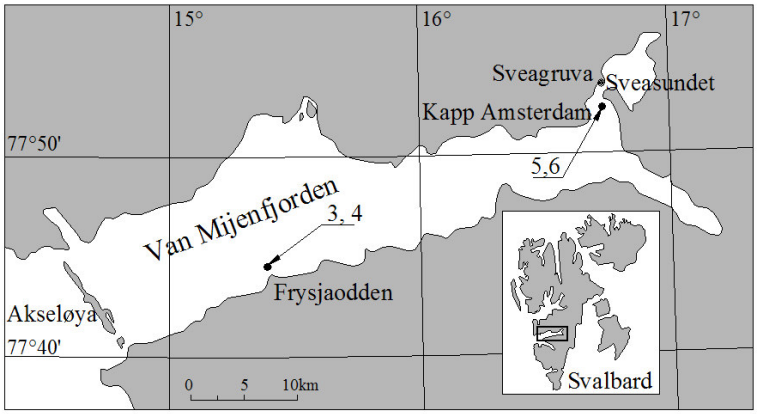

Fig. 1. The map of the test sites locations.
The sites are marked by the dots, number of site corresponds to the test number.

Table 1. Summary of the tests.

no.	Data	Location	Description	Depth[a]	Dir.[b]	n[c]
	Group A					
3.	1-2 May, 2004	Frysjaodden Van Mijenfjorden	Point-areas 1 and 2 4 differ. depths	0.2-0.8	V	86
4.	5-6 June, 2004	Frysjaodden Van Mijenfjorden	Point-areas 3 and 4 3 differ. depths	0.2-0.6	V	52
	Group B					
1.	21 March, 2004	Kapp Amsterdam Van Mijenfjorden	Area 10x10 m^2 step 1m	0.30	V	120
2.	7-8 April, 2005	Longyearbyen Adventfjorden	Area 3.13x3.13 m^2 step 0.78 m.	0.05	V	65
5.	20-21 April, 2004	Sveasundet Van Mijenfjorden	Area 150x150 m^2 step 25 m, Lines 150 m, step 25 m	0.30	V	77
6.	15-16 March, 2005	Sveasundet Van Mijenfjorden	Area 150x150 m^2 step 25 m	0.30	V	49

Note: [a] The depth is from the ice cover surface to the top of the sample, (m).
[b] The direction is either vertical (V) or horizontal (H).
[c] Number of compressed ice samples.

Group A

The ice cores were taken from a small area (< 0.25 m^2), which is called 'a Point-area'. Two different zones Point 1, 2 and Point 3, 4 were tested within Test 3 and Test 4 respectively. Ice cores from 4 different depths below the ice cover surface (0.2 m, 0.4 m, 0.6 m and 0.8 m) and 3 depths (0.2 m, 0.4 m, and 0.6 m) were cut out for the compression in Tests 3 and 4 respectively as shown in Table 1.

Group B

A detailed description including the map with the tests locations for the Test 1 and Test 2 were presented in Part I of this paper.

Test 5 and 6 investigated an area of 150x150 m^2 of the landfast ice sheet. The grid consisted of 49 sampling points with the horizontal distance (hereafter is called step) about 25 m between each point as shown in Fig. 2. As argued for in Part I the size of an area should be no less than 100x100 m^2, as at such size the heterogeneity over the area is commensurable with area of distribution of the stress-strain state zone arising from the ice-structure interaction (Seliverstov et al., 2001). Ice cores reaching from 0.3 to 0.5 m depth (hereafter called 0.3 m depth) below the ice cover surface were compressed. One ice core was taken at each sampling point. During Test 5, three ice cores from the same depth were taken as close as possible to each other for all sampling points in the lines 1/1-1/7 and 2/1-2/7 that corresponds to the two first lines along the x-axis (see Fig. 2).

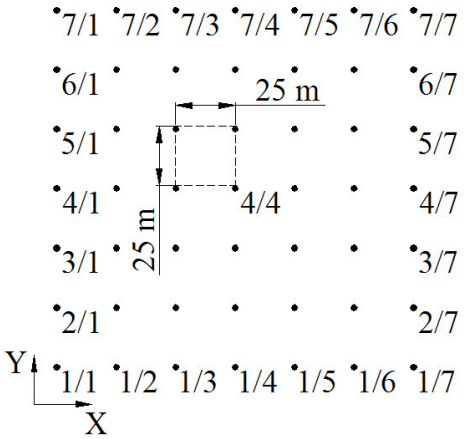

Fig. 2. Sampling area, Group B (Test 5 and 6).
The black dots are points of sampling.

Method

The ice strength distribution with respect to an absolute value is inconvenient to use. The ice strength is significantly affected by the physical properties of the ice, that continuously change in space and time. Thus, it is difficult to compare results from different field studies. The analysis of spatial ice strength variability were carried out according the idea presented by Surkov and Truskov (1993) and Truskov et al. (1996). The method is based on the representation of the ice strength as a relative value. Thus all data were recalculated in terms of relative values as:

$$\sigma_{rel} = \frac{\sigma_{ice}}{\sigma_{mean}}, \tag{1}$$

where σ_{rel} and σ_{ice} are the relative and absolute strength values for each test point.

σ_{mean} is the mean strength value of the current test series, MPa.

We assume that ice samples taken from the same ice depth had the same ice structure. Such samples for the current test area (Point-area, line or an area) were considered to be one sample series. Based on relative values the data for similar test areas for the separate test series can be summed together and formed a data block. Separate data series may be summed only when their variances are homogeneous. If so, the variability between the series is close to the variability within each series and as a result they corresponds to the same distribution and belongs to the same general population. The results of the sample tests for the Point-area (Group A) were subjected to analysis of variance, which shows that the values of the relative ice strength of separate test series belong to the same general population with a confidence probability of 0.95. The data obtained for the lines (Group B) was verified in the same way. Besides the both data sets (Group A and B) were satisfied to the Wilcoxon's test for the homogeneity of distributions (Box et al., 1978).

Furthermore verification for the presence of a trend between the variance and the mean value for ice strength in the separate data series were done. As an example the result for the lines 1/1-1/7 and 2/1-2/7 (Group B), where three ice cores were taken per each sampling point, is shown in Fig. 3. There is no correlation or trend between variance and mean ice strength. So, these data can be summed together and analysed by statistical method.

The results of the statistical analysis will be given as histograms of ice strength frequencies. The coefficient of variation (k_v), that is ratio of the standard deviation to the mean value, is assumed to be a measure of the ice strength heterogeneity. In addition the obtained histograms are characterized by skewness (S), which is a measure of degree of asymmetry of a distribution and excess (E), which is a degree of peakedness of a distribution.

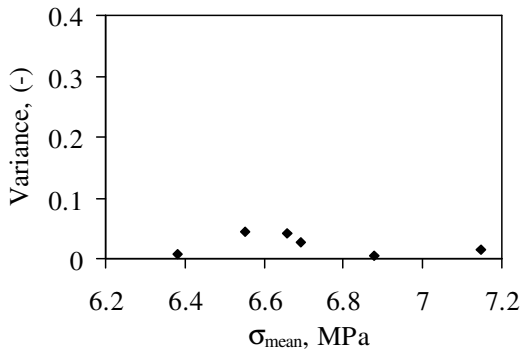

Fig. 3. Analysis of variance, Group B, Test 5 (Lines).
where σ_{mean} is mean value of the ice strength.

The following theoretical distributions were chosen in order to determine the best fit distribution law for the relative ice strength:

- normal, which characterized by mean value μ and variance σ^2
- t-location scale (scaled Student's distribution with υ degrees of freedom) with location parameter μ, scaled parameter σ and shape parameter υ
- gamma with parameters *a* and *b*
- lognormal with parameters μ and σ.

Results

Group A

The results of the statistical analysis as a histogram of the ice strength frequencies is given in Fig. 4. The symbols on the histogram represents the number of compressed ice samples (n) and coefficient of variation (k_v), skewness (*S*) and excess (*E*), which characterizes the current data set. The salinity of the ice samples was from 0.3 to 5.5 ppt. The temperature varied from -0.1°C to -2.4°C. In addition the ice strength variability for the Point-areas were analyzed in relation to the different depths. The results are summarized in Table 2.

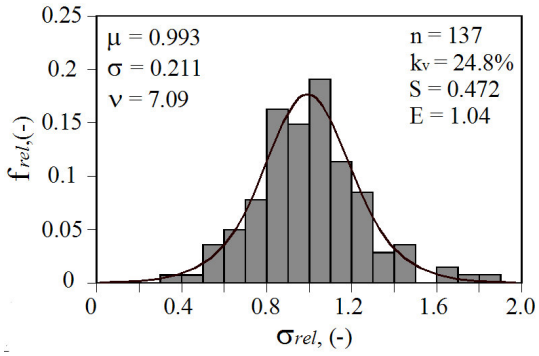

Fig. 4. Frequency histogram for relative ice strength for a Point-area, Group A, Test 3 and 4.

where n is the number of compressed ice samples, k_v the is coefficient of variation, S is the skewness, E is the excess; μ, σ, υ are the parameters of the t location-scale distribution.

Table 2. Ice strength variability for the different ice layers, Group A, Test 3 and 4.

	Test 3 Point-areas 1 & 2, May 2004			Test 4 Point-areas 3 & 4, June 2004		
Depth	n	$k_v(\sigma)$	σ_{mean}	n	$k_v(\sigma)$	σ_{mean}
0.20	21	31.8	1.43	15	33.1	1.27
0.40	23	24.6	4.22	15	23.7	0.85
0.60	20	16.7	6.30	21	28.6	2.09
0.80	22	16.5	5.99	-	-	

Note: The depth is from the ice cover surface to the top of the sample, (m).
σ_{mean} is the mean value of the ice strength, (MPa).
$k_v(\sigma)$ is the coefficient of variation of the ice strength, (%).
n is the number of compressed ice samples.

Group B

The maps of the absolute ice strength distribution from the uniaxail compression tests for the considered tests areas (Test 5 and Test 6 – 22500 m^2, Test 1 – 100 m^2, Test 2 – 10 m^2) are shown in Fig. 5, and the ice properties data for these test programs are summarized in Table 3. The absolute ice strength distribution and the corresponding frequency histogram based on the whole data set for the Test 1 is given in Fig. 6. The ice strength versus ice temperature for the Test 5 and Test 6 are given in Fig. 7. The results of statistical analysis for the test areas (Test 5 and Test 6) as a histograms are given in Fig. 8.

Table 3. Ice properties over considered test areas.

Test no.	T_{air} (°C)	σ_{ice} (MPa)			T_{ice} (°C)			S_{ice} (ppt)		
		min	max	mean	min	max	mean	min	max	mean
1	-2	2.26	11.9	6.40	-5.1	-3.5	-4.5	-	-	-
2	-15	3.60	8.05	6.18	-5.6	-2.9	-4.0	5.1	7.8	6.8
5	-6	3.23	10.7	6.28	-3.4	-2.3	-3.0	-	-	-
6	-18	2.97	12.6	6.35	-12.5	-5.7	-8.5	4.3	6.6	5.1

The ice strength variability versus corresponding ice temperature variability in terms of the coefficients of variation for the considered areas (Test 1, Test 2, Test 5 and Test 6) are shown on Fig. 9.

The air volume, brine volume and total porosity were determined for the each compressed sample from the Test 6. The air volume was in range of 0.28% to 1.54% for the brittle samples and from 0.2% to 5.6% for the ductile ones. The brine volume was varied from 2.3% to 3.7% and from 2.1% to 5.0% for the brittle and ductile samples respectively. The total porosity for the brittle and ductile samples was in range of 2.8% to 4.6% and from 2.9% to 7.9% correspondingly. The ice strength variability was higher for the brittle samples (k_v= 27.9%) than for the ductile samples (k_v= 22.9%).

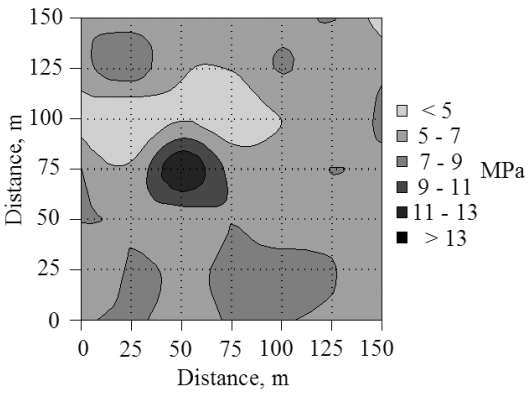

a) Test 5,
(Area 22500 m^2, step 25 m,
49 samples)

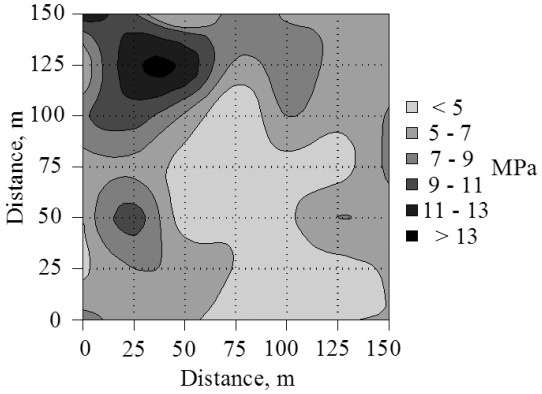

c) Test 6
(Area 22500 m^2, step 25 m,
49 samples)

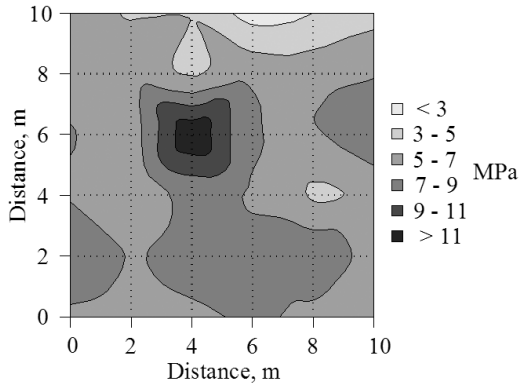

b) Test 1
(Area 100 m^2, step 2 m,
36 samples)

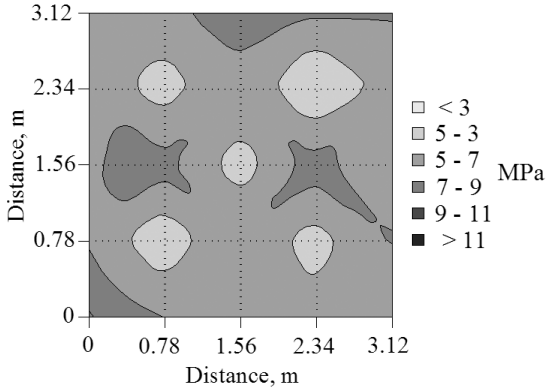

d) Test 2
(Area 10 m^2, step 0.78 m,
25 samples)

Fig. 5. The absolute ice strength distribution over areas, Group B.
Samples were taken at the points of intersections.

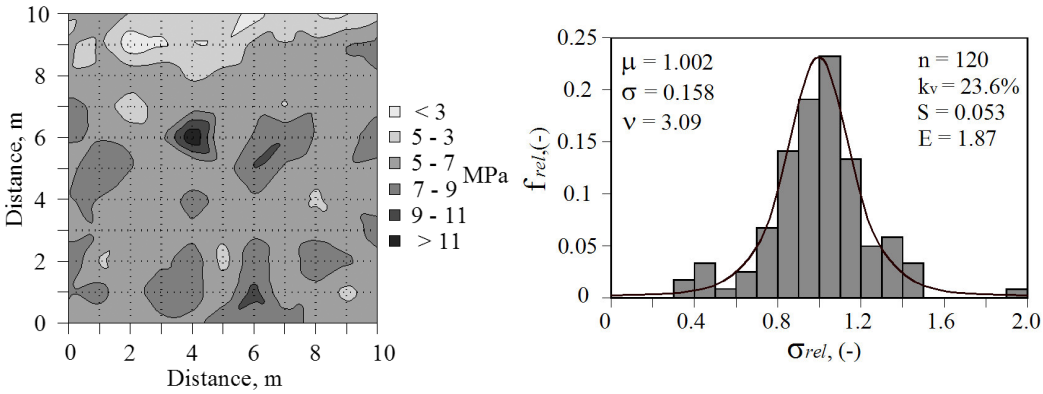

a) The absolute ice strength distribution
(Area 100 m^2, step 1 m, 120 samples)

b) Frequency histogram for the relative ice strength

Fig. 6. Ice strength distribution data, Test 1.
Samples were taken at the points of intersections

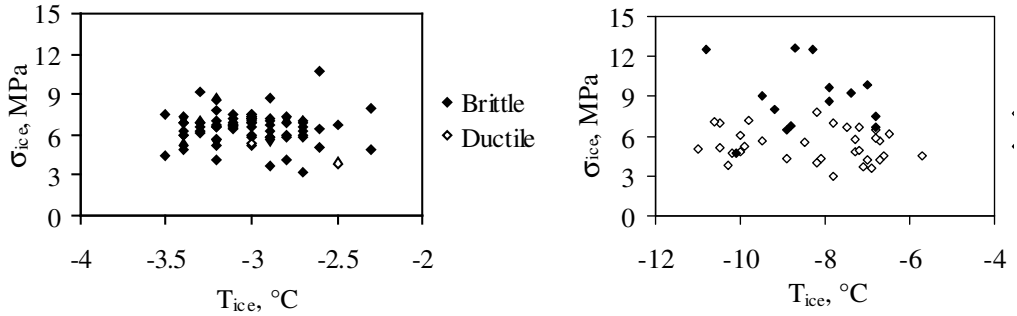

a) Test 5

b) Test 6

Fig. 7. Ice strength versus ice temperature, Group B.

In order to estimate the strength distribution along the line, three ice cores were taken per each sampling point in the two first lines (1/1-1/7 and 2/1–2/7) during Test 5. The result of this study is shown as a histogram in Fig. 10. The estimated coefficient of variation is 14.4%, which is less than 19.4% obtained for the corresponding test area (Fig. 8). Thus the ice strength heterogeneity decreases from an area to the line. The corresponding temperature variability for the line was about 6.1%, which is also less than 9.3% for the corresponding test area (Fig. 9).

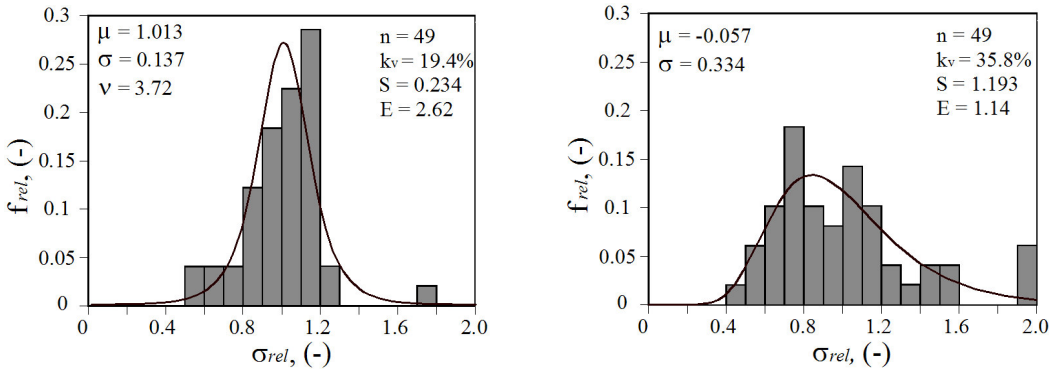

a) Test 5 b) Test 6

Fig. 8. Frequency histogram for the relative ice strength for an area, Group B.
where n is the number of compressed ice samples, k_v is the coefficient of variation, S is the skewness, E is the excess; μ, σ ,υ and μ, σ are the parameters of the corresponding t location-scale and lognormal distributions.

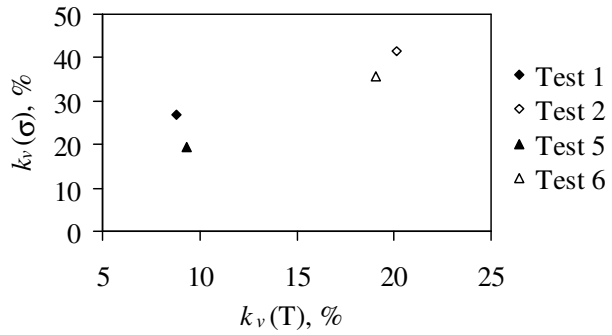

Fig. 9. Ice strength variability versus ice temperature variability for an areas, Group B.
where k_v(T) and k_v(σ) are the coefficients of variation of the ice temperature and ice strength.

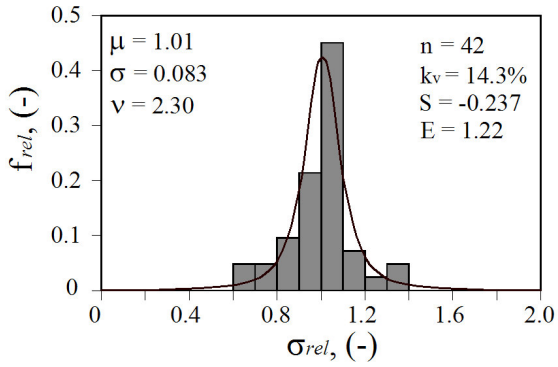

Fig. 10. Frequency histogram for relative ice strength for two first profiles, Test 5.

where n is the number of compressed ice samples, k_v is the coefficient of variation, S is the skewness, E is the excess; μ, σ, υ are the parameters of the t location-scale distribution.

Discussion

Group A

Four theoretical distributions (normal, t location-scale, gamma and lognormal) were chosen to determine the distribution law for the relative ice strength. The histogram in Fig. 4 is more similar to the symmetrical (normal and t location-scale) distributions than to the asymmetrical (gamma and lognormal) distributions. According to the coefficient of variation (24.8%) the normal distribution is more suitable as for such law k_v is equal to 24.9%. The t location-scale and gamma distributions have k_v of 25.1% and for the lognormal it is 26.3%. In respect to the skewness the gamma distribution is more suitable. In the view of the excess the lognormal law is better. In order to find the best fit theoretical distribution the Pearson's chi-squared and Kolmogorov-Smirnov goodness-of-fit tests were performed for the selected theoretical laws. The estimated parameters χ^2 and λ and corresponding probabilities of agreement of the chosen distributions to the empirical data are given in Table 4. Only the t location-scale distribution satisfy both of the tests criteria with the required probability (more than 0.1). So, the relative ice strength distribution for a Point-area is described by the t location-scale distribution with the location parameter μ= 0.993, the scale parameter σ= 0.211 and shape parameter υ= 7.09 as shown in Fig. 4.

Table 4. Results of goodness-of –fit analysis for a Group A (Test 3 and 4).

Distribution	χ^2_{crit}	χ^2	$P(\chi^2)$	λ_{crit}	λ	$P(\lambda)$
Normal	12.6	16.9	fail	1.36	0.775	0.586
t location-scale	11.1	5.02	0.413		0.475	0.972
Gamma	12.6	11.2	0.082		0.652	0.784
Lognormal	12.6	28.6	fail		0.852	0.465

The present results can be compared with the similar investigation done by Truskov et al. (1996) in Chaivo Bay. The 130 vertical ice cores from the different ice depths were tested under the in uniaxial compression for a Point-area. They reported that the relative ice strength distribution for the point is governed by a gamma-distribution law as shown in Fig. 11. This histogram is more flat and stretched along the x-axis compared to the our data. As a result the coefficient of variability of the ice strength obtained from Truskov et al. (1996) is equal to 42.2%, which is higher than our results of 24.9%. This can be explained by the temperature variation through the ice thickness. Our study was carried out at the end of the season and thus the ice temperature was in narrow range of -0.1°C to -2.4°C. As a result around 70% of the ice cores failed in ductile mode, which is proposed to be a predominate failure mechanism for the ice at the end of the season. Truskov's investigations were done during the cold season and the ice temperature variability was relatively high from -3°C to -13.4°C.

Based on our results (Fig. 4) and data from Truskov et al. (1996) (Fig. 11) it could be mention that the ice strength distribution for a Point-area varied seasonally. The ice strength variability is higher for the cold season because there is a stronger temperature gradient through the ice thickness. Therefore, the relative ice strength heterogeneity could be described by the asymmetrical lognormal or gamma theoretical laws. At the end of the season the ice is warmer and the temperature gradient through the ice thickness is weaker. As a result the ice strength variability for a Point-area decreases. So, the symmetrical t location-scale distribution become more suitable to determine the ice strength spatial variation at the end of the season.

Table 2 shows the ice strength variability versus ice depth for the Point-areas. It seems that the ice strength variability decreases from the top of the ice surface to the bottom. The higher variability (more than 30%) corresponds to the samples from 0.2 – 0.4 m depth below the ice cover surface. It looks reasonable, since the samples, which are closer to the ice surface are more affected by air and snow conditions.

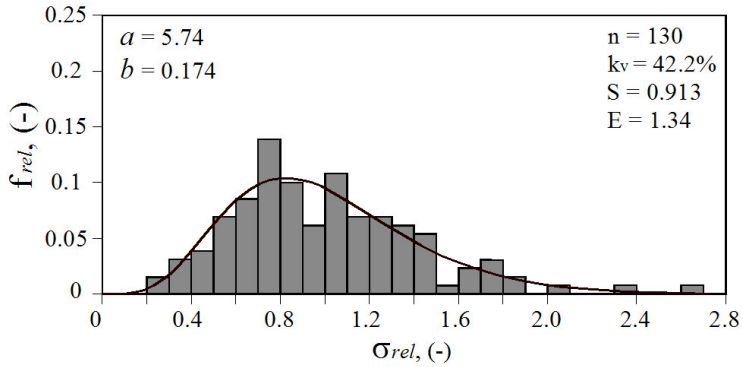

Fig. 11. Frequency histogram for the relative ice strength for a Point-area, after Truskov et al. (1996).

where n is the number of compressed ice samples, k_v the is coefficient of variation, S is the skewness, E is the excess, a, b are the parameters of the gamma distribution.

Group B

The absolute ice strength distributions over different test areas are given in Fig. 5. Three different test areas with dimensions of 150 m, 10 m and 3.12 m were shown. The ice strength variability for the 22500 m^2 areas was estimated in terms of the coefficient of variation $k_v(\sigma)$ about 19.4 % for the Test 5 and 35.8% for the Test 6. The variability is 26.8% and 41.4% for the 100 m^2 area (Test 1) and for the 10 m^2 (Test 2) correspondingly. In addition the absolute ice strength distribution for the 100 m^2 area based on 120 test results is presented in Fig. 6a. The variability was found of 23.6% for this data set. The dependence of the ice strength variability with reduction of the size of the area from 22500 m^2 to 10 m^2 was not found as shown in Fig. 12. The spots characterized by the local minimum or maximum values of the ice strength were observed in all cases as shown in Fig. 5. The ice properties and air temperature were similar for the both Test 5 and Test 1. The size of area for the Test 1 is 200 times less than for Test 5, but the strength variability observed during the tests corresponds to the same level. For 10 m^2 test area there are no clearly defined spots with the local maximum of the ice strength, but the variability itself is the highest one. This is probably a result of colder air temperature as discussed in Part I of this paper.

It seems that the ice strength heterogeneity resulted from the ice temperature variability. As shown in Fig. 9 the higher ice strength variability in the Test 2 and Test 6 corresponds to the high variation in the ice temperature data and the low variations were registered in case of the Test 1 and Test 5.

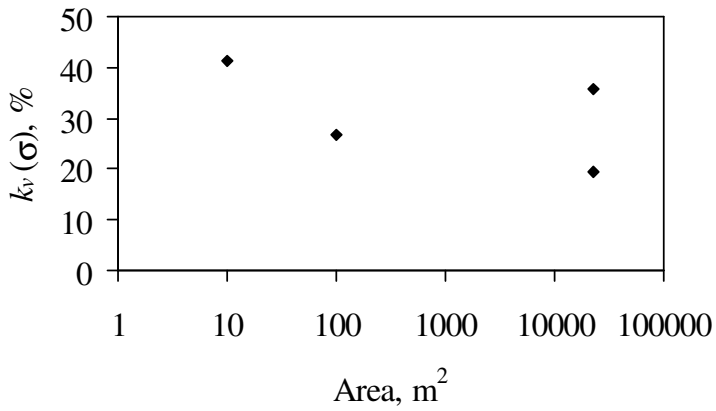

Fig. 12. Ice strength variability versus area.

where $k_v(T)$ and $k_v(\sigma)$ are the coefficients of variation for the ice temperature and ice strength.

Test 5 and 6 were done at Sveasundet in the Van Mijenfjorden in the 2004 and 2005 spring seasons respectively. The study areas during these tests were equal to each other. The mean values of the ice strength over these areas were 6.28 MPa and 6.35 MPa for the Test 5 and Test 6 correspondingly. But the ice strength distribution from the Test 5, which was carried out at the end of April, is more homogenous than from the Test 6 that was conducted at the middle of March as shown in Fig. 8. It could be explained by several factors.

Firstly, it is probably results from the temperature difference between the compressed ice and air during testing. As mentioned in Table 3 the air temperature during the Test 5 was -6°C and the compressed ice samples were quite warm and had uniform temperature around -3°C. For Test 6 the air temperature was -18°C. The ice itself was colder and its temperature ranged from -5.7°C to -12.5°C. The high temperature variation of the ice cores from the same depth could be explained by the presence of snow. Unfortunately, the snow depth, was not measured during testing. From the other point of view, the air temperature was colder than the ice temperature. Thus some ice cores may be cooled down slightly prior compression and this may increased the strength of the ice samples and as a result increased the ice strength variability.

Secondly, the brittle failure mode were predominant for the ice samples of the Test 5 as shown in Fig. 7a. Only two ice cores failed in ductile manner. (For the failure mode descriptions see Part I of the paper). For the Test 6, 60% of the ice cores failed in brittle manner and the rest correspond to the ductile failure mode. So, it was

observed that in case of the single failure mode the ice strength variability is less to compare to the situation where ice were failed into the different failure modes.

Furthermore in case of the Test 6 the ice strength variability was higher for the brittle samples (k_v= 27.9%) than for the ductile samples (k_v= 22.9%) (Fig. 7b). This was also found by Høyland (2007) for the ice ridges in the Barents Sea. The higher strength variability for the brittle samples seems reasonable as brittle failure depends on the local stress and strength distribution of the ice sample. So, the brittle failure is more erratic.

Finally, during Test 5 the compression equipment were operate by a single person. It was done in order to avoid effect of operator sensitivity. During Test 6 several persons were involved into the compression process. It seems that the ice strength heterogeneity from the Test 6 was slightly overestimated due to the weather conditions and operator sensitivity effect.

The brittle failure was found a predominant mode for the Test 5 as only two ice cores failed in ductile manner (Fig. 7a). It seems very interesting. Because the ice itself was relatively warm (average ice temperature of -3°C). Moslet (2007) found that there is no clear connection between ice temperature and corresponding failure mode. Our data from the Test 6 (Fig. 7b) shows the same. He was found that for the level ice the air volume was a critical value for the brittle-to-ductile transition and brittle behaviour occurred only when the air volume was below 7%. This means that for such condition no crack could propagate far enough to cause total failure of the ice sample. Our results from Test 6 are satisfied to this criteria. As given above all brittle samples had air volume less than 2% and total porosity less than 5%. Furthermore Høyland (2007) was also found that for the ice ridges the brittle failure was occurred basically for the low porosities. But he suggests that the transition from the brittle-to-ductile seemed to be more sensitive to the brine volume than to the air volume. We found no threshold neither for the brine volume nor for the temperature in the Test 6.

It seems that for the cold ice the temperature is a major contributor that affected the failure mode as the cold ice usually failed in a brittle failure mode. But in case of warm ice the air and brine volume became more important than the ice temperature. Unfortunately, we have no data about the porosity of the ice samples for the Test 5 in order to prove it. But we believe that the air volume and ice porosity itself were quite low that were suitable for the rapid crack propagation and as a result for the brittle failure of the ice samples.

Group A and B

The distribution laws for the relative ice strengths were determined for the different test areas as shown in Figs. 6b, 8 and 10. At the initial step the four theoretical distribution laws (normal, t location–scale, gamma and lognormal) were chosen. Then

based on the Kolmogorov-Smirnov test the distribution, which best fits to the data set, was determined. The results of goodness-of-fit analysis for the best fit distributions for the different test areas and lines are summarized in Table 5.

We found that the relative ice strength distribution is fitted by the symmetrical t location-scale distribution for the data sets with a coefficient of variation k_v (σ) less than 30% as shown in Figs. 8a and 10 for the Test 5 and in Fig. 6b for the Test 1. For more randomly distributed data the suitable theoretical law change over to the more asymmetrical lognormal distribution as shown in Fig. 8b for the Test 6.

Table 5. Results of goodness-of –fit analysis, Group A and B.

Test	Best fit distribution	$\lambda_{critical}$	λ	P(λ)
Test 5 (area 150x150 m, n=49)	t location-scale	1.36	0.715	0.685
Test 6 (area 150x150 m, n=49)	Lognormal		0.419	0.945
Test 1 (area 10x10 m, n=121)	t location-scale		0.467	0.975
Test 5 (lines 150 m, n=42)	t location-scale		0.441	0.984

Conclusions

Different types of in-situ uniaxial compressive tests programs have been performed in order to investigate the spatial variability of the ice strength for a Point-area, for a line and for an area in the first-year landfast sea ice. The following conclusion can be made so far:

- The ice strength distribution for a Point-area through the whole ice thickness was subjected to the seasonal variation. It was higher for the cold ice at the beginning of the season and became less for the warm ice at the end of the season.
- For the Point-area the ice strength variability over the layer decreased from the top of the ice cover surface down to the bottom of the ice.
- The dependence of the ice strength variability with the reduction of the size of the area of the ice cover from 22500 m^2 to 10 m^2 was not found.
- It was observed that the ice strength heterogeneity corresponds to the ice temperature variability. The strength variability over the area of the ice cover was less for the warm ice than for cold one. The degree of the ice strength variability was found about 35% for cold ice and around 20% for the warm ice for the ice samples from certain depth below the ice cover surface.

- The ice strength spatial variability increased from a line to an area for the certain depth below the ice cover surface.

Acknowledgement

We would like to thank the students of Arctic Technology department at UNIS springs of 2004 and 2005. We are grateful to all participants and contributors, especially to Basile Bonnemaire, Janne Valkonen and Rinat Kamalov. The encouragement and help from Knut V. Høyland and Sveinung Løset is greatly appreciated.

References

Box G.E.P., Hunter, W.G. and Hunter, J.S. (1978). Statistics for experiments. John Wiley and Sons, Inc, New York, 654p.

Høyland, K.V. (2007). Morphology and small-scale strength of ridges in the North-western Barents Sea. *Cold Regions Science and Technology*, (48): 169-187.

Moslet, P.O. (2007). Field testing of uniaxial compression of columnar sea ice. *Cold Regions Science and Technology,* (48): 1–14.

Seliverstov, V.I., Gomolski, S.G., Farafonov, A.E. (2001). Experimental studies of ice cover inhomogeneity. *In Proc. of the 11th Int. Offshore and Polar Engineering Conference (ISOPE)*, Stavanger, Norway, Vol. 1, pp. 744-748.

Surkov, G.A. and Truskov, P.A. (1993). Analysis of spatial heterogeneity of ultimate ice compressive strength. *In Proc. of the 3rd Int. Offshore and Polar Engineering Conference (ISOPE)*, Singapore, Vol. 2, pp. 596-599.

Truskov, P.A., Surkov, G.A. and Astafiev, V.N. (1996). 3-D variability of the sea ice uniaxial compressive strength. *In Proc. of the 13th Int. Symp. on Ice (IAHR)*, Beijing, China, pp. 94-101.

4 INFLUENCE OF ICE STRENGTH HETEROGENEITY ON ICE LOADS

4.1 Introduction

This chapter presents the numerical study of heterogeneous ice field/structure interaction processes. The load dependence on the ice strength heterogeneity was investigated. The motivation behind this study was the following:

1. To improve the knowledge of the ice loads dependence on the ice strength spatial heterogeneity. So far, the dependence of the ice loads on the scale (size of structure) as a result of the ice field strength non-homogeneity effect has not been considered in detail yet.

2. To study the influence of the ice strength heterogeneity on the ice loads and to investigate the all phenomena that accompanies the process of interaction. It can be important for the ice loads estimation on the structures of the different size under the given probability of exceedance.

The scale effect is a very important factor for evaluation of full scale loads on the structure. Different factors can account for the dependence of the ice loads on a scale. One of the factors, which may be responsible for this effect, has been poorly studied so far. This is an in-plane nonhomogeneity of the entire ice field property.

Weibull, Freidental and others developed a statistical theory of the scale effect. This theory was usually applied to explain the ice strength dependence on the sample size and volume. It was proposed that the greater material volume is , the higher is the probability for weak points to occur.

It was found that weak zones existed in situ in the ice field. It is evident that under these conditions the probability for a weak zone to be found in the ice field is significantly higher for the wide structure (e.g. 70-100 m) than for the narrow one. The failure starting at a weak point in the ice field diminishes the ice resistance to the structure penetration. Therefore the effective pressure (load divided by the structure width and ice thickness) may be lower for the wide structure than for the narrow one.

The chapter consists of one paper and is almost identical to the referred paper with some misprints corrected. Prof. Karl N. Shkhinek is the principal author of this paper.

Publication reference:

(4.2) Shkhinek, K., Blanchet, D., Jilenkov, A., Shafrova, S. (2007). Ice loads dependence on the field heterogeneity. In Proceedings of the 19th International Conference on Port and Ocean Engineering under Arctic conditions, (POAC), Dalian, China, Vol. 1, pp. 245-255.

4.2 Ice loads dependence on the field heterogeneity

Shkhinek, K[1]., Blanchet, D[2]., Jilenkov, A[1]., Shafrova, S.[3]

[1]*Saint-Petersburg State Polytechnic University, Russia*

[2]*BP, Houston, Texas, USA*

[3] *The University Centre in Svalbard, Norway*

Abstract

The influence of the ice strength heterogeneity on loads was considered in this paper. The special Finite Difference program "Inhomogeneity" was developed for investigation of this phenomenon and wide range of numerical experiments were conducted. It was shown that the ice heterogeneity might be one of the reasons of the scale effect. Some other effects: optimal ice management and influence of ice properties on the normal stress distribution over the structure surface were considered also.

Introduction

Investigations that were conducted recently (1991-2006) in the different regions (Northern Sakhalin, Spitsbergen area and Arctic Ocean, Vladivostok) showed the significant in-plane heterogeneity of the ice strength both for the landfast and for the drift ice. The results of the published field studies was summarized by Shafrova and Høyland (2007) and given in Table 1. One can see that the strength deviation from the average value in different locations of the ice field can reach several times. The horizontal dimensions of areas with the maximal strength may be as high as 50-60 m (Fig. 1).

It is evident that this heterogeneity will influence the ice loads but it is difficult to predict beforehand the level of this influence for the structures of different size. The problem has been poorly studied so far and the available (published) information is scarce. Because of the complexity of the problem, it is difficult to model the phenomenon in the ice tank and to obtain an analytical solution. The generally used numerical complexes do not offer an adequate means to describe this phenomenon, which requires the development of a special PC program. A 2D computer Finite Difference program "Inhomogeneity", which gives possibility to determine the load dependence on the ice strength heterogeneity, has been developed.

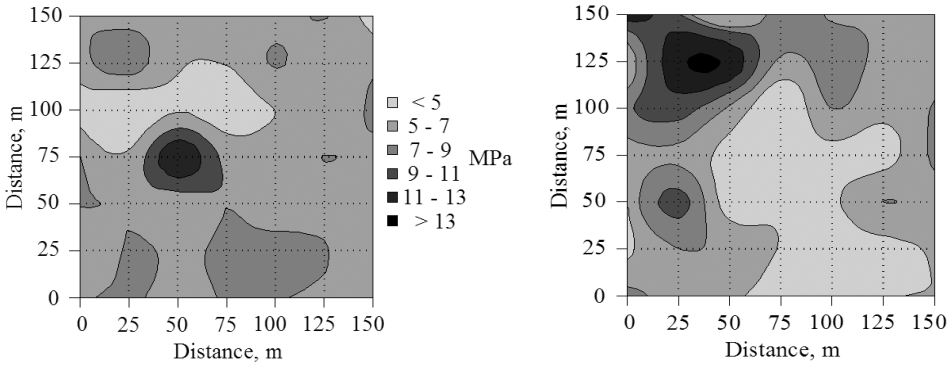

a) March, 2004 b) April, 2005

Fig. 1. Unconfined strength variation in space (after Shafrova & Moslet, 2006).

Computer program

The problem statement

An ice field (Fig. 2) with length W is considered. The field width (S) can be limited or unlimited. The border Y=W at the time moment t=0 begins to move with the constant velocity U_0. The center of the cylindrical structure with diameter (D) is located at any distance B from the origin of coordinates. Some inclusions are located in the field as well. Number of inclusions is limited only by a reasonable sense. Each inclusion has the elliptical form with the definite axis and angle of inclination of the main axis to horizon. Positions, dimensions and properties of inclusions can be set stochastically or probabilistically. The stress/strain field, the ice particles velocity and the total load on the structure as well as the failure process induced by interaction are determined in solution.

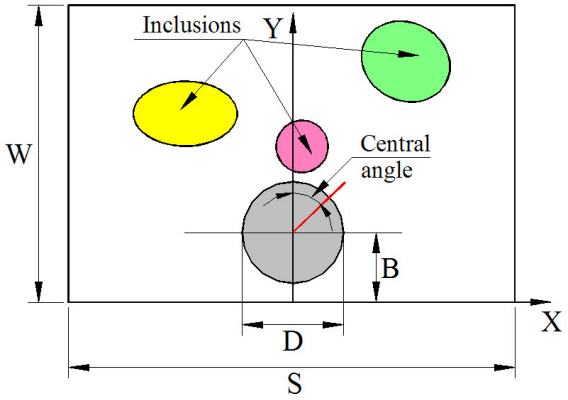

Fig. 2. The principal scheme for calculations.

Table 1. Key data on ice strength in-plane distribution (Shafrova & Høyland, 2007).

Author(s)	Type of ice and location	k_v (%)	Strength variation	D[1]	n[2]	Comments
Surkov & Truskov, (1993)	Landfast ice, Chaivo Bay	45	< 3 times	V	125	Line 100 m, step 10 m, 2-4 depths
Takeuchi et al. (1995)	Landfast ice, lake Saroma	26	> 3.5 times 0.6-2.2 MPa	H	256	Line 38 m, step 0.15 m, 1 depth
Truskov et al. (1996)	Drift ice, Sakhalin	-	< 3 times 1.3-3.7 MPa	V	125	Cross 100x100 m, step 20 m, 5 depths
Farafonov (2006)	Landfast ice, Amur Bay	8-45	1.5-8 times 0.73-9 MPa	3)	536	8 areas 100x100m^2 step 0.39 - 25 m
		-	5-7 times 0.4-4.4 MPa	V	28	Cross 160x160 m, step 20 m, 2 depths
Shafrova & Moslet (2006)	Landfast ice, Spitsbergen fjords	41	> 2 times 3.6-8.1 MPa	V	25	Area 3x3 m^2, step 0.78 m, depth 0.05 m
		27	> 5 times 2.3-12 MPa	V	36	Area 10x10 m^2, step 2 m, depth 0.3 m
		20-36	3-4 times 3.2-13 MPa	V	98	2 areas 150x150m^2, step 25 m, depth 0.3 m
Shafrova & Høyland (2007)	Drift ice, Arctic Ocean	30-55	2.5-4 times 0.58-7 MPa	V	41	Lnes 10m, step 1m, 3-4 depths
		20-38	1.7-5 times 0.35-1.8MPa	H	41	

[1] The direction of ice samples is either vertical (V) or horizontal (H).
[2] Number of compressed ice samples.
[3] Express method, drop ball test.

The main equations

Commonly used equations of the solid mechanics are considered. For the 2D phenomenon they are written in the form (i,j =1, 2):

Conservation of mass:

$$\rho V = \rho_0 V_0 \tag{1}$$

Conservation of momentum:

$$\rho \frac{dU_i}{dt} = \frac{\partial S_{ij}}{\partial x_j} - \frac{\partial P}{\partial x_i} \tag{2}$$

The constitutive equations for the ice are used in the following form:

$$\frac{DS_{ij}}{Dt} = 2G\left(\dot{e}_{ij} - \frac{1}{3}\dot{e}_{kk}\delta_{ij} - \dot{\lambda}S_{ij}\right) \tag{3}$$

$$\frac{dP}{dt} = -K\left(\dot{e}_{kk} - 2\Lambda\dot{\lambda}\tau\right), \tag{4}$$

where

$$\dot{e}_{ij} = \frac{1}{2}\left(\frac{\partial U_i}{\partial x_j} + \frac{\partial U_j}{\partial x_i}\right) \tag{5}$$

is the strain rate tensor.

Summation is made on the recurring index and the following indications are used:

$x_1 \equiv x, \quad x_2 \equiv y;$ ρ, ρ_0 are the ice density in the current and the initial states;

V, V_0 are the volume of the cell in the current and the initial states; U_i is the projections of the velocity vector on the axis x_i of the global system of coordinates;

t is the time; G is the shear modulus, that depends on pressure; K is the bulk modulus, that depends on pressure and loading conditions: $K = K_n$ during loading ($dP > 0$) and $K = K_r$ during unloading ($dP < 0$); $\frac{D}{Dt}$ is the Jaumanns derivative; Λ is the velocity of dilatancy, that depends on pressure (it was proposed equal to zero in numerical experiments); $\tau^2 = \frac{3}{8}S_{ij}S_{ij}$ is the intensity of the shear strength; $\dot{\lambda}$ is the factor to be determined from the conditions that the stress is on the ultimate strength surface (otherwise $\dot{\lambda}$=0); σ_{ij} is the Cauchy stress tensor.

The components of the stress tensor are considered as a sum of components of the spherical tensor and of the tensor deviator, so they can be written as following:

$$\sigma_{ij} = -P\delta_{ij} + S_{ij}, \tag{6}$$

where $P=-\sigma_{kk}/3$ is the pressure; δ_{ij} is the Kroneker's symbol ($\delta_{ij} = 0$ if i ≠ j; $\delta_{ij} = 1$ if i=j).

The plane stress conditions are proposed.

Boundary conditions:

$$\sigma_y = \sigma_{yx} = 0 \text{ at Y=0, } U=U_0 \text{ at } Y=W. \tag{7}$$

If the field dimensions in the direction X are not bounded then the conditions (7) are replaced by the more complicated.

Conditions on the structure surface are:

$$U_{nn}=0,\ \sigma_{n\theta} = f\sigma_{nn}, \tag{8}$$

where U_{nn} is the velocity normal to the structure surface, $\sigma_{n\theta}, \sigma_{nn}$ are the shear and normal stress on the structure border, f is the ice /structure friction coefficient.

The failure criteria

Compressive failure: The main equations of the compressive failure criterion are used in the Mohr-Coulomb form:

$$\sigma_3^{\,f} = -R_c + K_1\sigma_1,$$
$$K_1 = (1+\sin\varphi)/(1-\sin\varphi), \tag{9}$$

where σ_1 is the maximal principle stress (compressive stresses are negative), σ_3^f is the minimal principle stress on the failure surface, R_c is the unconfined strength, φ is the ice angle of internal friction.

If the ratio σ_3/σ_1 reaches some limit (Sanderson (1988), p. 96) then the Tresca law replaces the Mohr-Coulomb one. During the unloading process (in cell), the ice strength moves step by step to the residual state.

Criteria of the tensile failure: It was proposed that the tensile failure takes place if the maximal principle stress reaches the tensile strength σ_t. As soon as the criterion of the tensile failure is reached then the maximal principle stress is proposed to be zero.

Method of solution

The finite difference solution is used. The explicit method is applied, and the handling of the problem is based on the well-known Wilkins et al. (1973) methodology. The whole field is divided on the cells by the net and integration of the main equations (that shown above) is performed.

Some results of calculations

Two problems were considered: the influence of the ice field dimensions and the influence of the ice field strength heterogeneity on the loads.

Influence of the ice field dimensions

The ice load dependence on the ice field dimensions has its own engineering importance and is essential for the ice management. It is useful (as it was done during the KULLUK exploitation) to divide the big ice field into the smaller blocks which action induces lower loads. But if these blocks are too small and generate the negligible loads then a lot of the icebreakers energy will be wasted without great effect. Special numerical experiments were conducted to determine the load sensitivity to the field dimension. The experiments were carried out for structures of two diameters differed two-fold. The effective pressure (the load divided on the structure diameter and the ice thickness) versus the field width to structure diameter ratio (*S/D*) are plotted in Fig. 3. These results demonstrate that diminishing of the ice field dimensions leads to the pressure reduction. Especially intensively the pressure decreases if $S/D < 7$. This information is useful with respect to ice management.

The influence of ice strength heterogeneity on the loads

The structure interaction with the single inclusion was considered in this paper. This inclusion was located in the central part on the front side of the structure but on the different positions in relation to the structure surface. The properties of the whole (homogeneous) ice field and parameters of inclusions are given in Table 2 and Table 3, respectively.

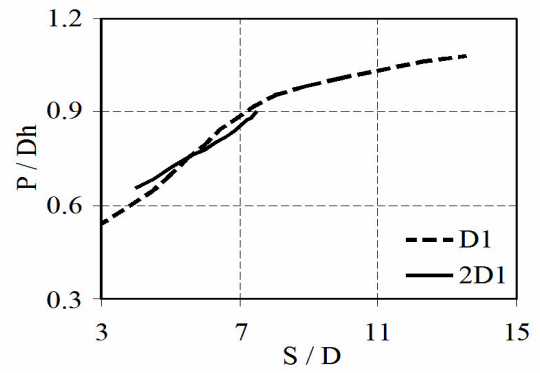

Fig. 3. Dependence of the average pressure over the structure surface on the ratio of ice field width to the structure diameter.

Table 2. Input data for calculations

Ice velocity	0.05 m/s
Ice thickness	1 m
Velocity of the longitudinal waves in ice	2800 m/s
Poisson's number	0.25
Angle of internal friction	30º
Unconfined strength (R_{ch})	1 MPa
Tensile strength (R_{th})	0.15 MPa
Ice/structure friction coefficient	0.2

Table 3. The inclusions property

a/D	2		1.0		0.5	
R_c, MPa	3	0.5	3	0.5	3	0.5
R_t, MPa	0.5	0.15	0.5	0.15	0.5	0.15

Here *a* is the dimension of the maximal axis of the inclusion. The cylindrical inclusions were considered in the current experiments. As only unconfined strength was measured in the field, this parameter varied in the numerical experiments. The failure pattern for the a/D=2 in case of R_c/R_{ch} =0.5 (a) and R_c/R_{ch} =3 (b) are shown in Fig. 4. One can see that the failure patterns significantly depend on the inclusion properties. If inclusion is weak then the failure develops basically inside the inclusion. The sliding lines (shear failure) form system usually shown in the theory.

The inclusion defenses the structure because the residual strength of the pulverized ice is lower than the strength of the surrounding ice in field.

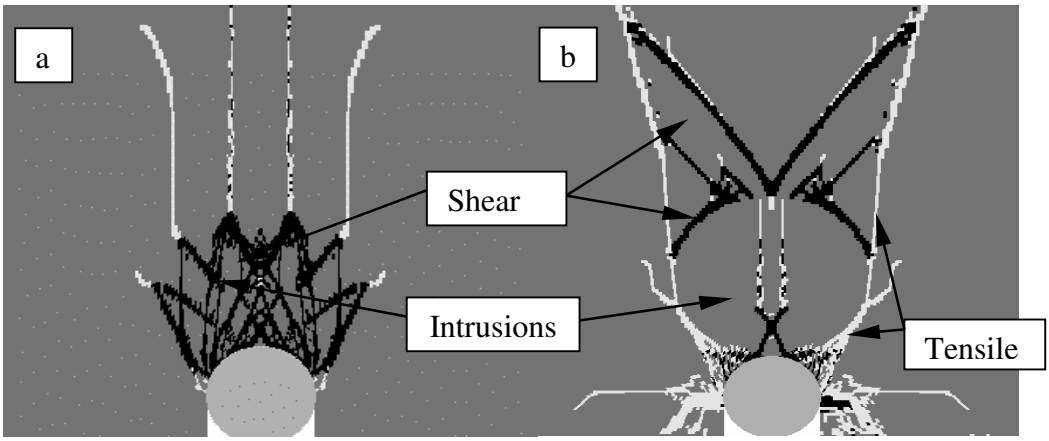

Fig. 4. The failure pattern *a/D*=2, (a) R_c/R_{ch} =0.5, (b) R_c/R_{ch} =3.

Tensile failure - white lines, shear failure – black ones.

On the contrary, there is about lack of failure inside the strong intrusion. The failure develops on its sides. The tensile failure takes place over the inclusion's side presented to the structure whereas the shear one occurs on the opposite side. In this case the loads are collected on the inclusion's outer side and transmitted to the structure. The inclusion's surface is greater than the structure's one. Therefore it collects the greater load and transmits it on the structure. The dependence of the non-dimensional total load (the ratio of the total load in the heterogeneous ice field (*P*) to the load in the homogeneous ice field (P_{homog})) versus the distance between centers of the inclusion and the structure (*L*) divided by the structure diameter (*D*) is presented in Fig. 5. One can see that the strong inclusion gives rise to the global load more than twice whereas the weak inclusion diminishes the load about 40%. It is interesting that the load depends not only on the strength level but as well on the relative structure/inclusion position. In order to understand this phenomenon the normal stress distribution over the structure surface should be analyzed. This distribution for three relative the structure/ inclusion positions is plotted in Fig. 6.

It can be seen in Fig. 6 that if *L/D*=0.5 (for *a/D* =2 this means that the inclusion envelopes the frontal part of the structure) then the load transmitted to the structure is distributed over the whole structure surface. Contrary at *L/D*=1.2 the same load is collected by the intrusion acts only on the central part of the structure surface. As the normal stresses on the side elements of the structure surface do not influence on the total load in the direction Y the load at *L/D*=1.2 is greater.

Similar analysis was done for other *a/D*. The maximal and minimal loads dependence on inclusions is collected in Fig. 7.

Ductile and brittle ice behaviour

Influence of the brittle and ductile ice behaviour was studied for homogeneous ice. The normal stress distributions over the structure surface (in the time moment corresponding to the maximal load) are plotted in Fig. 8. This figure explains why for the ductile ice the global load sometimes may be greater. Local loads are higher in the brittle ice.

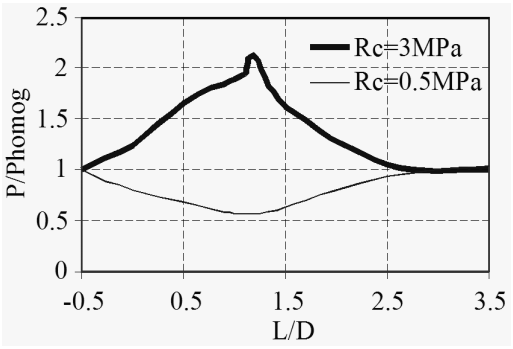

Fig. 5. The ice field heterogeneity influence on the loads.

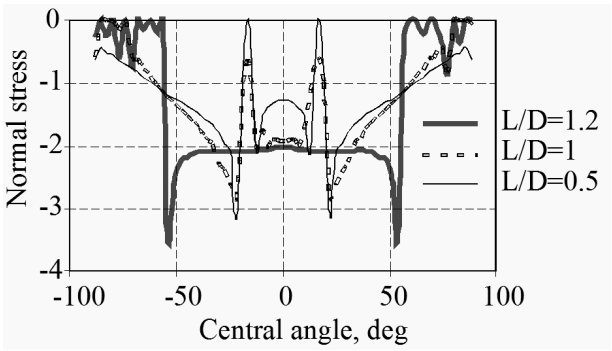

Fig. 6. Normal stress distribution over the structure surface at three relative structure/ inclusion positions. R_c=3MPa.

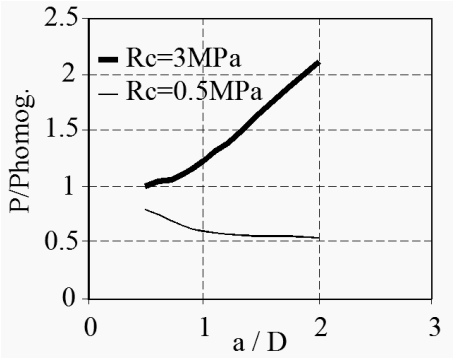

Fig. 7. The maximal and minimal influence of strong and weak inclusions on the ice load.

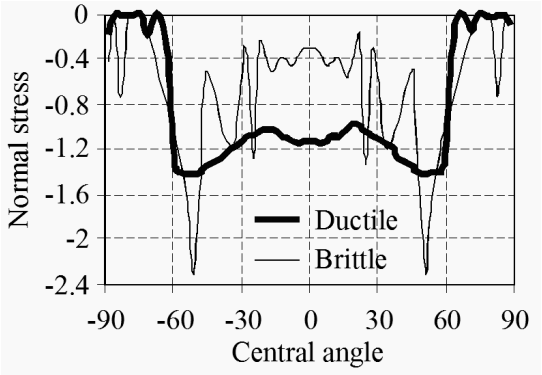

Fig. 8. Distribution of the normal stress over the contact area in the ductile and brittle homogeneous ice.

Discussion

The results, testify that the influence of the ice field strength heterogeneity on loads can be significant. For the considered cases and input data the load increased more than two–fold (for the strong inclusion) and decreased about 40% (for the weak inclusion). When the inclusion is stronger than the surrounding ice and is wider than the structure, then the ice failure by shear occurs over the inclusion's outer surface and by tension over the inner border. The inclusion collects the ice loads on its greater than structure's surface and transmits it to the more narrow structure. The external load from the surrounding ice acting on the inclusion does not depend significantly on the inclusion's position in relation to the structure. But the load transmitted to the structure and the stress distribution over the structure's surface depends on these objects position relative to each other. If the inclusion/structure contact area is large i.e. the inclusion envelops the structure, then the transmitted action is distributed over the greater contact area. This means that not only the central part of the structure but also its sides is loaded. On the contrary, if the common area is narrow the whole load is transmitted to the central part. This can be seen in Fig. 6. At L/D=0.5 the main pressures are located in the zone of the central angles ranged about $\pm(20\text{-}90)^{o}$, whereas for L/D=1.2 it appears in the ranges of $(0\pm55)^{o}$. But the pressure on the structure's sides does not lead to the significant increase of the total load in the Y-direction and mainly induces compression of the structure in the X-direction and also increases the friction force. At the same time if the contact area is small and located in the central part of the structure, then almost the whole action generated by the inclusion is concentrated in the central zone of the structure and acts about in the same direction.

The weak inclusion fails earlier than the surrounding ice and defenses the structure because after its failure the surrounding ice acts on the structure through the weak pulverized ice. Therefore the load on the structure reduces. The failure of the inclusion leads to the more evenly distribution of the pressure over the structure surface. Both the load increase due to the stronger inclusion existence and decrease due to the weaker one have a local character, typical for the particular location in the ice field, where inclusion is placed. Increase of the load in this particular place is important because the load corresponding to other positions of the structure is lower. But the local influence on loads of the weak inclusions can be ignored because the load in other places is higher than in this particular place.

The results obtained in this work show that the ice heterogeneity gives rise to the scale effect. It can be seen in Fig. 7. Let us assume that structures with diameters D=25 m and D=100 m interact with the same inclusion with a=50 m. For the smaller structure a/D=2. This means that for this particular case the loads on the small structure can increase more than two-fold whereas the load on the greater structure

(a/D=0.5) will not change. Finally the effective pressure on the smaller structure will be two times higher than the pressure on the wider one.

Conclusions

1. A numerical program for calculation of ice loads on structures located in heterogeneous ice was developed. This program gives the chance to estimate not only the influence of the ice heterogeneity on the global loads but also to consider all phenomena that accompanies the process of interaction.
2. The program was used in order to determine the load dependence on the homogeneous ice field dimension. It was shown that for reduction of the ice load on the structure the field should be divided into parts not bigger than 4-5 the structure diameter. This result may be used in operations for ice management.
3. Strong inclusion may increase the load significantly. For the current study the load increased twice. This happens because the inclusion collects the ice loads over its surface and transmits them to the structure.
4. Strong inclusions contribute to the scale effect. Structures of different dimensions interact differently with the same inclusion. The load on the small structure during its interaction with relatively narrow inclusion may arise whereas the load on the wide structure will not change. Therefore, effective pressure for the small structure will be large.
5. Weak inclusions may diminish the load but this diminishing has a local character and should not be taken into account because higher loads are met before or after this inclusion.

Acknowledgements

The authors would like to express their sincere thanks to the BP Company and professor Sveinung Løset (UNIS/NTNU) for support and funding this work.

Reference

Farafonov, A.E. (2006). Heterogeneity of the ice cover and its estimation for the ice loads evaluation on the sea water engineering constructions. Abstract of the Candidate of Science thesis. Far-East State Technical University, Vladivostok, Russia, 24p (in Russian).

Sanderson, T.J.O. (1988). Ice mechanics risks to offshore structures. Graham and Trotman, London, 253p.

Shafrova, S. and Moslet, P.O. (2006). In-situ uniaxial compression tests of level ice. Part II: Ice strength spatial distribution. *In Proc. of the 25th Int. Conf. on Offshore Mechanics and Arctic Engineering (OMAE)*, Hamburg, Germany, OMAE-92451, 10p.

Shafrova, S. and Høyland, K.V. (2007). Morphology and 2D spatial strength distribution in two Arctic first-year sea ice ridges. *Cold Regions Science and Technology,* doi:10.1016/j.coldregions. 2007.05.011.

Surkov, G.A. and Truskov, P.A. (1993). Analysis of spatial heterogeneity of ultimate ice compressive strength. *In Proc. of the 3rd Int. Offshore and Polar Engineering Conference, (ISOPE)*, Singapore, Vol. 2, pp. 596–599.

Takeuchi, T., Akagawa, S. and Iwai, T. (1995). On the distribution of strength of in-situ sea ice sheet. *In Proc. of the Civil Engineering in the Ocean Conference,* Vol. 11, pp. 241-245 (in Japanese).

Truskov, P.A., Surkov, G.A., Astafiev, V.N. (1996). 3-D variability of sea ice uniaxial compressive strength. *In Proc. of the 13th Int. Symp. on Ice (IAHR),* Beijing, China, pp. 94-101.

Wilkins, M.L. French, S. and Sorem, M. (1973). Finite-difference scheme for solving the 3D problems depending on time. Chislennie methody v hydromechanike, pp. 115-119 (in Russian).

5 SMALL SCALE TESTING OF ICE RUBBLE PROPERTIES

5.1 Introduction

This chapter presents field and laboratory test results of thermo-mechanical properties of ice rubble with particular focus on the strength of the freeze bonds in between the ice blocks. The motivation for this work was the following:

1. To improve the knowledge about strength of the freeze bonds.
2. To study the strength of freeze bonds and the local strength of ice blocks in the ice rubble. The main point is how these values are affected by different factors such as time of submerging, size of the ice blocks, confining pressure and initial properties of the ice. These data are vital for the numerical simulation of the ice rubble deformation behaviour that is described in Chapter 7.

The nature of freeze bonds is not well known yet. It is obvious that the ice blocks within an ice ridge can easily freeze to each other at the points of contact forming the freeze-bonding boundary between separate ice blocks. But how strong is this boundary compared to the surrounding submerged ice blocks that formed the boundary? Furthermore the freeze-bonds develop through the lifetime of the ridge, increasing during the initial phase and thereafter decreasing as the rubble is eroded. So, it would be useful to know how much time it takes before the maximum value is reached, how high it becomes and how fast it decreases thereafter.

The chapter consists of one paper that is identical to the referred paper.

Publication references:

(5.2) Shafrova, S. and Høyland, K.V. (2007). Thermo-mechanical properties of ice rubble. Freeze-bond experiments. Submitted to Journal of Cold Regions Science and Technology.

5.2 Thermo-mechanical properties of ice rubble. Freeze bond experiments

Svetlana Shafrova[1] and Knut V. Høyland

The University Centre in Svalbard (UNIS), Longyearbyen, Norway

Norwegian University of Science and Technology (NTNU), Trondheim, Norway

Abstract

The strength of freeze-bonds in-between blocks in first-year ridges has been investigated through field and laboratory tests. A series of small scale field tests with submerged ice blocks were carried out in Adventfjorden on Svalbard in March-April 2005. An opening was made in the landfast level ice and the ice was sawed into cubes with dimensions of 0.24 m. Some of the cubes were cut in two parts and then frozen together to simulate freeze bonds between the ice blocks. The other blocks were submerged without forming adfreeze bonds. In addition to that, laboratory tests with both laboratory made layered (fresh- and seawater) and sea ice were conducted in February-April 2006 at UNIS. The strength of the freeze bonds, the strength of the submerged ice blocks and their changes with time of submerging, confining pressure, block size and physical properties of ice were investigated. The average strength of freeze bonds was found to be 0.032 ± 0.018 MPa after 48 hours of being submerged in the field. The corresponding values from the laboratory tests were 0.067 ± 0.052 MPa for the sea ice testing and 0.274 ± 0.142 MPa for the laboratory made layered freshwater ice up to 60 hours of being submerged. The initial physical properties of ice, the confining pressure applied to the ice pieces before and during submerging together with the size of the ice blocks are the main parameters that affect the freeze bond strength. Besides the correlation between physical and mechanical properties of submerged ice was registered.

Key words: Ice rubble; Properties; Freeze-bonding strength.

[1] Corresponding author.
E-mail address: svetlana.shafrova@unis.no

1. Introduction

Ridges are common ice features in the Arctic, they move due to wind and sea currents and may cause loads to offshore structures. In the Arctic region, first-year ice ridges and icebergs govern the design load level for such structures. The ridge load on structures depends on external parameters such as geometry of the ice features and ice drift, and internal parameters such as the internal structure of the ridge and its mechanical characteristics.

Ice ridges are often divided into two parts: a sail and a keel. Typically, the sail consists of ice blocks, snow and voids filled with air and snow. The keel consists of a consolidated layer of refrozen ice and unconsolidated or partly consolidated ice rubble beneath. During the initial phase of the consolidation process the ice blocks freeze to each other at the points of contacts and form freeze bonds. Thus, typically an ice ridge is a mixture of ice blocks (that make up the ice matrix), slush, water and air between them. The unconsolidated part (the rubble) is important in many practical applications such as sea-bed scouring, but neither the mechanical behaviour nor the processes determining them are well understood. We suggest that they are basically governed by the following:

- The strength of the freeze bonds between the ice blocks
- The dimensions and orientation of the ice blocks
- The strength of the submerged ice in the rubble.

When ice rubble deforms, we suggest that at least three different physical mechanisms can take place:

- Failure of the freeze bonds
- Rotation and rearrangement of the ice blocks
- Failure of the ice blocks themselves.

Ettema and Urroz (1989) discuss the freeze bonds, and argue that they govern the initial strength of ice rubble. They further state that these bonds get broken during the initial stage of interaction. Surkov and Truskov (1993) and Surkov et al. (2001) conducted experiments where small cubic models of ridged ice were made from the natural sea ice. They compressed these models uniaxially and found that the failure often took place along the freeze bonds.

Shafrova et al. (2004), Liferov (2005) and Shafrova (2007) conducted numerical simulations of ice rubble with a pseudo-discrete continuum model and treated the rubble as a combination of ice and voids. Contact elements joined the ice block elements and simulated the freeze bonds. The mechanical properties of these contact

elements were different from those of the ice blocks. In those numerical simulations, the initial failure of the rubble was also associated with the freeze bond failure.

Liferov and Bonnemaire (2005) analyzed in-situ punch tests of ice rubble and concluded that the initial failure of the ice rubble corresponds to the peak load. They argue that during the initial failure, the strength of the rubble skeleton is dominated by the cohesion, whereas the angle of internal friction is less important. Based on the literature review presented above we suggest that the freeze bonds define the cohesion, the cohesion governs the initial collapse of the rubble, and the initial collapse of the rubble corresponds to the peak load in punch tests. Thus, the freeze bonds are vital to find the peak load of ice rubble.

The freeze bonds strength develops through the lifetime of the ice ridge, first increasing during the initial phase, and thereafter decreasing as the rubble is eroded. If we further accept that the cohesion is strongly related to the strength and the stress concentrations in the freeze bonds, this leads to conclusion that the cohesion initially increases, but then start decreasing. If this is correct, it would be important to know how long it takes before the maximum value is reached, how high it becomes and how fast it decreases.

The strength of the freeze bonds σ_{fb} (hereafter called FB strength) and the strength of the submerged ice σ_{si} (SIB strength) is governed by the initial ice conditions (before submerging) and the oceanic conditions. Thus, it would be vital to investigate the relationship between the FB - and SIB strength and a strength ratio ($\sigma_{fb} / \sigma_{si}$) may be a useful tool since the ice rubble block strength is better known than the freeze bond strength.

Furthermore, it is vital to estimate the temporal development of FB strength and their changes with size of the ice blocks, confining pressure and ice properties such as temperature, salinity and porosity.

2. Theory

Correct interpretation of model test results requires scaling the problem and establishing certain similitude laws. For complete similitude, a model must satisfy geometric, kinematic and dynamic similitude criteria. Using appropriate length and time scales will ensure the first two. The correct scaling of the forces is required for the dynamic similarity. Since, it is not possible to satisfy all these requirements, only the most important parameters should be scaled. For the testing submerged ice, the two processes namely heat and mass transfers are important.

The geometric and time scaling factors (λ and λ_t) are introduced as following:

$$\lambda = \frac{L_p}{L_m}, \tag{1}$$

$$\lambda_t = \frac{t_p}{t_m}, \tag{2}$$

where L is the linear dimension; t is the time; the variable with a p subscript means that it is a prototype scale and the variable with a m subscript means that it is a model scale.

2.1 Heat conduction and Fourier number

The heat transfer in the submerged ice blocks is assumed to be purely conductive. If the internal mass flows for the freezing/melting and the convective heat transfer are neglected, the Fourier number (Fo) can be used for scaling. It is defined as a ratio of heat conduction rate to the rate of internal thermal energy storage in a solid (Incropera and DeWitt, 2002):

$$F_O = \left(\frac{tk_i}{L^2 (\rho c_v)_i} \right) = \left(\frac{\alpha_i t}{L^2} \right), \tag{3}$$

where k_i is the sea ice thermal conductivity; $(\rho c_v)_i$ is the volumetric heat capacity of ice; $\alpha_i = \left(\frac{k_i}{(\rho c_v)_i} \right)$ is the thermal diffusivity of ice.

Substituting (1) and (2) into (3) the time scale factor can be written as:

$$\lambda_t = \lambda^2 (F_O)_p / (F_O)_m, \tag{4}$$

where the variable with a p subscript means that it is a prototype scale and the variable with a m subscript means that it is a model scale.

Unless the Fourier number changes with the scale the Eq. (4) can be written as:

$$\lambda_t = \lambda^2 \tag{5}$$

For the freshwater ice Eqs. (4) and (5) define well the similitude criteria, whereas for the saline ice, the situation is more complicated, due to the brine migration in the ice.

2.2 Salinity exchange and Froude number

In order to characterize the salinity exchange in the ice, the Froude number can be applied. It is the ratio between the inertia and gravity forces:

$$F_r = \left(\frac{V}{\sqrt{Lg}} \right), \tag{6}$$

and the time scale factor is:

$$\lambda_t = \sqrt{\lambda} (F_r)_p / (F_r)_m \tag{7}$$

For the sea ice, Eq. (7) can be written similarly to Eq. (4) as:

$$\lambda_t = \sqrt{\lambda} \tag{8}$$

Scaling requirements (5) and (8) contradict each other. As will be shown later, the heat conduction is predominate process during the first day of testing, while the salinity transfer becomes important at later stages. This means, it is not possible to satisfy both requirements in a single model.

The prototype scaling time (t_p) for fresh and sea ice was estimated based on Fourier and Froude similitude laws and results are given in Table 1. For these estimate, salinity of the prototype ice was assumed to be constant and equal to 6 ppt, whereas the ice temperature was the variable parameter changing from -20ºC to -4ºC for both the prototype and the model ice. The ice salinity variation for the model ice was chosen from 0 to 10 ppt. The thermal properties of ice were calculated as functions of salinity and temperature based on the theory by Schwerdtfeger (1963).

Table 1. Calculation of the prototype scaling time.

Model scaling time, t_m (days)	Prototype scaling time, t_p (days)		
	Fresh ice	Sea ice	
	Fourier[a]	Fourier[b]	Froude
1	31…97	7…27	1.9
2	61…193	13…54	3.8
2.5	76…242	16…68	4.7

[a] $Fo = f(T)$, T_p, T_m varied from -20ºC to -4ºC; S_p=6 ppt, S_m=0 ppt.

[b] $Fo = f(T, S)$, T_p, T_m varied from -20ºC to -4ºC; S_p=6 ppt, S_m varied from 10 ppt to 2 ppt.

3. Experimental set-up

3.1. Field tests

3.1.1 General

In March and April 2005, field tests with submerged ice blocks were carried out in Adventfjorden, Longyearbyen on Svalbard. Two types of tests were conducted:

- Freeze bonding test (FB test)
- Test of submerged ice blocks (SIB test).

The purpose of the FB test was to estimate the freeze bond strength between ice blocks and its relation to the strength of the submerged ice blocks through uniaxial compression test. We also wanted to examine how the FB strength is affected by different aspects such as the time of submerging, the size of the ice blocks, the confining pressure and the physical properties of the ice.

Investigations of physical and thermo-mechanical properties of submerged ice with special attention to their temporal development was the goal for the SIB test program. The field test program is shown in Table 2.

Table 2. Field tests on landfast level ice, Adventfjorden, March – April 2005.

Test no.	Date[a]	t_m (hours)	Type of test	n[b]	Description
Series 2	22 March	72	SIB	10[1]	6 SIB blocks
Series 4	25 March		SIB	8[1]	4 SIB blocks
Series 5	26 March	48	SIB + FB	2 + 6[2] (0)	1 SIB +2[3] FB blocks
Series 6	30 March		SIB + FB	17 + 0 (all)[4]	3 SIB +3 FB blocks
Series 7	11 April		SIB + FB	18 + 8 (4)	3 SIB +3 FB blocks
Series 8	13 April		SIB + FB	17 + 9 (3)	
Series 9	27 April		SIB + FB	17 + 5 (7)	

[a] Date of the beginning of the test.
[b] Number of compressed samples (number of FB samples that failed during cutting).
[1] Vertical cylindrical ice samples were compressed.
[2] Including 4 samples from the big ice block.
[3] Including the big ice block (0.34 m).
[4] The FB blocks were broken along the freeze bond during transportation from the site to the laboratory.

Type of test: SIB - Test of submerged ice blocks, FB - Freeze bonding test.

3.1.2 Test description

An opening of 0.8 x 1.6 m was made in the ice cover. The landfast level ice thickness grew from 0.35 m to 0.56 m and ice cubes with dimensions of 0.24 m were used for testing. They were taken at the same depth from the ice cover surface. The orientation of the block inside the cage was the same as its original position in the level ice body.

Six ice blocks from the level ice were prepared during each test series except for Series 4, where only four ice blocks were examined. For the FB test, three ice blocks were cut in two pieces by 45° vertical cut and then put together as shown in Fig. 1a. The SIB blocks were left intact without forming the adfreeze bonds. Then all blocks were put inside the aluminium cages and submerged at approximately 0.15 m below the water level as shown in Fig. 2.

a) Before submerging b) After submerging, 48 hours

Fig. 1. Ice block with freeze bonds.

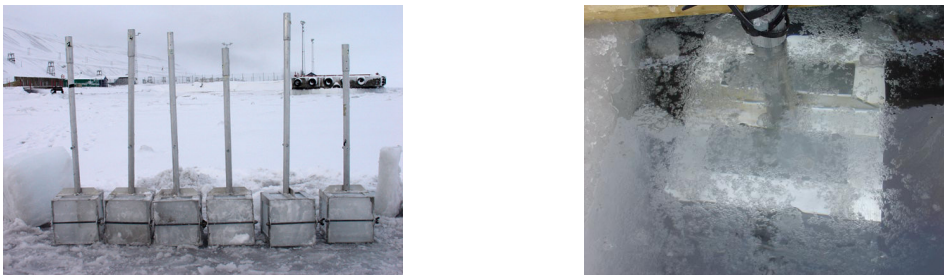

a) Ice blocks before submerging b) Submerged ice block

Fig. 2. Ice blocks inside cages.

The final test set-up for Day 1 is shown in Fig. 3a. The cages were submerged along the shore and parallel to the direction of the current. The position of the different ice blocks in relation to each other was always the same as shown in Fig. 3b. For the heat transfer investigation, the dimensions of the ice blocks were measured before and after submerging. The air and water temperatures were registered each day.

After 24 hours of submerging, one SIB block was lifted out of the water. The remaining blocks (3 with the adfreeze bond and 2 without it) were kept under water for 48 hours and then lifted out of the water. The summary of measurements and observations are given in Table 3.

During Series 5, a larger ice block with side length of 0.34 m was submerged in addition to the small blocks. All blocks were submerged at the same time and kept under water for 48 hours.

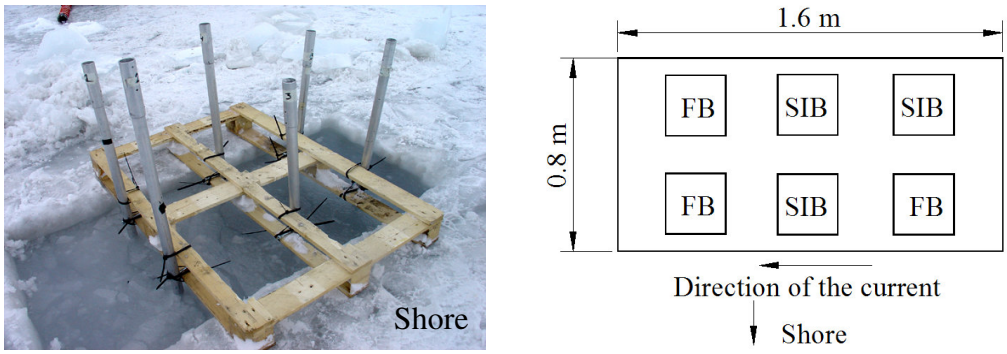

a) b)

Fig. 3. Final test set-up, Day 1.
(FB – Blocks with freeze bonds; SIB – Blocks without freeze bonds).

Table 3. Summary of measurements and observations. Field tests.

no.	Description
	Day 1 Before submerging (t_m=0 hours)
1.	Temperature profile, salinity and strength of the ice prior to submerging
2.	Geometry of the ice blocks subjected to submerging
3.	Air and water temperature
4.	Photo and video
	Days 2-3 (t_m=24 hours, 48 hours)
1.	Temperature profile, salinity and strength of the submerged ice blocks
2.	Geometry of the submerged ice blocks
3.	Freeze bonds strength (FB test, Day 3 only)
4.	Air and water temperature
5.	Photo and video

3.1.3 Strength measurements

Portable compression equipment that consists of band saw and the uniaxial compression machine 'KOMPIS' was used for the compression testing. The strength was defined as the maximum force divided by the initial sample cross-section, and is called σ throughout the paper. The piston speed corresponded to a nominal strain rate of $10^{-3}s^{-1}$. The compression rig is described by Shafrova and Moslet (2006) and Moslet (2007). Horizontal ice samples (in relation to the original ice cover surface) of prismatic shape with the dimensions of 62 x 62 x 175 mm were tested under uniaxial compression.

The ice samples were weighed before the test and then compressed. The density was estimated from the measured weight, assuming that the volumes of the samples were identical. Immediately after compression, the ice temperature was measured. Then the samples were melted and their salinity was estimated. The porosity was calculated as described by Cox and Weeks (1983) for ice colder than -2°C and by Leppäranta and Manninen (1988) for warm ice.

3.2 Laboratory tests

3.2.1 General

The 2005 field tests showed that the initial confinement is one of the key parameters that affected the FB strength, especially at the initial stage. Thus, the cages were modified in order to provide the confinement both initially and during the test. One of the modified cages is shown in Fig. 4. The pressure on the FB block was applied using a stainless spring. The spring was connected to the aluminium plate that was tightened to the cage by four stainless bolts. In addition to that, the plastic plate was used in order to transfer the uniform pressure distribution over the whole side of the ice block. Two different springs that can develop forces up to 20 N and 50 N were used in the laboratory test program.

3.2.2 Test description

There was hardly any sea ice in Adventfjorden in the spring of 2006 so the testing was done only in the UNIS laboratory. An overview of the laboratory test program is given in Table 4.

The laboratory tests were carried out during the February-March 2006, where three different types of the laboratory made ice were tested: sea ice from the ice tank (SIFIT), layered saline ice (LSI) and layered freshwater ice (LFI). The LFI ice was submerged in the tap water, while the sea water was used for the sea ice testing. The air temperature in the laboratory together with the water temperature in the ice tank and testing containers was around –2°C all the time.

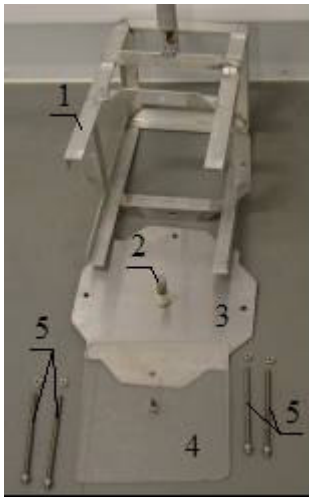

1 Aluminium cage
2 Stainless steel spring
3 Aluminium plate
4 Plastic plate
5 Stainless steel bolts
6 Ice block
7 Freeze bond

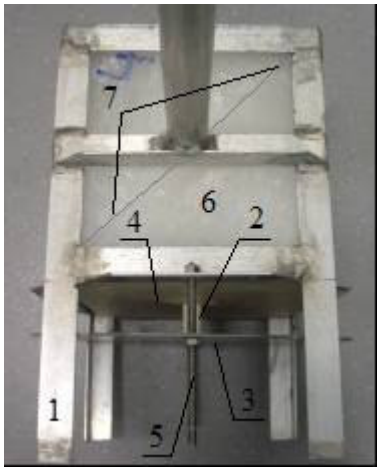

Fig. 4. Modified cage equipment.

For Test 1, sea ice was grown in the ice tank (FRYSIS) in the laboratory. FRYSIS has dimensions of 1.0 x 0.5 x 1.3 m and was first used as ice production basin and then as a testing pool. Three cubic ice blocks with size of 0.24 m were cut out from the ice sheet, submerged in the ice tank for the 48 hours and than tested under uniaxial compression.

For Tests 2-11, FRYSIS was used as a testing pool only. The ice was grown in plastic boxes (0.4 x 0.3 x 0.185 m) using a layering technique. FB cubes (0.24 m) were saw out from the two separate ice blocks in such way that the ice layers were parallel to the freeze bond and inclined at 45° to the horizontal. The ice blocks without freeze bond were made from a single ice block and thus have a thickness of 0.17 m. For Test 2 (LSI ice), a mixture of sea and fresh (tap) water with a ratio of 1:1 was used to prepare the ice blocks. For Tests 3-11, the ice blocks were prepared using the fresh tap water (LFI ice). A typical view of the layered ice samples before the compression test is shown in Fig. 5.

In March 2006, six sea ice blocks 0.6 m thick and linear dimensions of about 0.35 m were sampled in the Van Mijenfjorden (60 km away from UNIS), transported to the cold laboratory and stored there for subsequent testing. This ice was tested in Tests 12-13. Furthermore, ice from the ice foot the Adventfjorden was used in Test 14. In addition to that, a thin ice cover was discovered in a shallow protected area in the Adventfjorden (Test 15).

Table 4. Laboratory tests, February – April 2006, the initial temperature ($(T_{init})_{av}$) and initial salinity ($(S_{init})_{av}$) of the ice prior submerging.

Test no.	t_m (hr)	Type of test	Type of ice	$(T_{init})_{av}$ (°C)	$(S_{init})_{av}$ (ppt)	n[a]	Description
Ice tank testing							
1	48	FB	SIFIT	-5	9.7	7 (4)	3 FB blocks under different confinement (WS, S20, S50)
2	48	FB	LSI	-6.4	10.3	5 (8)	
3	60	FB	LFI	-7.0	-	12 (0)	
4	60	SIB	LFI	-5.9	-	18	3 SIB blocks
5	60	SIB + FB	LFI	-10.6	-	6 + 8 (0)	1 SIB + 2 FB blocks under different confinement (S20, S50)
6	60	SIB + FB	LFI	-14.5	-	(6 + 7 (1))[b]	
7	48	SIB + FB	LFI	-5.1	-	3 + 8 (0)	
8	48	SIB + FB	LFI	-10.1	-	6 + 8 (0)	
9	24	SIB + FB	LFI	-5.0	-	7 + 3 (5)	
10	24	SIB + FB	LFI	-6.4	-	6 + 7 (1)	
11	24	SIB + FB	LFI	-10.2	-	6 + 8 (0)	
Container testing							
12	60	SIB + FB	SI1_T	-5.6	2.64	27 + 0 (12)	3 SIB + 3 FB blocks under the same confinement (S50)
13	60	SIB + FB	SI1_B	-17.8	2.82	29 + 12 (7)	
14	60	SIB + FB	SI2	-19.3	1.76	12 + 10 (2)	
15	60	SIB + FB	SI3	-19.9	3.16	12 + 12 (2)	

[a] Number of compressed samples (number of FB samples that failed during cutting).
[b] The stationary uniaxial compression machine 'Knekkis' was used for testing.

Type of test: SIB is the test of submerged ice blocks, FB is the freeze bonding test.

Type of ice: SIFIT is the sea ice that was grown in the ice tank in the laboratory.
LSI and LFI are the laboratory made layered saline and freshwater ice that was grown in plastic boxes in the laboratory.
SI1_T and SI1_B are the sea ice from Van Mijenfjorden, top and bottom parts, respectively.
SI2 and SI3 are the sea ice from Adventfjorden, the ice foot and floe ice, respectively.

Type of confinement: WS without spring, S20 spring, maximum load 20 N,
S50 spring, maximum load 50 N.

a) Sample without freeze bond b) Sample with freeze bond

Fig. 5. The laboratory made layered freshwater ice (LFI) samples prior compression testing.

In order to increase the efficiency of the laboratory work, six plastic containers with dimensions of 0.5 x 0.6 x 1.0 m were used as pools for the sea ice testing (Tests 12-15, Table 4). Thus, six ice blocks (3 FB and 3 SIB blocks) were submerged at the same time. Pairs of ice blocks (1 SIB and 1 FB) were lifted out of the water after 24 hours, 48 hours and 60 hours of exposure respectively and their physical and mechanical properties were examined.

3.2.3 Strength measurements

Horizontal ice samples (relative to the growth direction) of prismatic shape were used for the strength measurements during all tests except for Tests 3-11, where the FB blocks were prepared in such way that ice layers were parallel to the freeze bond (Fig. 5a). For a proper density evaluation, the size of ice samples were measured prior the compression by a slide gauge. The sample preparation and the testing procedure were the same as in the field program.

4. Results

4.1 Field tests

The initial properties of the ice prior submerging and general information about the field tests are summarized in Table 5.

Table 5. Initial properties of the ice prior to submerging and general information about the field tests, the air and water temperature (T_{air}) and (T_{water}), the thickness of the level ice ($(h_{init})_{av}$), the ice temperature ($(T_{init})_{av}$), the salinity of ice ($(S_{init})_{av}$), the density of ice ($(\rho_{init})_{av}$) and the strength of ice ($(\sigma_{init})_{av}$).

Test no.	T_{air} (ºC)	T_{water} (ºC)	$(h_{init})_{av}$ (m)	$(T_{init})_{av}$ (ºC)	$(S_{init})_{av}$ (ppt)	$(\rho_{init})_{av}$ (kg/m^3)	$(\sigma_{init})_{av}$ (MPa)
Series 2	-15	-	0.56	-7.2	7.16	904	5.48[a)]
Series 4	-18	-	0.45	-3.9	6.94	897	3.67[a)]
Series 5	-9	-1.7	0.45	-3.8	6.80	897	-
Series 6	-6	-1.5	0.35	-2.9	6.45	910	1.86[b)]
Series 7	-2	-1.6	0.54	-3.2	5.21	906	2.77[b)]
Series 8	-4	-1.7	0.50	-2.2	6.06	905	1.71[b)]
Series 9	-10	-1.6	0.44	-1.8	4.47	859	0.96[b)]

[a)] Vertical cylindrical ice samples were compressed.
[b)] Horizontal rectangular ice samples were compressed.

4.1.1 FB Test

Altogether 28 uniaxial compression tests were conducted with the FB ice samples. These samples failed along the freeze bond surface as shown in Fig. 6. The FB strength (σ_{fb}) varied from 0.014 to 0.073 MPa for the ice that had been submerged for 48 hours. The average strength data is given in Table 6. We introduce the ratio between FB strength and SIB strength (σ_{fb}/σ_{si}) and it varied from 0.008 up to 0.082, with an average value of 0.03.

Fig. 7 shows the strength of freeze bonds versus the initial (parent) ice porosity and the porosity of the submerged ice. Furthermore, the porosity of the submerged ice as a function of initial properties is given in Fig. 8. The initially colder and less porous ice gave a higher FB strength.

The volume of the samples changed during the submersion and we define the relative volume as the current volume divided by the initial volume. Fig. 9 gives the correlation between the FB strength and the relative volume of the ice blocks. The smaller relative volume, the weaker FB.

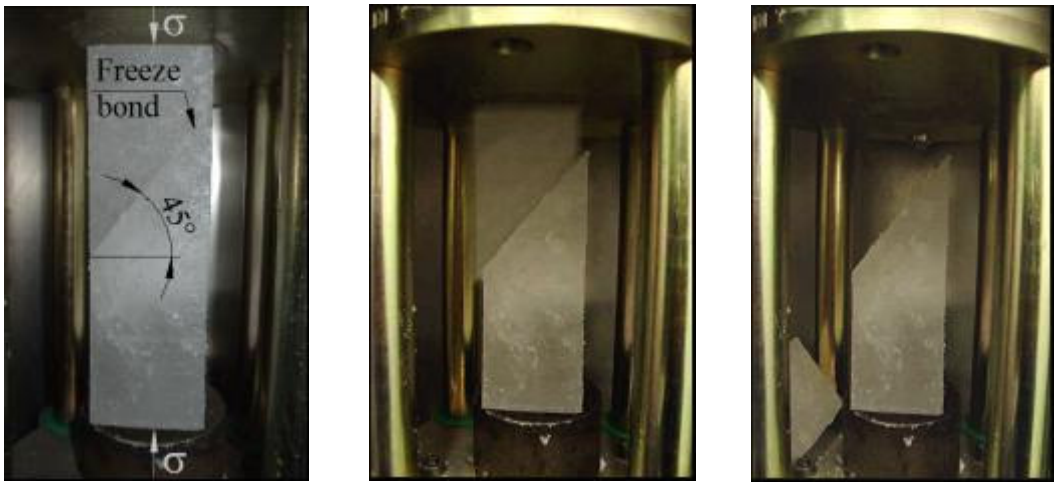

a) Before test b) During test c) End of test

Fig. 6. Uniaxial compression tests of the ice samples with freeze bonds.

Table 6. Strength data. Field tests, t_m=48 hours (small cages only), the freeze bond strength ($(\sigma_{fb})_{av}$ ± the standard deviation), the strength of the submerged ice ($(\sigma_{si})_{av}$ ± the standard deviation).

Test no.	$(\sigma_{fb})_{av}$ (MPa)	n	$(\sigma_{si})_{av}$ (MPa)	n	$(\sigma_{fb}/\sigma_{si})_{av}$ (-)
Series 5	0.019	2	1.37 ± 0.57	2	0.015 ± 0.005
Series 7	0.044 ± 0.019	8	1.46 ± 0.29	4	0.031 ± 0.016
Series 8	0.034 ± 0.016	9	1.46 ± 0.33	8	0.024 ± 0.013
Series 9	0.017 ± 0.004	4	0.61 ± 0.20	8	0.035 ± 0.017

All FB ice blocks were normally submerged for 48 hours except for Series 9, where one FB block was lifted out of the water after 24 hours of submerging. Only one FB sample from this block was tested, the three other samples broke during preparation. The FB strength of this single sample was 0.027 MPa. The FB samples from Series 9 tested on the next day (after 48 hours of submerging) had lower strength values of 0.014 MPa, 0.015 MPa, 0.016 MPa and 0.023 MPa.

Four FB samples were taken from the big block (0.34 m) and tested in Series 5. Two samples were taken from the internal part of the ice block and had FB strength of 0.024 MPa and 0.028 MPa. These results are somewhat higher than 0.019 MPa measured on FB samples from the small blocks (Table 6). The strength of the two edge samples was 0.083 MPa and 0.089 MPa.

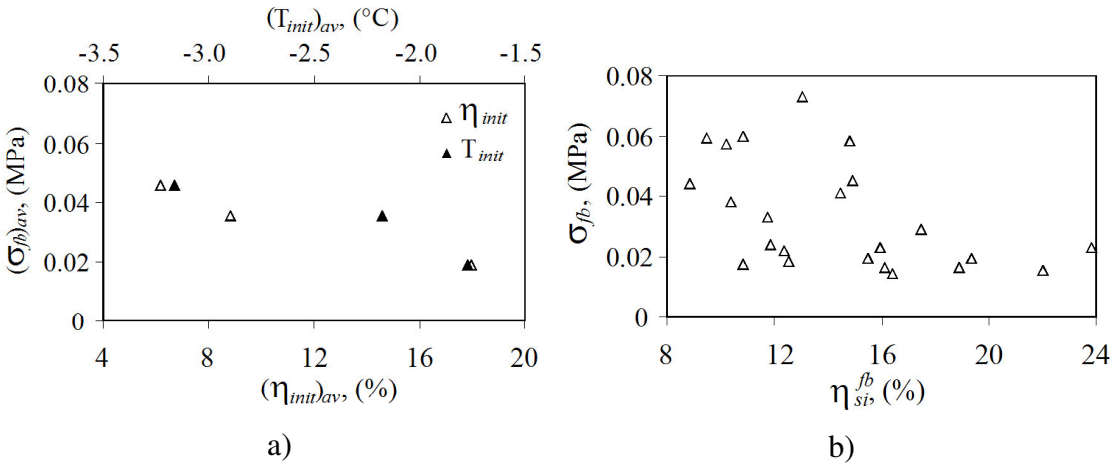

Fig. 7. Freeze bond strength as a function of: a) initial temperature and porosity of the ice prior submerging and b) porosity of the submerged ice (FB blocks) at the time of compression testing. Field tests, t_m=48 hours.

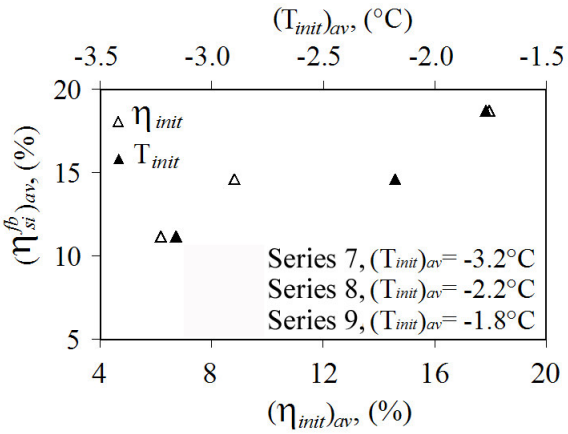

Fig. 8. Porosity of the submerged ice (FB blocks) at the time of compression testing as a function of initial temperature and porosity of the ice prior submerging. Field tests, t_m=48 hours.

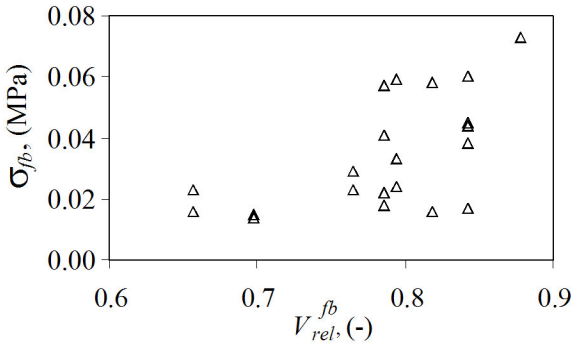

Fig. 9. Freeze bond strength versus relative volume of the submerged ice blocks that formed the freeze bonds. Field tests, t_m=48 hours.

4.1.2 SIB test

The average strength of the SIB blocks is given in Table 6. The change of the ice blocks dimensions during submerging in terms of relative volume is shown in Fig. 10. Typical profiles of temperature and salinity before and after submersion are shown in Fig. 11. The development of density, porosity and SIB strength versus time is given in Fig. 12, while the SIB strength as a function of porosity and density is given in Fig. 13. The temperature increased up to -2°C within the first 24 hours of submerging, the salinity decreased and the porosity increased and consequently the SIB strength decreased with time.

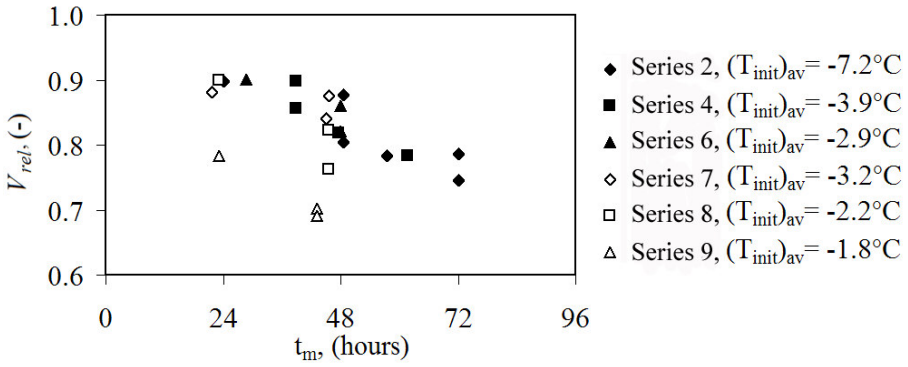

Fig. 10. Relative volume of the SIB ice blocks versus time. Field tests.

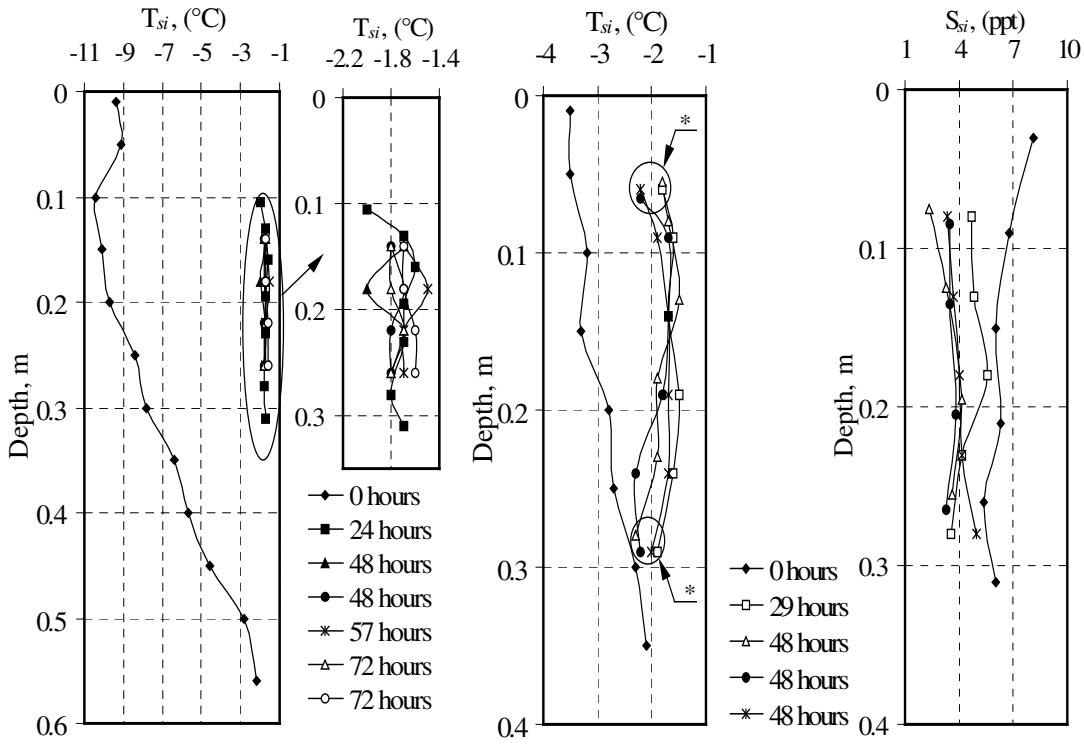

a) Serie 2 b) Serie 6

Fig. 11. Temperature and salinity profiles of the ice blocks, SIB data. Field tests.
* The blocks were slightly cooled down during transportation from the site to the laboratory.

4.2 Laboratory tests

4.2.1 FB Test

Altogether 106 uniaxial compression tests were conducted with the FB ice samples. Both laboratory made ice (72 samples) and sea ice (34 samples) were tested in the laboratory conditions. The main part of samples (60 samples) was taken from the laboratory made layered freshwater ice (LFI ice). No difference was observed between the FB strength in ice blocks that were subjected with the confinement of 20 N and 50 N. Thus, the FB results are given for the whole data set without distinguishing to the confining pressure.

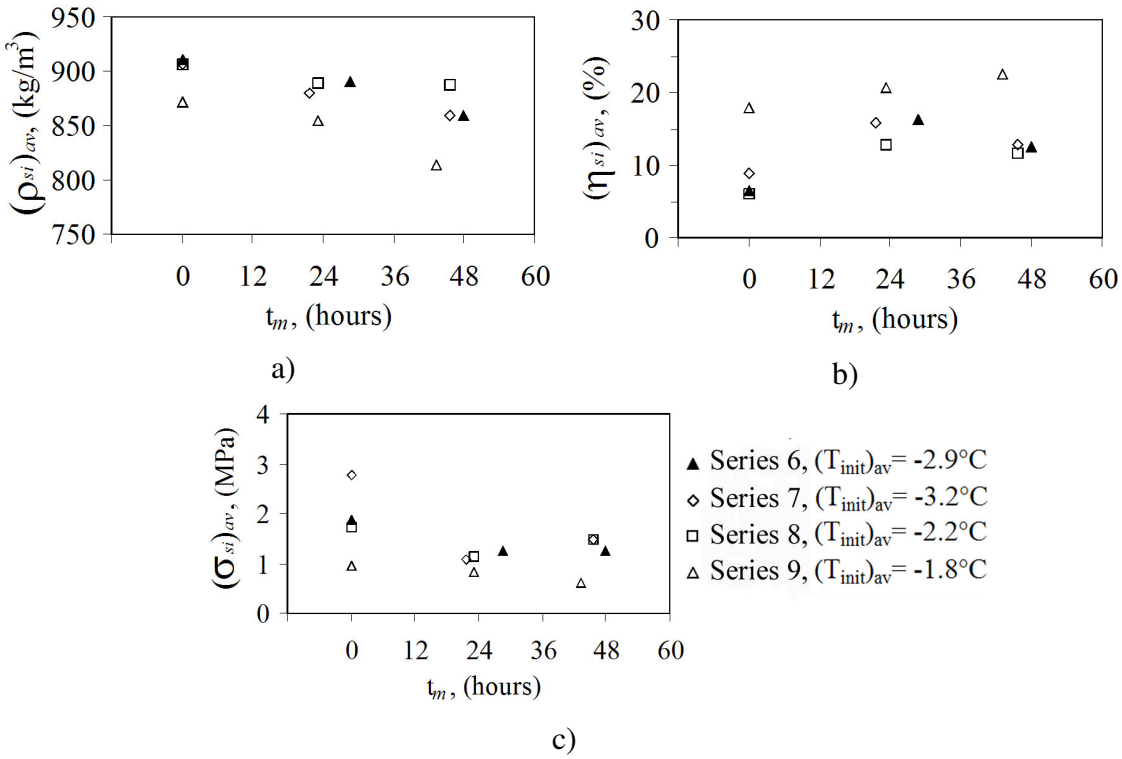

Fig. 12. Properties of the SIB blocks versus time. Field tests.
(based on the data from the compressed samples).

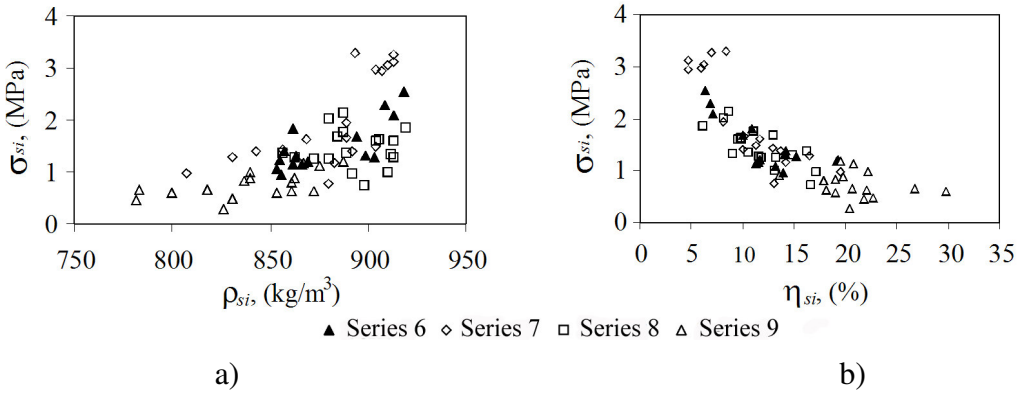

Fig. 13. Density and porosity of the SIB blocks versus strength. Field tests.

A summary of strength data from laboratory tests is given in Table 7. The average FB strength was found to be 0.23 ± 0.08 MPa (T_{init} =-6°C), 0.28 ± 0.09 MPa (T_{init} =-10°C), 0.45 ± 0.22 MPa (T_{init} =-14.5°C) for the LFI ice and 0.067 ± 0.052 kPa (T_{init} =-19°C) for the sea ice up to 60 hours of submerging.

In Tests 13-15, some of the FB samples were taken from the internal part of the block and some from the edges of the block. The average FB strength from the internal part of the ice blocks only and corresponding SIB strength data are given in Table 7. Based on these results, the strength ratio ($\sigma_{fb} / \sigma_{si}$) was found to be: 0.21 ± 0.12 for the LFI ice and 0.15 ± 0.15 for sea ice up to 60 hours of submerging. Note that FB strength for the sea ice varied significantly, even for the ice blocks with the same initial temperature.

The FB strength both from the internal part and from the edges of the ice block is given in Table 8. The edge samples exhibited higher FB strength compared to the FB samples from the internal part of the same ice block.

The FB strength versus initial ice properties (temperature and salinity) is shown in Fig. 14, whereas the FB strength is plotted against properties of the submerged block in Fig. 15. The same trends as for the field tests can be seen, except that there was a decreasing FB strength with increasing salinity. Finally, Fig. 16 shows the FB strength as a function of submerging time.

4.2.2 SIB test

The SIB strength is given in Table 7, and its time dependence is given in Fig. 17. The LFI block expanded during the submerging, whereas the size of sea ice blocks did not change significantly even after 60 hours in the water. Fig. 18 show the SIB strength as a function of the total porosity separately for the field (also given in Fig. 13b) and laboratory tests.

Table 7. Strength data. Laboratory tests (samples from the internal part of the block only), the freeze bond strength ($(\sigma_{fb})_{av}$ ± the standard deviation), the strength of the submerged ice ($(\sigma_{si})_{av}$ ± the standard deviation).

Test no.	Type of ice	t_m (hr)	$(\sigma_{fb})_{av}$ (MPa)	n	$(\sigma_{si})_{av}$ (MPa)	n	$(\sigma_{fb}/\sigma_{si})_{av}$ (-)
Ice tank testing							
1	SIFIT	49	0.036 ± 0.022	7	-	-	-
2	LSI	49	0.079 ± 0.045	5	-	-	-
9, 10, 4	LFI	24	0.23 ± 0.12	10	1.44 ± 0.32	18	0.17 ± 0.08
7, 4		48	0.17 ± 0.05	8	1.25 ± 0.24	9	0.14 ± 0.05
3, 4		60	0.26 ± 0.12	11	1.06 ± 0.23	6	0.31 ± 0.24
11	LFI	24	0.34 ± 0.14	8	1.24 ± 0.29	6	0.29 ± 0.14
8		48	0.30 ± 0.07	8	1.69 ± 0.53	6	0.20 ± 0.08
5		60	0.21 ± 0.10	8	1.30 ± 0.26	6	0.17 ± 0.09
6[a]	LFI	60	0.45 ± 0.22	7	1.27 ± 0.68	6	0.38 ± 0.21
Container testing							
12	SI1_T	24	-	-	2.11 ± 0.11	4	-
		48	-	-	1.76 ± 0.33	4	-
		60	-	-	1.23 ± 0.31	4	-
13	SI1_B	24	0.032	1	1.25 ± 0.15	4	0.026 ± 0.003
		48	0.015	1	1.12 ± 0.41	4	0.015 ± 0.005
		60	0.025 ± 0.001	2	1.02 ± 0.08	4	0.024 ± 0.002
14	SI2	24	0.054 ± 0.029	3	0.45 ± 0.13	4	0.13 ± 0.06
		48	0.151 ± 0.010	3	0.49 ± 0.18	4	0.36 ± 0.17
		60	0.195	1	0.58 ± 0.25	4	0.40 ± 0.21
15	SI3	24	0.053 ± 0.017	3	0.71 ± 0.20	4	0.08 ± 0.03
		48	0.049 ± 0.028	4	0.39 ± 0.06	4	0.13 ± 0.07
		60	0.049 ± 0.028	3	0.39 ± 0.25	4	0.17 ± 0.13

[a] The stationary uniaxial compression machine KNEKKIS was used for testing.

Table 8. Freeze bonding strength data. Laboratory tests. Sea ice (all samples).

Test	t_m	Internal samples		Edge samples	
	(hours)	$(\sigma_{fb})_{av}$ (MPa)	n	$(\sigma_{fb})_{av}$ (MPa)	n
13	24	0.032	1	0.063 ± 0.015	2
	48	0.015	1	0.026 ± 0.003	3
	60	0.025 ± 0.001	2	0.029 ± 0.013	3
14	24	0.054 ± 0.029	3	-	-
	48	0.151 ± 0.010	3	0.117 ± 0.055	2
	60	0.195	1	-	-
15	24	0.053 ± 0.017	3	-	-
	48	0.049 ± 0.028	4	0.076	1
	60	0.049 ± 0.028	3	0.066	1

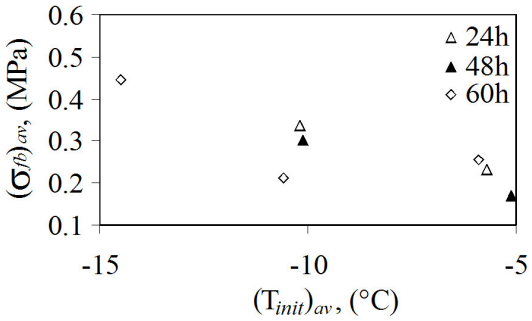

a) Freshwater ice (LFI)

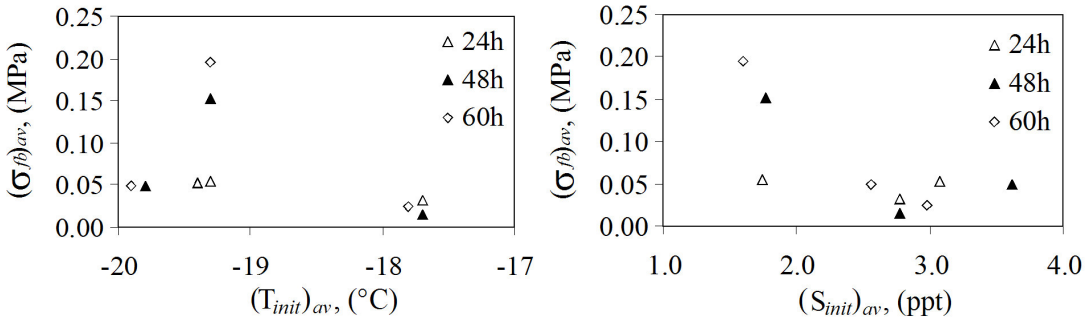

b) Sea ice (Tests 13-15)

Fig. 14. Freeze bond strength as a function of initial temperature and salinity of the ice prior submerging. Laboratory tests.

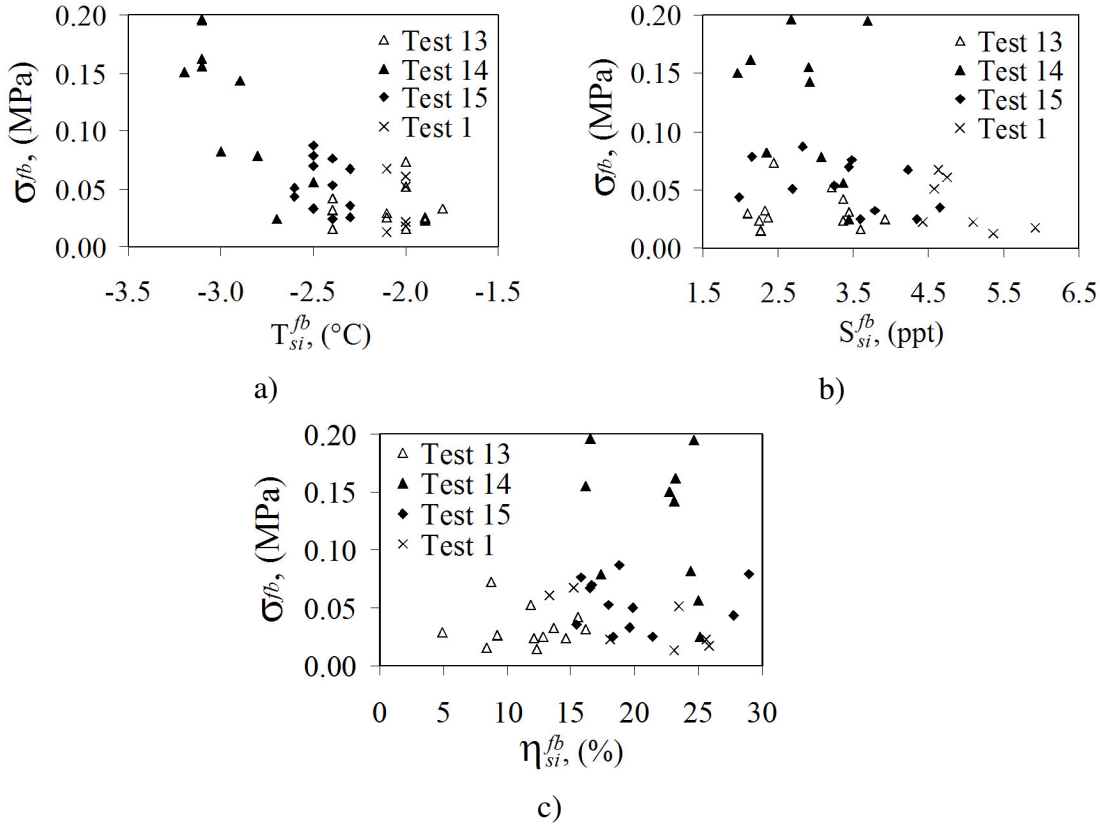

Fig. 15. Freeze bond strength versus properties of submerged ice.
Sea ice. Laboratory tests (all data).

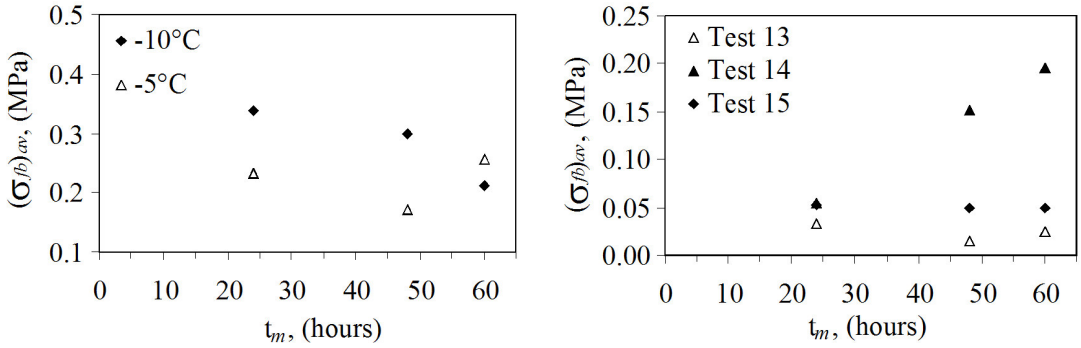

Fig. 16. Freeze bond strength versus time of submerging. Laboratory tests.

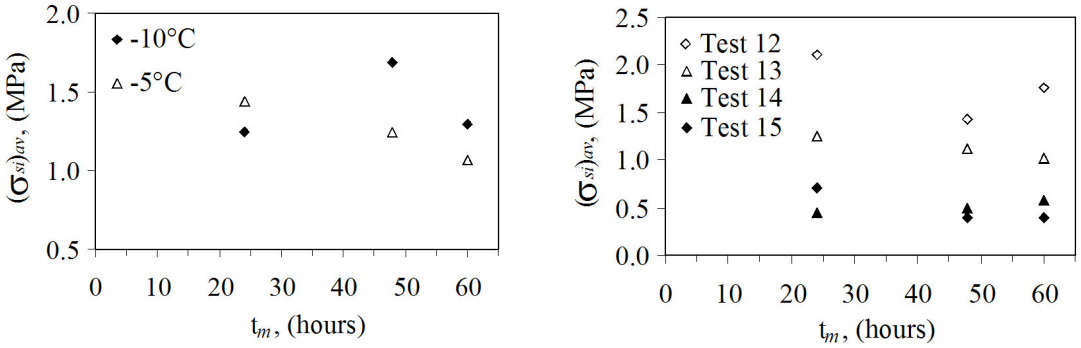

a) Freshwater ice (LFI) b) Sea ice

Fig. 17. Strength of SIB blocks versus time of submerging. Laboratory tests.

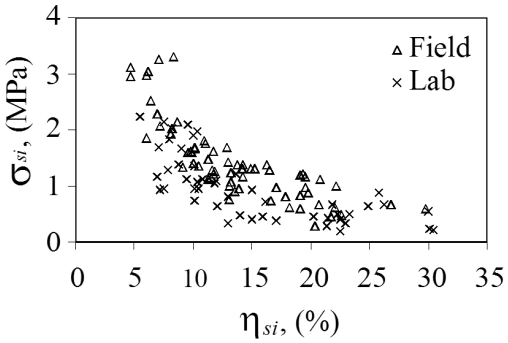

Fig. 18. Strength of SIB blocks versus porosity (All tests).

5. Analysis

5.1 FB Test

5.1.1 FB strength versus ice properties

Both the strength of the freeze bonds and the strength of submerged ice are functions of the initial ice properties. Basically these strengths decreased for increasing initial temperature and increasing initial porosity and partly for increasing initial salinity. In particular there was a strong correlation between the FB strength and the ice temperatures (for both initial and current values). Any changes of the initial temperature even within 1-2°C had a significant effect on the FB strength.

The initial salinity of the field tests varied between 4.5 and 7 ppt, and we found no correlation between the initial salinity and FB strength. However, when including the laboratory tests a wider range of salinities (including freshwater ice) is covered and some patterns become evident. The FB strength from freshwater ice was roughly

5-10 times that of the saline ice, so ridges in rivers and lakes should have substantially higher freeze bond strength. It was further a trend of decreasing strength with increasing initial salinity for salinities below about 3 ppt. For higher salinities the brine volume is more sensitive to the temperature variations, and at some point the effect of small temperature variations overcomes that of the total salinity.

We further found a FB strength dependence on the initial porosity. This should also be clear as a higher ice fraction contains more potential (negative) energy that can be spent in creating freeze bonds. However, the ice foot (Test 14) was an interesting exception; the ice had high porosity (25%), high FB strength and a low SIB strength. The ice temperature at testing was relatively low (about -3°C) and since the FB ice had a higher salinity than the SIB ice, its strength was more sensitive to temperature variations. This only partly explains the measurements, the key is the ratio of air to brine volume. The samples had high air volume (20%) and low brine volume which produces two effects, firstly a high thermal conductivity that slows down the temperature diffusion and secondly more holes speed up the mass diffusion. A combination of these factors explains the high FB strength in combination with the low SIB strength for the ice foot.

5.1.2 FB strength versus time

Our results with respect to the time dependency are not unambiguous. The field tests (Serie 9) show that σ_{fb} (t_m= 24 h) > σ_{fb} (t_m= 48 h), but only one 24 hour FB sample was compressed. The freshwater tests show partly decreasing strength (T_{init}= -10°C) and partly no development (T_{init}= -5°C). The saline laboratory tests neither show any trends with the exception of Test 14 where the strength increased with time. This ice had a higher thermal conductivity that slowed down the speed of the temperature diffusion and delaying the point of maximum strength. We suggest a general temporal development of the strength as sketched in Fig. 19. For a more precise trend it is necessary to carry out more experiments preferably in the field.

5.1.3 FB strength versus block size

The results show two things about size dependence; first that the FB strength was lower in the interior of the sample (Series 5 and Table 8), second that the FB strength of small blocks were smaller than the average strength of large blocks: σ_{fb} (small block) ≈ σ_{fb} (interior of the large block) < σ_{fb} (edges of large block) after 48 hours of submerging (Series 5). The higher average strength can be explained by two aspects. A large block has a higher volume/area ratio than a small block and if we consider the freeze bonds as a 2D feature, there will be more thermal energy (negative) available to create freeze bonds in a larger block. In a big block the effect

of the conductive flux in relation to the thermal inertia will also be less making the time progress more slowly.

The difference between interior and edge samples has to do with the mass transfer (salt expulsion). The salinity exchange or drainage process through the freeze bond takes more time in a larger block. Ice salinity within freeze bonds measured close to the edges was lower than corresponding values in the middle part of the same bond. Thus, the FB strength from the internal part of the ice block should be weaker than the corresponding strength from the edges of the same block as observed for both laboratory and field tests.

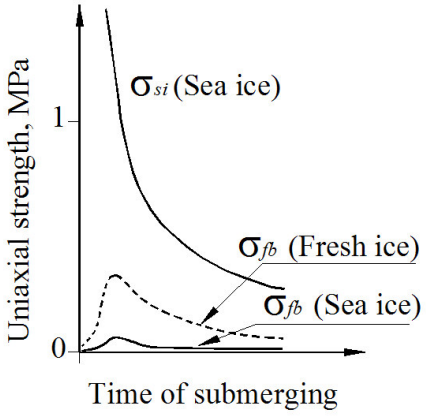

Fig. 19. Typical strength development diagram.
(σ_{fb} is the freeze bond strength and σ_{si} is the strength of SIB blocks).

5.1.4 FB strength versus confinement

In ice ridges the buoyancy, the thermal expansion and the pressure applied by the driving forces give initial pressure between the ice blocks, but we don't know their relative importance in relation to the creation of freeze bonds. However, we are convinced that the FB strength depends on the initial pressure that is applied to the ice blocks prior to - and during submerging. In the field experiments, the FB ice blocks were tested with almost no confinement before, and during submerging. Thus, FB strength results from field tests (2005) were underestimated. The ice blocks from field tests that were perfectly fitted (without any gaps) to the cages (Series 7 and 8) finally gave higher FB strength. By contrast, during Series 6 the FB blocks had dimensions slightly less than 24 cm and as a result they were broken into pieces along freeze bonds during transportation.

The experiments with varying confinement (and FB strength measurement) were only carried out on freshwater samples. Freshwater ice has a positive coefficient of thermal expansion for all temperatures, and this effect is stronger than the 20 or 50 N applied as confinement. Thus, in rives and lakes the thermal expansion may be of high importance in ridges and river jams. In sea ice the coefficient of thermal expansion changes sign for the proper combination of salinity and temperature, and sea ice above -5°C does not expand for increasing temperature. This explains the lack of quantitative information about the effect of confinement in our tests, but the observations in the field tests clearly showed that the confinement is important, at least up to a certain pressure. There will be a gradient of buoyancy induced pressure in a keel so that blocks in the lower parts of the keel is subjected to a lower confinement, which probably results in lower FB strength and cohesion.

5.1.5 FB strength versus Fourier number

As discussed in Section 2, the Fourier and Froude numbers can be used to scale the tests results. Furthermore, it was shown that for the sea ice the salinity effect is less important compared to the temperature influence. Thus, the Fourier number was calculated for all FB samples and the results are given in Fig. 20 separately for the freshwater and the sea ice.

The Fourier number for the LFI ice is a time dependent parameter that increases with the time of submerging as the latent and oceanic heat disappears. It corresponds to the same data level for the same groups of samples in relation to the time of submerging. The coefficient of variation varied within 1-2 % for the different time groups. Furthermore, it was observed that the Fourier number is almost 10 times higher for the freshwater ice compared to the sea ice. This is due to the specific heat capacity of fresh ice being less than the corresponding value for the sea ice.

For the sea ice testing, no clear threshold in relation to the time of submerging was observed for the Fourier number. The specific heat capacity of “warm” sea ice is very sensitive to its temperature (Schwerdtfeger, 1963). In addition, the salinity fluctuations made the situation even more complicated. Thus, any uncertainties with the measurements of the physical properties of the ice lead to a huge variability in the specific heat capacity value for the “warm” sea ice. It was concluded that for the sea ice the Fourier number’s data sets (Fig. 20b) corresponds to the same level. Based on χ^2 and Kolmogorov-Smornov’s tests it was found that the Fourier number’s data set is stochastically distributed and the obtained variability belongs to the uncertainties with the measurements of the physical properties of the sea ice.

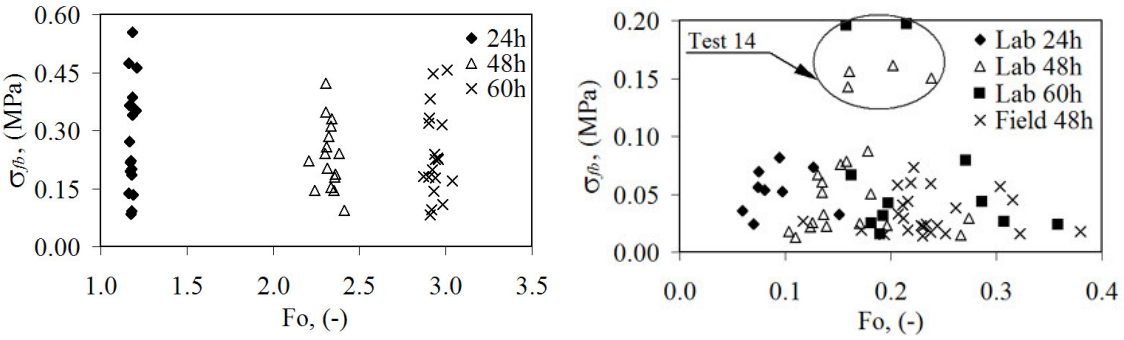

a) Freshwater ice (LFI) b) Sea ice

Fig. 20. Freeze bond strength versus Fourier number.

5.1.6 The σ_{fb}/σ_{si} strength ratio

We have investigated the short-term FB/SIB strength ratio (σ_{fb}/σ_{si}) as given in Tables 6-7. The results can be generalized as follows:

$$(\sigma_{fb}/\sigma_{si})_{\text{LFI lab}} > (\sigma_{fb}/\sigma_{si})_{\text{Sea ice lab}} > (\sigma_{fb}/\sigma_{si})_{\text{Sea ice field}}$$

As given in Fig. 5, the FB blocks for LFI ice were prepared in such way that ice layers were parallel to the freeze bond and inclined at 45° to the horizontal. However, the corresponding SIB ice samples were compressed along the frozen layers. Thus, the SIB layered samples exhibited lower strength than they potentially might have with the same structure as the FB layered samples. Hence, the strength ratio for the laboratory testing may have been overestimated. By contrast, the field FB strength results can be underestimated, since no confinement was applied to the pieces of the FB ice blocks before and during the tests. We believe that the typical strength ratio (σ_{fb}/σ_{si}) for the ice rubble of this age and size is in the range of 0.06-0.1 (Our general view of the temporal development of this ratio is given in Fig. 19).

5.2 SIB test

5.2.1 Ice melting/expansion

The field samples lost volume during their submersion. In the laboratory tests, the sea ice had more or less a constant volume, whereas the freshwater ice became larger while being submerged (Fig. 21). This is due to differences in coefficient of thermal expansion between saline and non-saline ice as discussed in Section 5.1.4 as well as different oceanic flux in the laboratory basin and in the Adventfjorden.

The ice blocks in field lost around 10-11% of their initial volume during the first 24 hours of submersion. For the second and the third day the losses were 7-8% and 6-7% respectively. Thus, the rate of ice melting decreases with the time. Generally, the ice blocks lost a quarter of their initial volume by the end of the third day (after 72 hours). Thus, rate of ice melting depends on the initial conditions, the higher initial temperature the lower relative volume (Fig. 10).

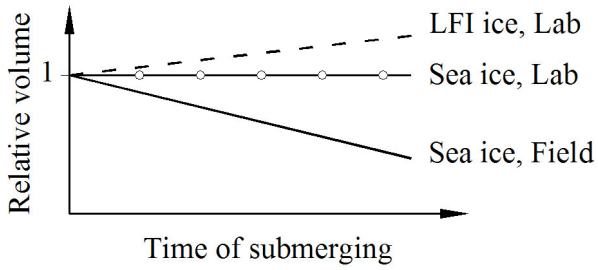

Fig. 21. Typical block size development diagram.

5.2.2 Physical properties of submerged ice

In the field tests the temperature in the ice blocks reached the freezing point within 24 hours of submerging both for warm ice (Series 6) and cold ice (Series 2) as given in Fig. 11. In the laboratory this was not the case (Fig. 15a), in particular for the non-ordinary sea ice in Tests 14 and 15. A high air volume combined with no water velocity gave a long duration of the temperature diffusion in Test 14. This clearly demonstrates the importance of the oceanic flux in the melting of ridge keels.

The salinity decreased during submersion partly because of brine migration towards higher temperatures and partly because a mass concentration gradient between the sea water ($S_w \approx 34$ ppt) and the brine in the sample ($S_b \geq S_w$).

5.2.3 Strength of submerged ice

The SIB strength of the field samples decreased for the first 24 hours of submerging and then partly increased. The porosity developed in a similar manner, and the reason for this apparent strange behaviour is different exposure to oceanic flux as a result of the test set-up and sampling routines. As shown in Fig. 3b the SIB block (that was submerged for 24 hours) was located at the edge of the opening towards to the current direction, whereas the two other SIB blocks were situated between the blocks being protected from the current. This means that the decrease of the SIB strength was high for first 24 hours and then flattened out. This corresponds nicely to the porosity development, and the SIB strength-porosity plots (Figs. 13b and 18) fits well into the plots presented by Shafrova and Høyland (2007) and Høyland (2007) where ice rubble blocks were tested in uniaxial compression.

A general trend of SIB strength reduction with time of submerging was also found in four out of six cases during the laboratory test (Table 7 and Fig. 17). In the cold LFI test the strength increased and then decreased. We don't know why, but assume that it was a coincidence. Test 14 gave slightly increasing strength and this has to do with the porosity. The high air volume allowed for brine to penetrate and freeze inside the ice, reducing the total porosity and compensated for the increasing temperature so that the strength actually increased.

6. Conclusions

A series of field and laboratory small scale tests were conducted with submerged ice blocks. The freeze bond strength between the ice blocks, the local strength of the submerged ice blocks and their changes with time of submerging, confinement, block size and physical properties of ice were investigated. The ice samples with the freeze bonds were formed both in the field and in the laboratory and than tested in uniaxial compression. The laboratory made ice and the sea ice were tested. The main conclusions are:

- The freeze bond strength was found to be in the range of 0.014 MPa to 0.073 MPa with the average value of 0.032 ± 0.018 MPa after 48 hours of submerging in the field.
- The freeze bond strength from the laboratory tests were observed to be in the range of 0.015 MPa to 0.197 MPa (on average 0.067 ± 0.052 MPa) for the sea ice tests and in the range of 0.083 MPa to 0.744 MPa (on average 0.274 ± 0.142 MPa) for the LFI ice up to 60 hours of submerging.
- The $\sigma_{fb} / \sigma_{si}$ strength ratio for the field tests was found in range of 0.008 to 0.082, with the average value of 0.03 after 48 hours of submerging.
- In the laboratory tests, the $\sigma_{fb} / \sigma_{si}$ strength ratio varied from 0.06 to 0.69 (on average 0.21 ± 0.12) for the LFI ice and from 0.009 to 0.69 (on average 0.15 ± 0.15) for the sea ice up to 60 hours of submerging.
- The initial properties of ice determine the properties of the submerged ice and as a result the freeze bond strength between the ice blocks.
- The initial physical properties of ice, the confining pressure applied to the ice pieces before and during submerging together with the linear dimensions of the ice blocks are the main parameters that affect the freeze bond strength.
- The correlation between physical and mechanical properties of submerged ice was found during both FB and SIB test programs.

The nature of freeze bond contacts between the ice blocks is important for understanding the shear strength and deformation behaviour of the ice rubble blocks in the first-year ice ridges. Thus, further in-situ and field investigations of the temporal development of the FB strength between ice blocks with various dimensions under different confinement should be conducted.

Acknowledgement

We would like to thank all participants and contributors for their crucial assistance during the field and laboratory testing, especially the following people without whom the experiments have not be done: master student Rinat Kamalov, NTNU, (2005), PhD student Per Olav Moslet, UNIS, (2005), master student Ekaterina Kim, UNIS, (both years), master student Ragnar Ekker, NTNU, (both years), student Pavel Belyaev, UNIS, (2005) and master student Ulrich Neuman, UNIS, (2006). The authors would like to thank Professor Lars Grande (NTNU/UNIS) for the improving the original test idea, Dr. Pavel Liferov (Barlindhaug Consult, now Statoil ASA) for the idea of modification of the cages equipment. The encouragement and help from Professor Karl N. Shkhinek (SPbSPU) and Professor Sveinung Løset (NTNU/UNIS) are greatly appreciated. The authors would like to thank Dr. Dmitri G. Matskevitch for comments and review of this paper. We are thankful to Jørgen Haagensli (UNIS) for the manufacturing of the cage equipment.

References

Cox, G.F. and Weeks, W.F. (1983). Equations for determining the gas and brine volumes in sea ice samples. *Journal of Glaciology*, Vol. 29, (102): 306-316.

Ettema, R. and Urroz, G.E. (1989). On internal friction and cohesion in unconsolidated ice rubble. *Cold Regions Science and Technology*, (16): 237–247.

Høyland, K.V. (2007). Morphology and small-scale strength of ridges in the North-western Barents Sea. Cold Regions Science and Technology (2007), doi:10.1016/j.coldregions. 2007.01.006.

Incropera, F.P. and DeWitt, D.P. (2002). Fundamentals of heat and mass transfer. The 5th edition. John Wiley and Sons, Inc, New York, 981p.

Leppäaranta, M. and Manninen, T. (1988). The brine and gas content of sea ice with attention to low salinities and high temperatures. Technical Report 1988(2), Finnish Institute of marine research, 14 p.

Liferov, P. (2005). Review of ice rubble behaviour and strength, Part II: Modelling. *Cold Regions Science and Technology*, (41): 153–163.

Liferov, P. and Bonnemaire, B. (2005). Review of ice rubble behaviour and strength, Part I: Testing and interpretation of the results. *Cold Regions Science and Technology*, (41): 135–151.

Moslet, P.O. (2007). Field testing of uniaxial compression of columnar sea ice. *Cold Regions Science and Technology,* (48): 1–14.

Schwerdtfeger, P. (1963). The thermal properties of sea ice. *Journal of Glaciology*, Vol. 4, (36): 789-807.

Shafrova, S. (2007). Initial failure of the ice rubble in plane strain direct shear tests. *In Proc. of the 19th Int. Conf. on Port and Ocean Engineering under Arctic conditions, (POAC)*, Dalian, China, Vol. 1, pp. 256-266.

Shafrova, S. and Høyland, K.V. (2007). Morphology and 2D spatial strength distribution in two Arctic first-year sea ice ridges. *Cold Regions Science and Technology*, doi:10.1016/j.coldregions. 2007.05.011.

Shafrova, S., Liferov, P., and Shkhinek, K. (2004). Modelling ice rubble with a pseudo-discrete continuum model. *In Proc. of the 17th Int. Symp. on Ice (IAHR)*, Saint-Petersburg, Russia, Vol. 2, pp. 265-273.

Shafrova, S. and Moslet, P.O. (2006). In-situ uniaxial compression tests of level ice. Part I: Ice strength variability versus length scale. *In Proc. of the 25th Int. Conf. on Offshore Mechanics and Arctic Engineering (OMAE),* Hamburg, Germany*,* OMAE-92450, 9p.

Surkov, G.A. and Truskov, P.A. (1993). Method for evaluation of the First-Year Ice hummock strength. *In Proc. of the 3rd Int. Offshore and Polar Engineering Conference (ISOPE)*, Singapore, Vol. 2, pp. 640-642.

Surkov, G.A., Astaf'yev, V.N., Polomoshnov, A.M., Zemlyuk, S.V., Truskov, P.A. (2001). Strength characteristics of hummock formations. *In Proc. of the 11th Int. Offshore and Polar Engineering Conference (ISOPE)*, Stavanger, Norway, Vol. 1, pp. 770-774.

6 ICE RUBBLE MATERIAL MODEL

6.1 Introduction

Two different approaches can be used to simulate the constitutive behaviour of the ice rubble: a continuum and a discrete modelling. The continuum models assume that the ice rubble is homogeneous and isotropic material and describe its the behaviour in average sense in which the details of the rubble are smoothed out. The stress and strain fields are described by the constitutive laws of continuous functions.

By contrast discrete models take into account the behaviour of each individual ice block within ice rubble that is considered as a single particle. As a result the constitutive laws in terms of stress and strain are replaced by a contact law formulated in terms of contact forces (normal and tangential components) and relative displacements.

The pieces of ice within the ice rubble are too large for the hypothesis of continuum. It is doubtful that ice blocks may be compared to the grains of a soil. In addition during the initial phase of the consolidation the ice blocks freeze to each other at the points of contacts and form the freeze bonds. Thus the size and the shape of the individual ice blocks and freeze bonds between ice blocks may affect the global behaviour of the ice rubble material. Whereas the problems with the accurate modelling of both the internal structure of the rubble and the contact phenomena are usually occur using the discrete model.

In order to avoid such problems and take into account the complicated structure of the ice rubble the pseudo-discrete approach was chosen to study the ice rubble behaviour. This implies that ice rubble is treated as heterogeneous material: a combinations of the ice blocks and voids. Contacts elements joined the ice block elements simulating the freeze bonds and the mechanical properties of these contacts elements were different from those of the ice blocks. Based on such assumptions the pseudo-discrete continuum model (PDCM) is developed. The 2D plane strain tests simulations on ice rubble is given in Chapter 7.

This Chapter presents a brief review of theory of elasto-plasticity and gives introduction into finite element numerical modelling.

6.2 Theory of elasto-plasticity

The review of classical theory of elasto-plasticity with emphasis on granular material is given in this section. The attention is focused on application of the classical Mohr-Coulomb model. Before applying the Mohr-Coulomb elasto-plastic model to the behaviour of the ice rubble the following assumptions are made:

- Time-dependent deformations are neglected
- Ice rubble is considered as an isotropic, homogeneous material
- The stresses and strains within the sample are uniform.

The necessary ingredients in an elasto-plastic stress strain model are summarized below:

- The basic principle of elasto-plasticity is that the strains and strain rates are decomposed into elastic and plastic contributions:

$$\boldsymbol{\varepsilon}^{tot} = \boldsymbol{\varepsilon}^{e} + \boldsymbol{\varepsilon}^{p} \text{ and } d\boldsymbol{\varepsilon}^{tot} = d\boldsymbol{\varepsilon}^{e} + d\boldsymbol{\varepsilon}^{p} \tag{6.1}$$

- The elastic contributions based on linear elastic model can be written using Hook's law as:

$$d\boldsymbol{\varepsilon}^{e} = (\boldsymbol{D}^{e})^{-1} d\boldsymbol{\sigma}, \tag{6.2}$$

where $\boldsymbol{\sigma}$ and $\boldsymbol{\varepsilon}^{e}$ are the stress and strain vectors in rate form, $\boldsymbol{D}^{e}$ is an elastic material stiffness matrix containing two independent elastic constants: modulus of elasticity (Young's modulus) E and Poisson's ratio ν. The elastic material stiffness matrix for the plane strain condition is given by Ottosen and Petersson (1992) as:

$$\boldsymbol{D}^{e} = \frac{E}{(1+\nu)(1-2\nu)} \begin{bmatrix} 1-\nu & \nu & 0 \\ \nu & 1-\nu & 0 \\ 0 & 0 & \frac{1}{2}(1-2\nu) \end{bmatrix} \tag{6.3}$$

The relationship between modulus of elasticity and other stiffness modules such as the shear modulus G and bulk modulus K is given by :

$$G = \frac{E}{2(1+\nu)} \text{ and } K = \frac{E}{3(1-2\nu)} \tag{6.4}$$

- The plastic contribution is controlled through: a) yield criterion, b) flow rule, c) hardening rule. The derivations below are given after Nordal (2004):

a) A yield criterion is a function of stress tensor components and state variables. Normally the criterion is denoted $F(\boldsymbol{\sigma}, \boldsymbol{\kappa})=0$ and this equation must be satisfied if any plastic strain is developed. If $F < 0$ the material is in elastic stress state. The $\boldsymbol{\kappa}$ is a general letter for a state variable which may be, for example, a degree of mobilization *f*. It is a control parameter for the amount of plastic strains which occur when approaching the failure. Thus the Mohr-Coulomb yield criterion may be given in terms of the principal stresses as:

$$F=(\sigma_1+a)-N(\sigma_3+a), \tag{6.5}$$

where the stress state is described by the major (σ_1) and minor (σ_3) principle stresses and the following state parameters are used: $N=(1+sin\rho)/(1-sin\rho)$, ρ is the mobilized friction angle, $tan\rho=f\cdot tan\varphi$ and φ is the angle of internal friction; $a=c/tan\varphi$ is the attraction where *c* is the cohesion.

The failure criterion is an ultimate yield criterion that distinguishes the obtainable stress states from the unobtainable stress states. If a stress space is defined by stress components σ_{ij} then the yield criterion will define a yield surface in this stress space. The initial yield surface provides the elastic limit, while the failure surface is the surface, which is defined by the failure criterion. An application of the general definitions in Eq. (6.5) is presented in Fig. 6.1.

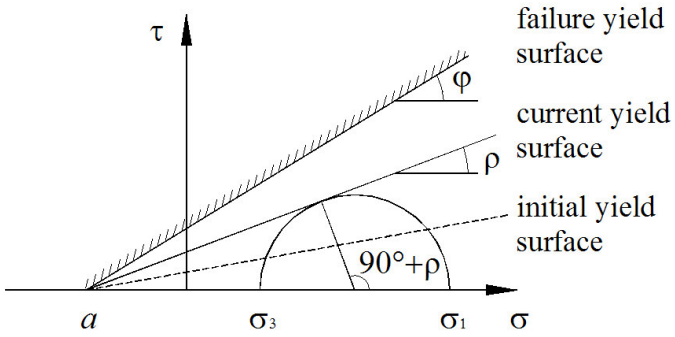

Fig. 6.1. Yield surfaces in $\tau:\sigma$ stress space.

b) The flow rule should be introduced to handle plastic deformations or plastic strains. The classical theory of plasticity (Hill, 1950) is referred to an associated plasticity. This means that the plastic strain rates can be represented as vectors normal to the yield surfaces. However, for the Mohr-Coulomb type yield functions, the theory of associated plasticity leads to overprediction of dilatancy when the plastic

volume increase or a plastic dilation is far above the values that can be experimentally observed. In order to avoid this unrealistic behaviour, the plastic potential function (*Q)* is introduced. As a result the plastic strain rate can be written in terms of the potential function and this expression is called a non-associated flow rule*:*

$$d\boldsymbol{\varepsilon}^p = d\lambda \frac{\partial Q}{\partial \boldsymbol{\sigma}}, \tag{6.6}$$

where the $d\lambda$ is the plastic multiplier (for purely elastic behaviour $d\lambda$ is zero, whereas in case of plastic behaviour $d\lambda$ is positive).

c) The hardening rule defines the scalar $d\lambda$ in Eq. (6.6), which determines the size of the plastic strain increment. It relates the development of plastic strains to a movement of the yield surface, which is associated by plastic resistance and causes plastic strains to develop. The requirement of $F = 0$ during hardening for the small increments may be written as consistency equation, which insures that the stress state lies on the yield surface all the time:

$$dF = \left\{\frac{\partial F}{\partial \boldsymbol{\sigma}}\right\}^T d\boldsymbol{\sigma} + \frac{\partial F}{\partial \kappa} d\kappa = 0, \tag{6.7}$$

where κ is the scalar hardening parameter (degree of strength mobilization *f).*

The formulation of the Mohr-Coulomb criterion fits well for isotropic strain hardening (when the yield surface expands isotropically) with $\sin\rho$ as a hardening parameter. The scalar measure for the amount of plastic strains can be given as:

$$\bar{\varepsilon}^p = \sum d\lambda \sqrt{\left\{\frac{\partial Q}{\partial \boldsymbol{\sigma}}\right\}^2}, \tag{6.8}$$

Thus the consistency equation may be rewritten in the following form:

$$dF = \left\{\frac{\partial F}{\partial \boldsymbol{\sigma}}\right\}^T d\boldsymbol{\sigma} - A d\lambda = 0 \text{ and } d\lambda = \frac{1}{A}\left\{\frac{\partial F}{\partial \boldsymbol{\sigma}}\right\}^T d\boldsymbol{\sigma}, \tag{6.9}$$

where A is a plastic resistance number that for strain hardening can be expressed as:

$$A = -\frac{\partial F}{\partial \kappa}\frac{\partial \kappa}{\partial \bar{\varepsilon}^p}\frac{\partial \bar{\varepsilon}^p}{\partial \lambda}, \tag{6.10}$$

The plastic resistance number is zero when the failure surface is reached.

The components that were determined above can be used to derive a constitutive relationship between stresses and strain. Thus the elasto-plastic constitutive equation can be established as:

$$d\boldsymbol{\sigma} = \boldsymbol{D}^{ep} d\boldsymbol{\varepsilon}\,, \tag{6.11}$$

where elasto-plastic stiffness matrix can be defined as:

$$\boldsymbol{D}^{ep} = \left[\boldsymbol{D}^{e} - \frac{\boldsymbol{D}^{e} \left\{ \frac{\partial Q}{\partial \boldsymbol{\sigma}} \right\} \left\{ \frac{\partial F}{\partial \boldsymbol{\sigma}} \right\}^{T} \boldsymbol{D}^{e}}{\left[A + \left\{ \frac{\partial F}{\partial \boldsymbol{\sigma}} \right\}^{T} \boldsymbol{D}^{e} \left\{ \frac{\partial Q}{\partial \boldsymbol{\sigma}} \right\} \right]} \right], \tag{6.12}$$

In case of perfect plasticity which is defined by pure elastic behaviour below the fixed failure criterion the failure surface is independent of κ and according to Eq. (6.10) A is equal zero. As a result the elasto-plastic stiffness matrix $\boldsymbol{D}^{ep}$ is singular.

6.3 Finite element discretisation

The finite element programs (i.e. PLAXIS, ANSYS) providing non-linear analysis in which the equilibrium state describe that the mechanical effect of the forces on a body undergoing a kinematic allowable velocity field is equal to the deformation effect by a dynamical allowable stress field (Skallerud, 2004) and can be written in form of a virtual work principle as (PLAXIS, 2002):

$$\int_{V} \delta\boldsymbol{\varepsilon}^{\mathrm{T}} \boldsymbol{\sigma} dV = \int_{S} \delta\boldsymbol{v}^{\mathrm{T}} \boldsymbol{t} dS + \int_{V} \delta\boldsymbol{v}^{\mathrm{T}} \boldsymbol{b} dV\,, \tag{6.13}$$

where $\boldsymbol{\sigma}$ and $\boldsymbol{\varepsilon}$ are the stress and strain vectors, δ indicates the virtual differences, $\boldsymbol{v}$ is the velocity field, $\boldsymbol{t}$ is the vector of traction forces components acting on surface *S*, $\boldsymbol{b}$ is the vector of body forces components at any point within the considered volume *V*.

According to the finite element method a continuum is divided into the number of elements. Taking into account that the displacements is an independent field variable, the displacement field in the element is assumed to be described by a combination of the displacements at the nodal point defining the element. The displacement field is obtained from the discrete nodal values by shape functions as:

$$\boldsymbol{u} = \boldsymbol{N}\ \mathbf{v}_{N}\,, \tag{6.14}$$

where $\boldsymbol{u}$ is the displacement field, $\boldsymbol{N}$ is the matrix that contains the shape functions, $\mathbf{v}_{N}$ is the nodal displacement vector.

For the static conditions when the inertia forces are ignored, the following non-linear equilibrium equation was derived from virtual work principle (implicit solution):

$$\begin{aligned} \boldsymbol{R} &= \boldsymbol{R}^{ext} - \boldsymbol{R}^{int} = 0 \,, \\ d\boldsymbol{R} &= \boldsymbol{K}(\mathbf{v}_N)\ \mathrm{d}\mathbf{v}_N \,, \end{aligned} \tag{6.15}$$

where $\boldsymbol{R}$ is the nodal force vector, $\boldsymbol{R}^{ext}$ is the sum of external forces defined by the right side in Eq. (6.13), $\boldsymbol{R}^{int}$ is the sum of internal forces defined by the left side in Eq. (6.13), $\boldsymbol{K}$ is the tangential stiffness matrix.

Deformations measured by the strain are determined from displacements as:

$$d\boldsymbol{\varepsilon} = \boldsymbol{B}(\mathbf{v}_N)\ \mathrm{d}\mathbf{v}_N \,, \tag{6.16}$$

where $\boldsymbol{B}$ is the strain interpolation (kinematic) matrix that defines the kinematic relation based on the shape functions.

From a virtual work approach, the stiffness matrix can be written as:

$$\boldsymbol{K} = \int_V \boldsymbol{B}^T \boldsymbol{C} \boldsymbol{B}\ dV \,, \tag{6.17}$$

where $\boldsymbol{C}$ is the constitutive tensor in matrix form.

In simplest form $\boldsymbol{K}$ represents a linear elastic response. In this case the constitutive matrix is equal to elastic material stiffness matrix $\boldsymbol{D}^e$.

The development of stress state $\boldsymbol{\sigma}$ can be regarded as an incremental process:

$$\begin{aligned} \boldsymbol{\sigma}^{i+1} &= \boldsymbol{\sigma}^{i} + \Delta\boldsymbol{\sigma} \,, \\ \Delta\boldsymbol{\sigma} &= \int_t d\boldsymbol{\sigma} dt \end{aligned} \tag{6.18}$$

where $\boldsymbol{\sigma}^{i+1}$ is the actual state of stress which is unknown, $\boldsymbol{\sigma}^{i}$ is the previous state of stress which is known, $\Delta\boldsymbol{\sigma}$ is the stress rate integrated over a small time increment (stress increment).

If Eq. (6.13) is considered for the actual state $i+1$, then the unknown stress $\boldsymbol{\sigma}^{i+1}$ can be eliminated using Eq. (6.18):

$$\int_V \delta\boldsymbol{\varepsilon}^{\mathrm{T}} \Delta\boldsymbol{\sigma}\ dV = \int_S \delta\boldsymbol{v}^{\mathrm{T}} \boldsymbol{t}^{i+1} dS + \int_V \delta\boldsymbol{v}^{\mathrm{T}} \boldsymbol{b}^{i+1} dV - \int_V \delta\boldsymbol{\varepsilon}^{\mathrm{T}} \boldsymbol{\sigma}^{i} dV \tag{6.19}$$

The stress increments $\Delta\boldsymbol{\sigma}$ are obtained by integration of stress rates according to Eq. (6.18). For differential plasticity the strain increments can generally be written as:

$$\Delta\boldsymbol{\sigma} = \boldsymbol{D}^e\left(\Delta\boldsymbol{\varepsilon} - \Delta\boldsymbol{\varepsilon}^p\right), \tag{6.20}$$

where $\boldsymbol{D}^e$ represents the elastic material stiffness matrix for the current stress increment, $\Delta\boldsymbol{\varepsilon}$ and $\Delta\boldsymbol{\varepsilon}^p$ are the strain increments. For plastic material behaviour, the plastic strain increment can be estimated according to Vermeer (1979):

$$\Delta\boldsymbol{\varepsilon}^p = \Delta\lambda\left[(1-\alpha)\left(\frac{\partial Q}{\partial\boldsymbol{\sigma}}\right)^i + \alpha\left(\frac{\partial Q}{\partial\boldsymbol{\sigma}}\right)^{i+1}\right], \tag{6.21}$$

where $\Delta\lambda$ is the increment of the plastic multiplier, α is the parameter indicating the type of time integration. By choosing $\alpha = 0$, the method remains explicit known as the *Forward Euler* integration scheme. In this case the stable strain increment becomes too short for the failure modelling applications. By choosing $\alpha = 1$, the integration scheme becomes implicit, requires local iterations. The method is called as *Backward Euler* integration, providing a stable algorithm. Vermeer (1979) has shown that the implicit integration overcomes the requirement to update the stress to the yield surface in case of transition from elastic to elastoplastic behaviour.

For the implicit time integration the Eq. 6.18 can be modified to:

$$\boldsymbol{\sigma}^{i+1} = \boldsymbol{\sigma}^{tr} - \Delta\lambda\boldsymbol{D}^e\left(\frac{\partial Q}{\partial\boldsymbol{\sigma}}\right)^{i+1} \qquad \text{with } \boldsymbol{\sigma}^{tr} = \boldsymbol{\sigma}^i + \boldsymbol{D}^e\Delta\boldsymbol{\varepsilon}, \tag{6.22}$$

where $\boldsymbol{\sigma}^{tr}$ is an auxiliary stress vector, referred to as the elastic or trial stresses, which is the new stress state when considering purely linear elastic material behaviour.

The increment of plastic multiplier can be solved from the condition that the new stress state has to satisfy the yield condition and in case of perfectly plastic and linear hardening models can be written (Simo and Hughes, 1999) as:

$$\Delta\lambda^{(k)} = \frac{F_{i+1}^{(k)}}{\left\{\frac{\partial F}{\partial\boldsymbol{\sigma}}\right\}_{i+1}^{(k)}\boldsymbol{D}^e\left\{\frac{\partial Q}{\partial\boldsymbol{\sigma}}\right\}_{i+1}^{(k)} + \left\{\frac{\partial F}{\partial\boldsymbol{\kappa}}\right\}_{i+1}^{(k)}\boldsymbol{h}_{i+1}^{(k)}}, \tag{6.23}$$

where $\boldsymbol{h}$ is the hardening function, which is zero for the perfectly plastic models and constant for linear hardening models.

When the solution for the stress state is valid the constitutive matrix has to be defined at the end of each increment. This is done in order to create the global tangential stiffness matrix (Eq. (6.17)), which is needed for estimating the next increment when solving the global non-linear balance equation.

6.4 References

Hill, R. (1950). The mathematical theory of plasticity. Oxford, Clarendon Press, 355p.

Nordal, S. (2004). Soil modeling. Lecture notes to PhD course BA8304. Norwegian University of Science and Technology. Geotechnical Division. Trondheim, 264p.

Ottosen, N.S. and Petersson, H. (1992). Introduction to the Finite Element Method. Prentice Hall Europe, 410p.

PLAXIS Plaxis v. 8.2., (2002). Finite Element Code for Soil and Rock Analyses.

Simo, J.C. and Hughes, T.J.R (1998). Computational Inelasticity. Springer-Verlag, New York, 392p.

Skallerud, B. (2004). Nonlinear finite element analysis. Lecture notes to PhD course DIO 1015. Norwegian University of Science and Technology. Department Structural Engineering. Applied Mechanics Division. Trondheim, 134p.

Vermeer, P.A. (1979). A modified initial strain method for plasticity problems. *In Proc. of the 3rd Int. Conf. Num. Meth. Geomech.*, Balkema, Rotterdam, pp. 377–387.

7 NUMERICAL MODELLING OF ICE RUBBLE BEHAVIOUR

7.1 Introduction

This chapter presents the numerical study on the ice rubble deformation behaviour and its strength. The motivations for this work are summarized below:

1. To improve the knowledge about the properties of the unconsolidated part of the ice ridge i.e. ice rubble.
2. To study the deformation behaviour of the ice rubble material. It can be important for ice ridge scour studies and for ice ridge-structure interaction investigations.

Several test programs both in laboratory and in-situ were conducted in order to evaluate the strength properties of the ice rubble material. The analysis of such features is usually based on classical soil theory assuming simultaneous failure surfaces within the study item and the ice rubble being described as a Tresca, Mohr-Coulomb (2D) or Drucker-Prager (3D) material. But the reported strength parameters (angle of internal friction and cohesion) for the ice rubble show a great scatter. There are several reasons behind this. Firstly, as mention in Chapter 6 it is doubtful that the ice rubble blocks can be compared to the grains of the soil since the size of the blocks are too large for the hypothesis of continuum. The size, shape of individual rubble blocks and freeze bond contacts between them may affect the global behaviour. Secondly, the Mohr-Coulomb and Drucker-Prager failure criteria assume that the ice rubble fails only by shearing. However, in addition to the shear failure the ice rubble can fail by crushing due to compaction in the front of the structure during the ice ridge-structure interaction process. Finally, by contrast to soil material the ice rubble properties changes through the lifetime of the ice ridge corresponding to the initial, main and decay phase of formation. In this case the thermodynamic similarity between the prototype (unconsolidated part of ice ridge) and the ice rubble model become of high importance. This makes the situation even more complicated and leads to the following question: can we apply, if so how to apply, the soil theory (in particular the Mohr-Coulomb or Drucker-Prager theory) to the ice rubble modelling?

This chapter consists of two papers, each composing a section. Section 7.3 presents an introduction to the model that was extended and verified in Section 7.2. All sections are almost identical to the referred papers.

Publication references:

(7.2) Shafrova, S. (2007). Initial failure of the ice rubble in plane strain direct shear tests. In Proceedings of the 19th International Conference on Port and Ocean Engineering under Arctic conditions, (POAC), Dalian, China, Vol. 1, pp. 256-266.

(7.3) Shafrova, S., Liferov, P., Shkhinek, K. (2004). Modelling ice rubble with pseudo-discrete continuum model. In Proceedings of the 17th International Symposium on Ice (IAHR), Saint-Petersburg, Russia, Vol. 2, pp. 265-274.

7.2 Initial failure of the ice rubble in plane strain direct shear tests

Svetlana Shafrova

University Centre in Svalbard, Longyearbyen, Norway

Abstract

A pseudo-discrete continuum model was developed to study the behaviour of ice rubble blocks and particularly theirs initial failure mechanism. The model is a combination of discrete particle assembly generator and Finite Element analysis of this assembly. The model provides a possibility to simulate the contacts (bonds) between the ice blocks. The 2D plane strain direct shear test simulations on the ice rubble were performed. The influence of block size (contact size effect), rubble porosity and normal pressure was investigated. The sensitivity analysis of the input parameters on the overall variability of the model has been carried out. It was shown that the morphological and mechanical properties of the freeze bonds between the ice blocks are important for the strength evaluation and for understanding the deformation behaviour of the ice rubble in the first-year sea ice ridges.

Introduction

The first-year sea ice ridges are often divided into two parts: sail and keel. The sail comprises ice blocks, snow and voids that filled by air and snow. The keel consists of a consolidated layer of refrozen ice, which grows through and unconsolidated or partly consolidated ice rubble beneath. Immediately after formation the ice rubble consists of large amount of blocks of different size that can rotate around each other and the rubble strength results from contact friction and mechanical interlocking. This type of material is cohesionless. During the initial phase of the consolidation the originally low ice temperature is spent in creating freeze-bonds between the blocks. This type of ice rubble is apparently coherent. Typically, the first-year sea ice ridge is a mixture of crushed, broken ice blocks that frozen together with slush, water and air in between.

The analysis of such granular media is usually based on classical soil theory, where a Mohr-Coulomb state of failure is determine the material yielding. It is assumed that plastic flow occurs when the shear stress (τ) reaches the amount:

$$\tau = c + \sigma \tan \varphi \qquad (1)$$

where σ is the normal stress, φ is the angle of internal friction, c is the cohesion.

Several laboratory and in-situ programs on testing of the ice rubble properties have been carried out. The reported values of angle of internal friction (φ_r) and cohesion (c_r) for the ice rubble show a great scatter. Bruneau (1997) has reviewed the literature and summarized that the results were in range of φ_r= 8 - 70° and c_r=0 - 20 kPa.

Furthermore, several Finite Element (FE) and Discrete Element (DE) models have been developed so far. The ice rubble behaviour during punch test were simulated using FE approach by Heinonen (2003) and Liferov et al. (2003) where the ice rubble was treated as continuum homogeneous material which is not fully truthful. Thus the properties obtained from these simulations can be considered only as an indication of the strength of the rubble material.

The DE model has been developed by Hopkins and Hibler (1991) in order to study the behaviour and strength of the ice rubble in the direct shear tests. They indicate that the local rearrangement and breakage are competing mechanisms for the relief local forces on the nominal failure plane. The freeze-bonding effect (cohesion) was ignored during these simulations.

For the current study the pseudo-discrete approach was used to investigate the ice rubble deformation behaviour. This implies that ice rubble was treated as heterogeneous material that is a combination of the ice blocks (that connected to each other via freeze bonds) and voids between them. Based on such assumption the pseudo-discrete continuum model (PDCM) was developed as a tool to study initial failure of the ice rubble skeleton. The goal of the present work was to determine equivalent parameters of the homogeneous ice rubble medium. The attempt to extend this model for the large deformation was also presented.

Pseudo-discrete continuum model

The detailed description of the program is given by Shafrova et al. (2004) and by Liferov (2005) and only main aspects are repeated below.

The model is a combination of a discrete particle assembly generator and a FE analysis of this assembly. It provides the possibility to simulate the contacts between the ice blocks and their local failure. The modelling procedure consists of two basic steps. First, the assembly of blocks is developed using the custom-developed computer C++ program called the block generator. This program fills a closed contour with blocks of rectangular or cubical shape. In the second step, the generated assembly was used as a geometrical input to the FE analysis. The Plaxis FE code (Plaxis, 2002) was used for the numerical simulations.

The model consists of:

The ice blocks. They were assigned an elastic-plastic Mohr-Coulomb material model with a tensile cut-off (σ_t).

The contacts between the blocks. The ice rubble blocks are freeze to each other forming the freeze-bonds at the points of contacts. These contacts were modelled using the interface elements that are allowed to reduce the friction and to simulate thin zone of intensely shearing material at the points of contacts in between the blocks. The strength properties of the freeze-bonds are linked to the strength properties of the surrounding ice blocks via strength reduction factor (R_i) as follows:

$$c_{fb} = R_i \cdot c_{ice} \text{ and } \tan\varphi_{fb} = R_i \cdot \tan\varphi_{ice}, \quad (2)$$

$$\sigma_{t,fb} = R_i \cdot \sigma_{t,ice}, \quad (3)$$

where c_{fb}, φ_{fb} and c_{ice}, φ_{ice} are the cohesion and the angle of internal friction of the freeze bonds and ice blocks respectively.

The voids between the blocks. They were modelled using elastic material with a negligible stiffness.

The quasi-static approach was used in the simulations and the ice rubble was modelled as a weightless material, i.e. initially the rubble was unloaded. A plane strain FE model was chosen for the simulations. Iterative calculations were carried out until the overall stiffness of the material approached zero. This was an indication of complete failure of the initial rubble skeleton along the shear surface.

Direct shear box simulations

General description

The apparatus for the 2D direct shear box is shown in Fig. 1. The length/height ratio (L/H) of the shear box is equal to 2. The upper part of the box moves in a horizontal direction relative to the lower part, which is fixed. The vertical pressure (p_y) was constant and the horizontal pressure (p_x) was incrementally applied to move the upper part of the shear box. Table 1 presents properties for the ice blocks that were chosen after Sanderson, (1988) and Kämärinen, (1993).

Parametric analysis

The present simulations are based on the results by Shafrova et al. (2004), where the similar shear box was used. They argue that the initial failure mode is almost independent of the frictional component. Therefore angle of internal friction of the ice (φ_{ice}) was assumed to be constant.

The small-scale field and laboratory tests of the freeze-bonding strength were done by Shafrova and Høyland (2007a). They indicate that the average strength of the freeze-bonding contacts is 32 ± 18 kPa after 48 hours of submerging in the field and 67 ± 52 kPa within 60 hours of the laboratory testing. Besides Shafrova and Høyland introduce the ratio of freeze-bonding strength to the strength of the surrounding ice blocks (σ_{fb}/σ_{si}) that equal to the strength reduction factor (R_i) in Eq. (2) and (3) of the current paper. The ratio was found in range of 0.008 to 0.082 and in average 0.03 after 48 hours of submerging in the field. For the laboratory tests it was varied from 0.015 to 0.40 within 60 hours of submerging. Based on these results, the value of R_i for the current simulations was chosen to be 0.09 that corresponds to 40-50 kPa for the freeze bonding strength.

As a further examination of the model the influence of block size (contact size effect), rubble porosity and normal pressure was investigated.

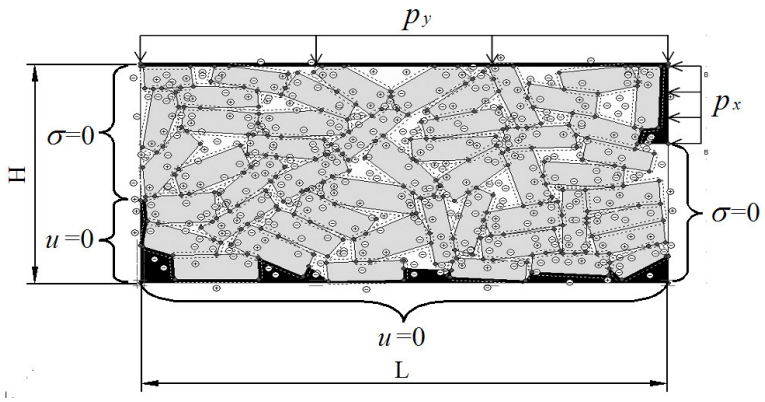

Fig. 1. The direct shear box.

(L, H are the length and height of the shear box, u is the displacement, σ is the stress, p_y is the normal pressure, p_x is the horizontal pressure).

Table 1. Ice block properties.

Property	Value	Property	Value
Young's modulus (E_{ice}), GPa	1.0	Angle of internal friction (φ_{ice}), °	30
Poisson's ratio (ν_{ice})	0.3	Tensile strength ($\sigma_{t,ice}$), MPa	0.2
Cohesion (c_{ice}), MPa	0.5		

Size effect (contact effect)

Four different geometry sets with respect to the size of the block were used. The length to thickness ratio (*l/t*) of the ice blocks was assumed constant and equal to 3.33. The *L/t* ratio (length of the shear box/thickness of the ice blocks) was varied from 12.7 up to 23.3. The geometric properties of the rubble assemblies for the performed simulations are shown in Table 2.

Three different random assemblies were conducted for the each geometry set. The porosity (η) of the ice rubble assembly and ratio of total length of the contacts (interface elements) between the blocks to length of the shear box (*A/L*) about 28% and 2.2 respectively for all assemblies. Based on the data from Shafrova and Høyland (2007b) the ratio of the average contact length to the average block length (*a/l*) was assumed to be in range of 0.19 to 0.31 for the different geometry sets. The number of blocks (N_b) and number of contact interface elements in between the blocks (N_c) were approximately the same for an identical geometrical set as shown in Table 2.

The shear stress τ (in the following referred as maximum horizontal force (derived from p_x) attained during the test divided by the area of the shear surface (*L*)) versus ratio *L/t* is given in Fig. 2. It can be seen that the shear stress decreases with increasing of the block size. The correlation between block size and average length of the frozen contacts was found and the results are given in Fig. 3. As will be shown further the size of the freeze bonding contacts is responsible for the changes of the strength of the ice rubble material. Thus, the 'size effect' is hereafter called as 'contact effect'.

Porosity effect

The typical macro porosity (η) of ice ridge is in range of 25-40%. Three assemblies of Set 1 from the previous part of the parametric study were used as geometrical input for the initial step of the current analysis. The N_b and N_c were kept to be equal for the assemblies with the same porosity. Further, the porosity was increased from 28% to 38%. The shear stress decreases with increasing porosity as given in Fig. 4. The correlation plot of rubble porosity versus total length of the frozen contacts is shown in Fig. 5.

Table 2. Geometric properties of the ice rubble assemblies.

(l, t are the average block length and thickness; L is the length of the shear box; N_b and N_c are the number of blocks and contact interface elements; η is the porosity of the ice rubble assembly; A and a are the total and average lengths of the contact interface elements).

No.	l x t (m)	L/t	N_b/N_c	η (%)	A/L	a/l	a/L (x10^2)
Set 1	1.0 x 0.3	23.3	50/81 50/82 50/83	~28	~2.2	0.19	2.69 2.71 2.71
Set 2	1.33 x 0.4	17.5	31/56 31/53 31/56			0.21	3.97 4.06 3.96
Set 3	1.67 x 0.5	14	20/32 19/34 19/32			0.28	6.75 6.45 6.72
Set 4	1.83 x 0.55	12.7	17/26 17/28 16/27			0.31	8.31 7.94 8.02

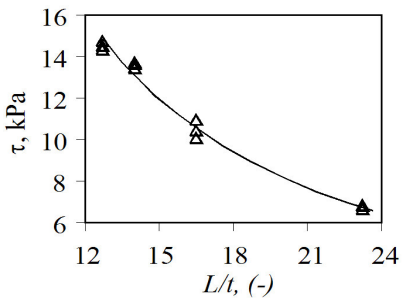

Fig. 2. Shear stress τ versus L/t.

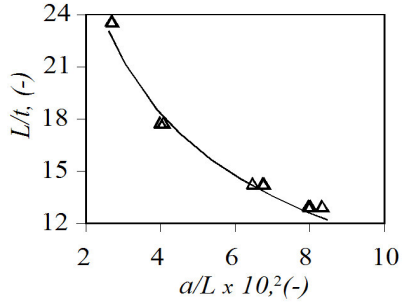

Fig. 3. Correlation plot L/t versus a/L.

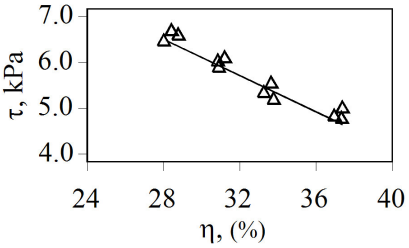

Fig. 4. Shear stress τ versus η.

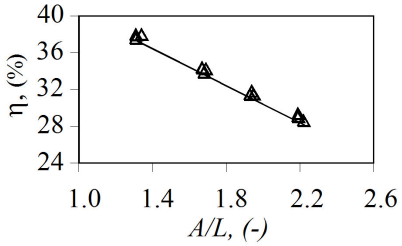

Fig. 5. Correlation plot η versus A/L.

Influence of normal pressure

Using the same geometry Sets 1-4 the influence of normal pressure was examined. For the range of the present analysis shear stress increased linearly with increase of normal pressure for the different ice rubble assemblies as shown in Fig. 6.

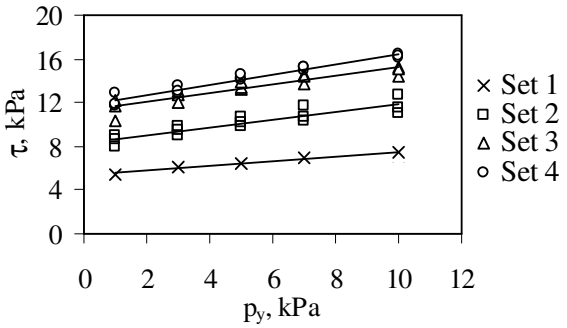

Fig. 6. Shear stress τ versus normal pressure p_y.

Sensitivity analysis

In order to identify the parameters, which uncertainty has the highest impact on the PDCM model, the on-way sensitivity analysis has been performed. The results are given in Fig. 7 as a Tornado diagram that clearly shows the impact of several parameters such as strength reduction factor, contact effect, cohesion and angle of internal friction of the ice, initial confinement, rubble porosity on the cohesion of the ice rubble. Besides, the diagram illustrates the influence of parameters uncertainty, representing the range of possible outcomes and ranks them in order of importance.

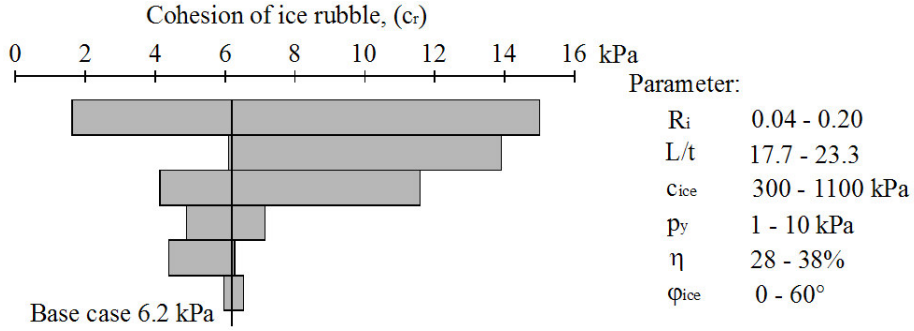

Fig. 7. Tornado sensitivity diagram.

(where R_i is the strength reduction factor, L/t is the length of the shear box/thickness of the ice blocks, c_{ice} is the ice cohesion, p_y is the normal pressure, η is the porosity of ice rubble, φ_{ice} is the angle of internal friction of the ice).

Discussion

Parametric analysis

Several programs on laboratory testing of ice rubble strength properties have been carried out in the direct shear boxes. Both unconsolidated (Prodanovic (1979), Weiss et al. (1981)) and partly consolidated (Leppäranta and Hakala (1992)) ice rubble were under investigation. These laboratory data together with current results from FE simulation are given in Table 3.

Table 3. FE simulation results in comparison with the laboratory direct shear tests.

Author(s)	L (m)	t (m)	L/t (-)	c_r (kPa)	c_r (L/t), kPa	Comments
Prodanovic (1979)	0.457	0.019 0.038	24.0 12.0	0.26 0.58	6.25 6.96	Artificially grown sea ice, UCR
Weiss et al. (1981)	1.8	0.08 0.15 0.20	22.5 12 9	1.45 1.85 3.75	32.6 22.2 33.8	
Leppäranta and Hakala (1992)	0.8	0.015	53.3	0.9…2.6	48…139	Artificially grown fresh water ice, PCR
Current simulations	-	-	23.3 17.5 14 12.7	6.1…6.3 9.3…10.2 12.6…13.3 13.5…13.9	142…147 162…178 176…186 173…176	PCR, sea ice properties used as input data, 2D tests

UCR – unconsolidated ice rubble, PCR – partly consolidated ice rubble.

As can be seen in Fig. 2 and Table 3 the strength of the ice rubble tends to increase as the size of the ice blocks increases. The same trend was also observed in the laboratory tests of the unconsolidated rubble.

The increasing of rubble strength results from increasing of resistance to the deformation within the ice rubble. The possible resistance mechanisms are: friction at the points of contact, mechanical interlocking and cohesion strength of freeze-bonds between ice blocks. Two first mechanisms are exhibited mainly in unconsolidated ice rubble and all three are found in partly consolidated rubble. Thus, the increasing of block size deals with increasing of the average length of the contact interface elements between the ice blocks as shown in Fig. 3. Since the smaller contact length characterized by less resistance that leads to smaller strength of the rubble material.

Weiss et al. (1981) have been proposed that the angle of internal friction of the ice rubble is not affected by changes in scale and the rubble cohesion changes proportionally to the geometrical scale factor. Fig. 6 shows that the angle of internal friction increased from 3º to 8º as the contact size increases. However, the increase of apparent angle of internal friction decreases as the size of the contacts increases. Thus for initial failure, the angle of internal friction is little of importance and the cohesion is a major contributor to the bearing capacity of the rubble.

In order to scale the material properties, the value c_r (L/t) was introduced. It was found in range from 138 to 186 kPa as shown in Table 3. The values are in order of magnitude with results by Leppäranta and Hakala (1992), where the artificial freshwater partly consolidated ice rubble blocks were tested. Besides, the values are significantly higher than the results by Prodanovic (1979) and Weiss et al. (1981) for the unconsolidated rubble made from the artificially grown saline ice, which seems to be reasonable.

The continue increasing or decreasing of the L/t ratio asymptotically leads some threshold values, which seems very interesting with respect to use of continuum mechanics approach. Unfortunately the current PLAXIS software can't provide capability to verify this. The limitation of the input geometry (effect of "complex geometry") was found during the mesh generation process. The mesh was generated only if the number of the non-contacting clusters was less than 25. As a result this leads to limitation in number of blocks and number of contacts between them in the assembly. The Set 1 (N_b=50, N_c=81-83) shows the most complicated geometry that can be achieved using PLAXIS software. As will be shown further the more advanced FE program (e.g. ANSYS) should be used for the complicated tasks.

Based on the analysis of different geometries the correlation between total length of the contacts and rubble porosity was found as shown in Fig. 5. The ridge porosity is better known than the morphology of the freeze bonds. Recently only investigations by Shafrova and Høyland (2007b) has been done. During this study, the typical dimensions of the freeze bonds and the ratio of the freeze bond length to the block length were estimated. These data was used as input for the current simulations. However, the total length of the freeze bonding contacts per section within ice ridge is still unknown. Thus the field investigation with focus on the block/freeze bonds morphology with subsequent probabilistic analysis should be done.

Sensitivity analysis

The Tornado diagram (Fig. 7) shows that results are strongly influenced by the input parameters such as strength and size of the freeze bonds between the ice blocks and ice cohesion. The major impact induced by strength reduction factor for the interfaces elements that correspond to the ratio of freeze-bonding strength to the strength of the

ice blocks. Besides it characterized by greatest uncertainty due to lack of data on the strength of freeze bonds. The first attempt to estimate this strength was carried out by Shafrova and Høyland (2007a), where the small-scale tests with the submerged ice blocks were conducted. In order to reduce this uncertainty a more thorough investigations are needed.

Further development

In order to avoid the 'complex geometry' effect and extend the model for the large deformation (that is associated with the rotation, rearrangement of the ice blocks and their breakage) the more advance ANSYS FE program was used for the further simulations.

The ice blocks were assigned an elastic-plastic Drucker-Prager material model. The 2D 8-node element was chosen for the mesh generation as given in ANSYS theory manual (Ansys, 2006). The voids between the ice blocks were left empty. In order to model contacts between the ice blocks two types of elements were considered, namely: target and contact. The node-to-surface contact elements were selected for the simulations, which enable to transmit the contact forces between the two bodies. These contact elements can carry shear stress up to a certain magnitude before they start sliding relative to each other. The contact elements were considered flexible. The friction between the ice blocks was taken into account. Such modelling technique permit to investigate the mechanism of ice blocks repacking together with the effect of the freeze bonds. This is one of advantages of the ANSYS FE software.

The proposed model is currently under development. More thorough results will be published in the nearest future.

Conclusions

The initial failure in case of direct shear tests was studied with PCDM. The initial failure of rubble skeleton that corresponds to the breakage of the freeze bonds between the ice blocks was observed during simulations.

The main concussions are:

- The strength of the ice rubble tends to increase as the size of the freeze bonds increases.
- The cohesion of partly consolidated rubble was found as 6.2±0.1 kPa.
- For the initial failure, the angle of internal friction has little of importance and the cohesion is a major contributor to the bearing capacity of the ice rubble.

- The PDCM is very sensitive to both freeze bonding strength, local strength of the surrounding ice blocks and morphology of the ice blocks and freeze bonds between them. As a result it is necessary to investigate these aspects both in laboratory and in-situ.

Acknowledgements

I would like to thank Dr. Pavel Liferov and Prof. Karl N. Shkhinek for the original idea and helpful discussions, Dr. Knut V. Høyland for the extensive review. The valuable support from Ms. Ekaterina Kim is greatly appreciated.

References

ANSYS Ansys v. 10, (2006). Ansys Release 10.0 Documentation Guide.

Bruneau, S. (1997). Development of a first-year ridge load model. PhD thesis, Memorial University of Newfoundland, St. John's, Newfoundland, Canada.

Heinonen, J. (2003). Continuum material model for ice rubble - combined shear-cap yield criterion with strain softening. *Proc. of the 17th Int. Conf. on Port and Ocean Engineering under Arctic Conditions (POAC)*, Trondheim, Norway, Vol. 2, pp. 547–557.

Hopkins, M.A. and Hibler, W.D. (1991). On the shear strength of geophysical scale ice rubble. *Cold Regions Science and Technology*, (19): 201-212.

Kämärinen, J. (1993). Studies in ice mechanics. Helsinki University of Technology. 182p.

Leppäranta, M. and Hakala, R. (1992). The structure and strength of first-year ridges in the Baltic Sea. *Cold Regions Science and Technology*, (20): 295–311.

Liferov, P., Jensen, A. and Høyland, K.V. (2003). 3D finite element analysis of laboratory punch tests on ice rubble. *Proc. of the 17th Int. Conf. on Port and Ocean Engineering under Arctic conditions (POAC)*, Trondheim, Norway, pp.599–610.

Liferov, P. (2005). Review of ice rubble behaviour and strength, Part II: Modelling. *Cold Regions Science and Technology*, (41): 153–163.

PLAXIS Plaxis v. 8.2. (2002). Finite Element Code for Soil and Rock Analyses.

Prodanovic, A. (1979). Model tests of ice rubble strength. *Proc. of the 5th Int. Conf. on Port and Ocean Engineering under Arctic conditions (POAC),* Trondheim, Norway, Vol. 1, pp. 89-105.

Sanderson, T.J.O. (1988). Ice Mechanics. Risk to offshore structures. 253p.

Shafrova, S., Liferov, P., Shkhinek, K. (2004). Modelling ice rubble with pseudo-discrete continuum model. *Proc. of the 17th Int. Symp. on Ice (IHAR)*, Saint-Petersburg, Russia, Vol. 2, pp. 265-274.

Shafrova, S. and Høyland, K.V. (2007a). Thermo-mechanical properties of the ice rubble. Freeze-bond experiments. *Submitted to Journal Cold Regions Science and Technology.*

Shafrova, S. and Høyland, K.V. (2007b). Morphology and 2D spatial strength distribution in two Arctic first-year sea ice ridges. *Cold Regions Science and Technology,* doi:10.1016/j.coldregions. 2007.05.011.

Weiss, R.T., Prodanovic, A. and Wood, K.N. (1981). Determination of ice rubble shear properties. *Proc. of the Int. Symp. on Ice (IAHR)*, Quebec, Canada, pp. 860-872.

7.3 Modelling ice rubble with pseudo-discrete continuum model

S. Shafrova[1,2)], P. Liferov[2,3)] and K. Shkhinek[4)]

[1)] *University Centre on Svalbard, Longyearbyen, Norway*
[2)] *Norwegian University of Science and Technology, Trondheim, Norway*
[3)] *Barlindhaug Consult AS, Tromsø, Norway*
[4)] *St. Petersburg State Polytechnical University, St. Petersburg, Russia*

Abstract

A pseudo-discrete continuum model was developed to study the breakage of the initial rubble skeleton. A special program was developed to generate a random assembly of rectangular blocks in a closed shape allowing to vary the block size and the resulting porosity of the assembly. The obtained assemblies were further used as geometrical input for the finite element model. The blocks were modelled as elasto-plastic bodies, contact elements were used to simulate the reduced strength at contacts between the blocks. Direct shear test simulation on the ice rubble were performed. The effect of the mechanical properties of the ice blocks and their contacts was investigated by applying different boundary conditions to assembly of the blocks.

Introduction

Several testing program on ice rubble mechanical properties have been done. Both laboratory and in-situ tests were performed. The results by Ettema and Urroz (1989) and Timco and Cornet (1999) confirmed that it is possible to describe ice rubble behaviour by elastic-perfectly plastic model, i.e. Mohr-Coulomb yield criteria.

Several methods to estimate the loads from ice ridges on offshore structures have been developed, both analytical and numerical models.

In the analytical approach the major difficulties are connected with the two-parametric Mohr-Coulomb failure criterion. The material properties (friction and cohesion) are not easy to determine. The cohesion term is mainly a function of freeze bonds between the ice blocks. Such bonds are broken at the initial stage in any interaction (Urroz and Ettema, 1987). The full frictional component cannot be mobilized until significant motion on failure plane has taken place. Thus, it is unlikely that frictional and cohesion terms will act simultaneously. Several assumptions and simplifications were done and ice rubble was often treated either as frictionless or as cohesionless material.

Numerical approaches used Finite Element (FE) and Discrete Element (DE) models that can describe the behaviour of ice rubble. Recently only few FE based modelling was conducted by Heinonen (2002, 2003) and Liferov et al. (2002, 2003). Punch tests were simulated in these models. The ice rubble was treated as a continuum and homogenous medium.

Discrete Element simulations by Hopkins and Hibler (1991) were done to study the behaviour and strength of ice rubble in the direct shear box. The freeze-bonding effect was neglected in these simulations. But it was suggested that a model of freeze-bonding might be used to explore various forms that such mechanism might take.

A pseudo-discrete continuum model, which simulates the initial breakage of the rubble skeleton, is described in this paper. The ice rubble was considered as discrete material and the effect of freeze bonds between individual ice blocks was taken into account. The model description and results of direct shear-box simulations are presented.

Pseudo-discrete continuum model

General description

The pseudo-discrete continuum model of ice rubble is a combination of the discrete particle assembly generation (i.e. ice rubble accumulation) and the FE analysis of this assembly. The primary goal for developing such model was to study numerically the initial failure mechanism of ice rubble. This model provides a possibility to simulate the contacts between the ice blocks and their local failure.

The modelling procedure consists of two basic steps. First, the assembly of blocks is generated. The block generator tool was developed to fulfill this task. In the second step, the generated assembly is used as a geometrical input for the FE analysis to study its behaviour under loading at the different boundary conditions.

Generation of discrete block assembly

Generation of the discrete block assembly was conducted in the custom-developed computer program called the block generator. This program fills the closed contour with blocks of rectangular shape. The blocks themselves are considered as solid bodies. Geometry of each block is defined by its centre of gravity x_c, y_c and four vertices. The assumed porosity of assembly is used to calculate the number of blocks needed to fill the area. In the process of generation it is possible to define the area within a contour (by means of top and bottom control lines) to estimate its effective porosity. The direction of gravity is specified by the attraction line that can be given different locations within the contour throughout the simulation. Fig. 1 shows a

typical interface view of the program during a simulation run. Detail description of the block generator is beyond the scope of this paper.

Finite element model

The generated assembly of ice blocks was used as a geometrical input for the FE analysis. It was conducted using the Plaxis FE code (Plaxis, 2002). The FE model of the ice rubble is shown in Fig. 2.

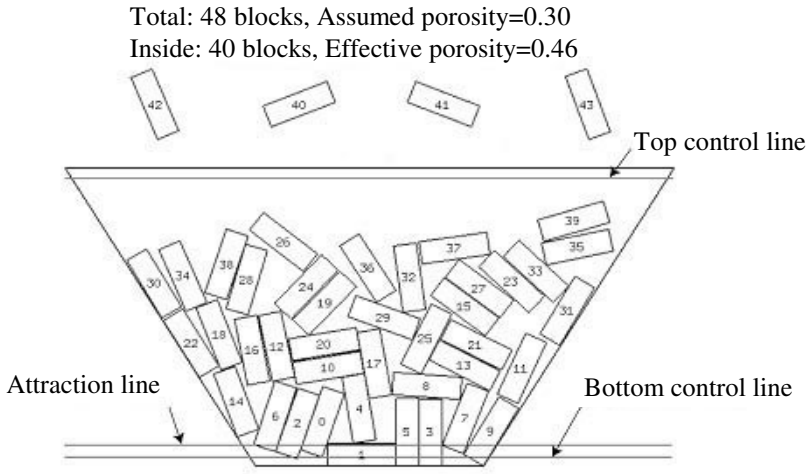

Fig. 1. Block generation in progress.

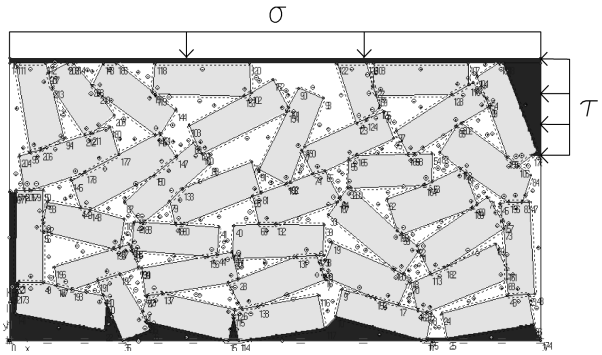

Fig. 2. The direct shear box.
(σ is the normal pressure, τ is the horizontal pressure).

The model consists of:

The ice blocks. They were assigned an elastic-perfectly plastic Mohr-Coulomb material model. It is a constitutive model with a fixed yield surface, i.e. a yield surface that is not affected by plastic straining. The yield surface thus always coincides with the failure surface that is defined by six yield functions of the following form when formulated in terms of principal stresses σ_i, σ_j:

$$F = (\sigma_i + a) - N(\sigma_j + a), \tag{1}$$

where the following state parameters are used: $N = (1 + \sin\varphi) / (1 - \sin\varphi)$, φ is the angle of internal friction, a is the attraction ($a = c/\tan\varphi$), c is the cohesion. For $c > 0$, the standard Mohr-Coulomb criterion allows for tension. However, the ice normally sustains smaller tensile stresses than those defined by the standard form of the failure criterion. In order to account for this, three additional yield functions are introduced:

$$F = \sigma_i - \sigma_t \text{ and } 0 \le \sigma_t \le a, \tag{2}$$

where σ_t is the tensile stress of ice.

The contacts between the blocks. They were modelled using the interface elements. Fig. 3 shows the close-up of contacts between ice blocks in the rubble (with the mesh on). The interface element shown in the figure to have a finite thickness, but in the FE formulation the coordinates of each node pair are identical, which means that the element has a zero thickness. Each interface has assigned to it a 'virtual thickness' which is an imaginary dimension used to define the material properties of the interface.

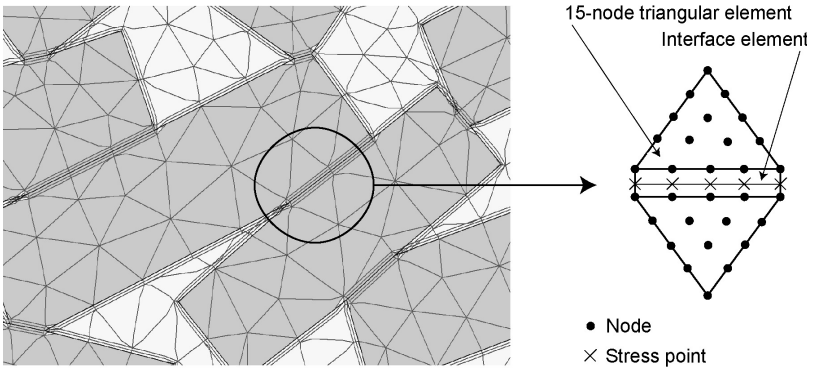

Fig. 3. Ice blocks in contact.

The length of contacts between the blocks is assumed to be a variable parameter. For the initial step the contact length is established to have a minimum value which can sustain the applied load combination. In case of smaller values the material fails during construction stage under compression, which operated by normal pressure. Thus the contact lengths have to be increased for the further simulations.

The strength properties of the interfaces are linked to the strength properties of the ice blocks via the strength reduction factor for interfaces (R_i) as follows:

$$c_i = R_i \cdot c \text{ and } \tan\varphi_i = R_i \cdot \tan\varphi \quad (3)$$

The voids between the blocks. They were modelled using elastic material with a negligible stiffness. This was done to avoid mesh problems - use of elastic material instead of leaving voids "empty". Verification was conducted on identical models with and without elastic material in the voids to prove that it doesn't affect the results.

The quasi-static approach was used in the simulations. The ice rubble was modelled as a weightless material, i.e. initially the rubble was unloaded. Iterative calculations were carried out until the overall stiffness of the material approached zero (or resistance to loading began to decrease). This was an indication of complete breakage of the initial rubble skeleton.

Numerical experiments

Direct shear box

The apparatus simulated in this set of numerical experiments is the two-dimensional direct shear box that is shown in Fig. 2. The inner length of the shear box is 6 m and the depth is 3 m. Load controlled deformation was applied to the upper part of material. The lid was free to move vertically in order to balance the normal confining pressure (σ) applied to its upper surface. The horizontal pressure (τ) was then incrementally applied to move the upper part of the shear box. The ice rubble used in the experiments was made up of rectangular blocks. Table 1 presents the characteristic parameters for the ice blocks that were chosen according to Kämärinen (1993).

Table 1. Ice block properties.

Property	Value	Property	Value
Length, m	~ 1.0	Angle of internal friction, °	0-30 (var.)
Thickness, m	~ 0.3	Tensile strength, MPa	0.2
Young's modulus, GPa	4.5	Porosity, %	~ 33
Poisson's ratio	0.3	Amount of blocks	~ 40
Cohesion, MPa	0.5		

Parametric analysis

A series of numerical tests were conducted with the direct shear box. The parametric study was performed in order to investigate the effect of mechanical properties of the ice blocks and their contacts on the strength of ice rubble skeleton. In addition the influence of normal pressure on the ice rubble strength was analyzed. The following parameters were assumed to be variable during the numerical experiments:

- Strength reduction factor for interfaces - R_i;
- Normal pressure – σ;
- Angle of internal friction - φ;
- Length of the contacts between ice blocks or contact area - A.

It was observed during simulation that initial failure of the ice rubble corresponds to breakage of the contacts between ice blocks. Therefore the initial strength is controlled by freeze bonding mechanism between separate blocks inside the ice rubble. The cohesion seems to be a major contributor to the bearing capacity of the ice rubble. Some local breakage of the individual ice blocks was also observed during simulations.

Influence of strength reduction factor

The shear strength τ versus strength reduction factor R_i for two different values of angle of internal friction is presented in Fig. 4. The normal pressure is assumed to be a constant and equal to 5 kPa.

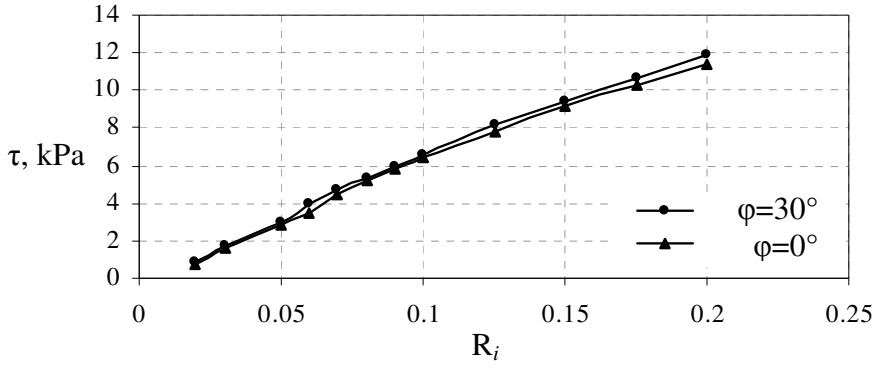

Fig. 4. Shear strength versus strength reduction factor, σ = 5 kPa.

The shear strength increases almost linearly with increasing strength of the interface elements. It is clearly shown in Fig. 4 that initial failure is independent of φ. Thus strength of the ice rubble is largely dominated by cohesion and tensile strength of freeze-bonds.

Weiss et al. (1981) have proposed that effective cohesion of ice rubble, *c,* may be proportional to the thickness of ice blocks, t, which form the rubble. They indicated the following relationship: $c/t = 16 \pm 8\ kPa/m$. Bruneau (1997) conducted analysis of several ice rubble shear strength laboratory test and reported: $c/t = 17\ kPa/m$. In the following we assume the average *c/t* value is about 20 kPa/m. Thus for present simulations of 0.3 m thick ice blocks *c* is expected to be about 6-7 kPa.

Ettema and Schaefer (1986) conducted a series of experiments on freeze-bonding between ice blocks. They reported that the shear strength of freeze-bond is about 1-5 kPa for small-to-medium scale tests. The ice blocks with contact area of 4.52 x 10^{-3} m^2 and 9.03 x 10^{-3} m^2 were used during these experiments that correspond to 9.5 x 4.75 cm and 13.4 x 6.70 cm block size respectively. The scaling of these results coincides with simulation data in Fig. 4. The curves show that shear strength is in the range of 5-7 kPa for the strength reduction factor from 0.08 up to 0.1, that corresponds to 40-50 kPa for the freeze-bond shear strength.

Influence of contact area

Fig. 5 shows a plot of shear strength τ versus total contact area A between the ice blocks. The normal pressure is assumed to be a constant and equal to 5 kPa. The strength reduction factor is chosen as 0.09 that is a freeze bonding strength of 45 kPa.

For the range of contact area used in the present study, the shear strength of the ice rubble is linearly increased with increasing of contact area. The simulation indicated that length of contacts or contact area between ice blocks A, has a great influence on the shear strength. This prompts that results depend significantly on block size and position. Table 2 shows the typical values of the average length of the contacts between the ice blocks in relationship with the total contact area.

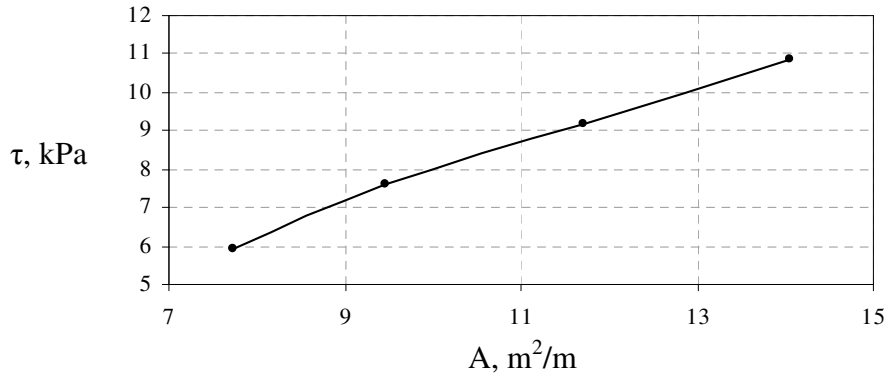

Fig. 5. Shear strength versus contact area, σ = 5 kPa, φ = 30º.

Table 2. Typical values of contacts between ice blocks as given by the block generator.

Total contact area A (m^2/m)	Average length $\bar{l}$ (m)
7.57	0.122 ± 0.085
9.31	0.150 ± 0.087
12.15	0.196 ± 0.092
14.74	0.238 ± 0.120

Additionally it was found that the total amount of blocks *N* and the inclination angles of contacts θ are very important as well. For the present simulation series the total amount of contacts was in narrow range of 60-62. It was also observed that θ is one of the contributors, which determined the failure mechanisms between the ice blocks and therefore has influence on the shear strength.

Influence of normal pressure

For the range of the present analysis shear strength τ increased non-linearly with increase of normal pressure σ as shown in Fig. 6.

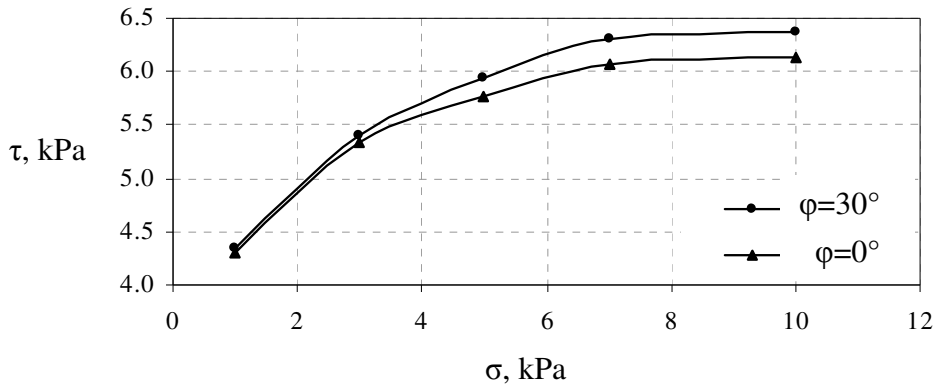

Fig. 6. Shear strength versus normal pressure.

The analysis shows that strength of the ice rubble is largely determined by the tensile strength. The stress states inside the ice rubble are illustrated in Fig 7. The plastic Mohr-Coulomb stress points are indicated with white dots and the tension cut-off points are indicated with black dots. For normal pressure σ = 1 kPa the ice rubble fails mostly in tension (Fig. 7a). The failure mode changes with increasing normal pressure up to 5 kPa. The local failure mechanism becomes a combination of tension and shear modes (Fig. 7b). It is possible to see from the Fig. 6 that shear strength increases approximately linearly with increasing of normal pressure up to 5 kPa. The failure mechanism remains the same with further increasing of normal pressure (Fig. 7c). Therefore the curves become non-linear and more flat as shown in Fig. 6.

a) b)

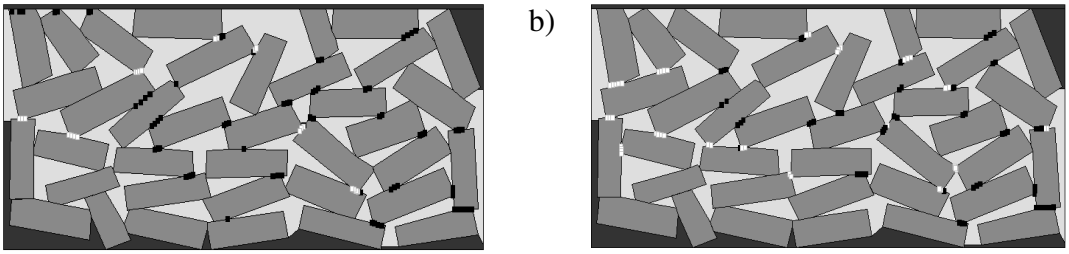

σ = 1 kPa σ= 5 kPa

c)

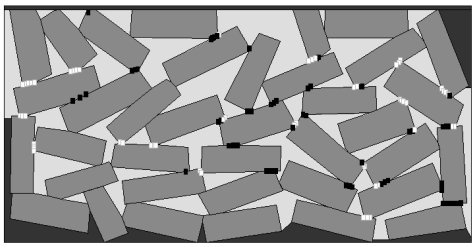

σ= 10 kPa

Fig. 7. Stress state inside the ice rubble, $R_i = 0.09$, $\varphi = 30°$.

(White dots - Coulomb stress points, Black dots - tension cut-off points).

Conclusions

The paper presents pseudo-discrete continuum model that simulates the breakage of rubble skeleton. A series of direct shear-box tests are done. The simulations were performed in order to investigate the effect mechanical properties of the ice blocks and their contacts. The influence of normal pressure on the ice rubble strength was analyzed.

The parametric analysis showed the following:

- The failure of the ice rubble mostly occurs between the ice blocks. But some local breakage of individual ice blocks was also observed during simulations. The initial failure mode is independent of frictional component. Therefore cohesion is a major contributor to the bearing capacity of the ice rubble.
- The freeze-bond properties and their relations to the properties of parent ice are important. The shear strength linearly increases with increasing strength of the interface elements.

- The shear strength of the freeze-bond linearly increases with increasing of contact area. Contact area between ice blocks, amount of contacts and inclination angles of contacts has a great influence on failure mode and shear strength. Thus it seems to be of high importance to estimate these aspects in-situ.
- The shear strength increased non-linearly with increasing of normal pressure. Strength of the ice rubble is mostly determined by tensile strength. But the some changes of failures mechanisms from tension to shear modes were observed, which probably is the result to the non-linear behaviour.

Acknowledgements

The authors would like to thank Alexey Privalov and Lev Videnski for programming support. We would also like to thank Dr. Knut Høyland for extensive review and valuable comments.

References

Bruneau, S. (1997). Development of a first-year ridge load model. *PhD thesis*, *Memorial University of Newfoundland*, St. John's, Newfoundland, Canada.

Ettema, R. and Schaefer, J.A. (1986). Experiments on freeze-bonding between ice blocks in floating ice rubble. *Journal of Glaciology*, Vol. 32, (112): 397-403.

Ettema, R. and Urroz, G.E. (1989). On internal friction and cohesion in unconsolidated ice rubble. *Cold Regions Science and Technology*, (16): 237–247.

Heinonen, J. (2002). Continuum material model with shear-cap yield function for ice rubble. *Proc. of 15th Seminar on Computational Mechanics*, Aalborg, Denmark, pp. 87-90.

Heinonen, J. (2003). Continuum material model for ice rubble–combined shear-cap yield criterion with strain softening. *Proc. of the 17th Int. Conf. on Port and Ocean Engineering under Arctic Conditions (POAC),* Trondheim, Norway, pp. 547–557.

Hopkins, M.A. and Hibler, W.D. (1991). On the shear strength of geophysical scale ice rubble. *Cold Regions Science and Technology*, (19): 201-212.

Kämärinen, J. (1993). Studies in ice mechanics. *Helsinki University of Technology*. 182p.

Liferov, P., Jensen, A., Høyland, K.V. and Løset, S. (2002).On analysis of punch tests on ice rubble. *Proc. of the 16th Int. Symp. on Ice (IAHR),* Dunedin, New-Zealand, pp. 101–109.

Liferov, P., Jensen, A. and Høyland, K.V. (2003). 3D finite element analysis of laboratory punch tests on ice rubble. *Proc. of the 17th Int. Conf. on Port and Ocean Engineering under Arctic Conditions (POAC),* Trondheim, Norway, pp. 599–610.

PLAXIS (2002). Plaxis v. 8.1. Finite Element Code for Soil and Rock Analyses.

Timco, G.W. and Cornet, A.M. (1999). Is φ a constant for broken ice rubble? *Proc. of the 10th Workshop on River Ice Management with a Changing Climate,* Winnipeg, Canada, pp. 318–331.

Urroz, G.E. and Ettema, R. (1987). Simple shear box experiments with floating ice rubble. *Cold Regions Science and Technology*, (14): 185-199.

Weiss, R.T., Prodanovic, A. and Wood, K.N. (1981). Determination of ice rubble shear properties. *Proc. of the Int. Symp. on Ice (IAHR),* Quebec, Canada, pp. 860-872.

8 SUMMARY, CONCLUSIONS AND RECOMMENDATIONS

8.1 Summary and conclusions

Ice strength heterogeneity: field testing

Several field uniaxial compression test programs have been performed in order to investigate the in-plane ice strength heterogeneity for the different ice fields in the first-year landfast sea ice in Spitsbergen fjords. In addition the ice strength distribution for a Point-area was examined. Furthermore, two first-year sea ice ridges (one in the North-Western Barents Sea and one in the Arctic Ocean nearby Spitsbergen) together with the surrounding level ice were investigated with respect to the 2D spatial strength distribution. The main conclusions of these studies are as follows:

- The ice strength distribution for a Point-area is subjected to the seasonal variation. The higher value corresponds to the cold ice at the beginning of the season and the lower variation is typical for the warm ice at the end of the season. Besides for a Point-area the ice strength variability over the layer decreases from the top of the ice cover surface down to the bottom of the ice.
- The strength of the ice samples taken from the certain depth from the ice cover surface at the different locations of the same landfast ice field varied by factor 3 to 4.
- For the landfast ice areas larger than 40 m^2 the typical ice strength heterogeneity is found in range of 20-30% for the vertical ice samples and about 10-20% for the horizontal ones.
- The hypothesis of decreasing of ice strength heterogeneity with the corresponding reduction of the size of an area in the landfast ice cover is considered to be doubtful.
- The ice ridges contain weak (and strong) zones and the local ridge strength varied by a factor of more than 3 in both vertical and horizontal directions. Due to their random structure, the first-year sea ice ridges are characterized by high strength heterogeneity - about 40-55%.
- A statistical correlation between physical and mechanical properties of sea ice was observed. The maximum strength of the drift ice for the both level ice and ice ridge can be estimated from the total porosity and the corresponding equations have been developed.

Numerical modelling of non-homogeneous ice field structure interaction

The special Finite Difference program "Inhomogeneity" was used to study the influence of ice strength heterogeneity on the global ice loads. The cylindrical structure was located in a non-homogenous ice field. The field heterogeneity was simulated by a number of inclusions of elliptical shape, which strength properties are weaker or stronger than corresponding values of the surrounding (homogeneous) ice field. This program gives possibility also to consider all phenomena that accompanies the process of the heterogeneous ice field structure interaction. The most important results are as follows:

- Strong inclusion may increase the load significantly. This happens due to inclusion that collects the ice loads over its surface and transmits them to the structure.
- Weak inclusions may diminish the load but this diminishing has a local character and should be ignored because zones with the higher strength always occur before or after weak ones.
- Strong inclusions may cause the scale effect. The ice load on a small structure during interaction with relatively narrow inclusion may arise whereas the load on the wide structure will not change.

Ice rubble: morphology and freeze-bond experiments

During scientific expeditions in 2005-2006, the ice blocks and freeze bonds between them were inspected in the ridge sails. Altogether 260 ice blocks and 130 freeze bonding contacts between them were examined with respect to their length, width, thickness and the angle of inclination to the horizontal plane. Furthermore the strength of the frozen contacts between the ice blocks were evaluated by the small-scale mechanical testing. Both field and laboratory experiments have been performed. The field tests were carried out in Adventfjorden on Spitsbergen. The laboratory tests with both artificial ice (fresh and sea water) and natural sea ice were conducted in the UNIS cold laboratory. The temporal development of the freeze bonding strength and the local strength of the submerged ice blocks were investigated.

The most important results of these investigations are as follows:

- The average length of the freeze bonds is 0.27 m, and width is 0.14 m. The average length to width ratios are 2.2 (2005) and 1.8 (2006).
- The average freeze bond length to the average block length ratio is introduced; this ratio is 0.33 (2005) and 0.35 (2006).

- The average freeze bonding strength is found as:

  32 ± 18 kPa for the sea ice that was tested in the field for 48 hours.

  67 ± 52 kPa for the sea ice that was tested in laboratory up to 60 hours.

  274 ± 142 kPa for the artificial freshwater ice that was tested in laboratory up to 60 hours.

- The ratio of freeze bonding strength to the strength of the surrounding submerged ice blocks is introduced and the results are:

  in range of 0.008 to 0.082 on average 0.03 ± 0.02 for the sea ice that was tested in the field for 48 hours.

  in range of 0.009 to 0.69 on average 0.15 ± 0.15 for the sea ice that was tested in laboratory up to 60 hours.

  in range of 0.06 to 0.69 on average 0.21 ± 0.12 for the artificial freshwater ice that was tested in laboratory up to 60 hours.

Numerical modelling of ice rubble behaviour

A pseudo-discrete continuum model used to simulate the micro-mechanical behaviour of the ice rubble was verified and extended. This model enables to study the initial failure mechanism of the ice rubble deformation behaviour. The parametric study and sensitivity analysis of the input parameters on the overall variability of the model has been performed for the 2D direct shear plane strain test simulations. Moreover the attempt to extend the program for the large deformation has been considered.

The main conclusions of this work are the following:

- The initial failure of rubble was mainly associated with the breakage of the freeze bonds between the ice blocks, though some local breakage of individual blocks also occurred.
- The strength of the ice rubble tends to increase as the size of the freeze bonds increases.
- The cohesion of partly consolidated rubble was found as 6.2 ± 0.1 kPa.
- For the initial failure, the angle of internal friction has little of importance and the cohesion is a major contributor to the bearing capacity of the ice rubble.
- The model is very sensitive to freeze bonding strength, local strength of the surrounding ice blocks and morphology of the ice blocks and freeze bonds between them.

8.2 Recommendations for further work

The following topics seem promising when extensions of the present work are being considered:

Field investigations of ice strength heterogeneity

- The 3D spatial and temporal variations of the mechanical properties of ice within sea ice features can be studied in the field using small-scale uniaxial compression tests. It can be important for the ice loads evaluation.
- The application of the borehole jack equipment together with the uniaxial compression machine for the field testing is considered to be useful for improving the knowledge of the ice strength heterogeneity.

Numerical modelling of non-homogeneous ice field structure interaction

- A statistical approach to determine the scale effects due to ice field heterogeneity can be developed. Analysis of probability of this effect for the structures of different dimensions should be carried out.
- The influence of several factors (e.g. strength of inclusions, theirs position in relation to the structure, the simultaneous interaction with several inclusions and the ice field behaviour) on the ice load can be investigated.

Ice rubble testing

- Further investigations on freeze-bonding strength preferably in full scale together with the morphology of the ice rubble would provide a valuable support for the numerical modelling of the ice rubble deformation behaviour.
- The special attention should be put on the thermodynamic scaling of the ice rubble test results.

Numerical modelling of ice rubble behaviour

- More work should be done to extend the pseudo-discrete continuum model for the large deformations in the ice rubble. This would enable to continue simulations after the global stiffness of material has approached zero.
- The ice sheet/ice rubble/structure interaction process can be studied using pseudo-discrete continuum model.